DOI:10.14753/SE.2018.2178

SEMMELWEIS EGYETEM

DOKTORI ISKOLA

# Ph.D. értekezések

# 2178.


# MOLNÁR KRISTÓF


**Celluláris és molekuláris biofizika**

című program

Programvezető: Dr. Kellermayer Miklós, egyetemi tanár

Témavezető: Dr. Jedlovszky-Hajdú Angéla, egyetemi adjunktus

DOI:10.14753/SE.2018.2178

# DEVELOPMENT OF BIOCOMPATIBLE POLYMER BASED FIBROUS MATERIALS FOR MEDICAL AND BIOLOGICAL USE

**Ph.D thesis**

**Kristóf Molnár**

Doctoral School of Basic and Translational Medicine

Semmelweis University



Supervisor: Angéla Jedlovszky-Hajdú, Ph.D

Official reviewers: György Marosi, D.Sc
Krisztina Ludányi, Ph.D

Head of the Final Examination Committee: Péter Mátyus, D.Sc

Members of the Final Examination Committee: Zoltán Hórvölgyi, D.Sc
Imre Klebovich, D.Sc

Budapest
2018

DOI:10.14753/SE.2018.2178

**Table of contents**

DOI:10.14753/SE.2018.2178

DOI:10.14753/SE.2018.2178

DOI:10.14753/SE.2018.2178

# 1 Abbreviations

| | |
|---|---|
| AFM | Atomic force microscope |
| ATR/fTIR | Attenuated total reflectance Fourier transform infrared spectroscopy |
| CL | Cross-linked |
| CYS | cystamine |
| CYSE | cysteamine |
| DAB | 1,4-diaminobuthane |
| DMF | dimethylformamide |
| DMSO | dimethylsulfoxide |
| DTA | differential thermal analysis |
| DTT | D,L-dithiothreitol |
| ECM | Extracellular Matrix |
| ESP | Electrospinning |
| EtOH | ethanol |
| GF | grafting number |
| KMH | Kuhn-Mark-Houwink equation |
| Magn | magnetite ($Fe_3O_4$) |
| NMR | Nuclear magnetic resonance spectroscopy |
| OA | oleaic acid |
| PASP | poly(aspartic acid) |
| PEO | poly(ethyleneoxid) |
| PSI | polysuccinimide |
| PVA | poly(vinyl alcohol) |
| SEM | Scanning electron microscope |
| TGA | Thermal gravimetric analysis |
| THD | 2,2,4(2,4,4)-trimethyl-1,6-hexanediamine |
| UV | Ultraviolet radiation |

DOI:10.14753/SE.2018.2178

**Further nomenclature**

| Name | Origin | Method |
|---|---|---|
| PSI-CYSE | CYSE modified PSI | grafting |
| PSI-DAB | DAB CL PSI | post ESP, dipping |
| PSI-CYS | CYS CL PSI | reactive ESP |
| PSI-OAMagn | magnetite doped electrospun PSI | reactive ESP |
| PSI-CYS-OAMagn | magnetite doped electrospun CYS CL PSI | reactive ESP |
| PSI-CYS-DAB | CYS and DAB double CL PSI | post ESP, dipping |
| PSI-THD | THD CL PSI/ | coaxial ESP |
| PSI-THD-PEO | THD CL PSI with added PEO | coaxial ESP, PEO was added to core solution |
| PASP-DAB | DAB CL PASP | hydrolysis from PSI-DAB |
| PASP-CYS | CYS CL PASP | hydrolysis from PSI-CYS |
| PASP-CYS-DAB | CYS and DAB double CL PASP | hydrolysis from PSI-CYS-DAB |
| PASP-CYSE-DAB | DAB CL PASP with thiol sidechains | cleavage of disulfide bonds of PASP-CYS-DAB |
| PASP-THD | THD CL PASP | post ESP, dipping of PSI then hydrolysis |
| PASP-THD-PEO | THD CL PASP with added PEO | coaxial ESP and hydrolysis, PEO was added to core solution |

DOI:10.14753/SE.2018.2178

# 2 Introduction

One of the most challenging tasks in medicine is the regeneration or complete replacement of damaged tissues. One of the solutions, or in other words, strategies, is the preparation of artificial matrices with embedded cells (preferably obtained by biopsy from the patient) and implantation of these matrices to the area of interest, where local regeneration might be induced. This field is called scaffold based tissue engineering or regenerative medicine. There are numerous requirements an artificial matrix must fulfill to mimick the structure of native tissues, such as biocompatibility, biodegradability and suitable chemical and last but not least physical structure.

Electrospinning enables the preparation of fibrous membranes with fiber diameters in the range of collagen fibers in natural tissues. Due to their inherent biocompatibility an obvious choice for basic materials would be the natural ones found in native tissues, such as collagen and hyaluronic acid. However, most of them are water soluble, and thus they tend to dissolve upon contact with biological fluids in the body. Although there are numerous non-water soluble polymers available, there is an emerging need for techniques making water soluble polymers available for electrospinning and finally for regenerative medicine. One solution can be the cross-linking of polymers, where in the case of water soluble polymers, a hydrogel is created, which tend to take up water and swell.

Hydrogel fibrous membranes resemble to the structure of native soft tissues especially when the appropriate polymer is used for their preparation. However, the available techniques for the preparation of hydrogel-fibers based on electrospinning have to be broadened, since there is no general strategy for the preparation of such fibers. This is the main motivation of the research behind the thesis, which is based on a synthetic poly(amino acids) and their derivatives.

## 2.1 Polymers, biocompatibility and biodegradability

Polymers are long macromolecules built from repeating units connected together covalently, called monomer units. Polymers can be divided into two mayor groups based on their origin: synthetic polymers, that are synthesized in laboratories or factories and bio-polymers, that are of natural origin, extracted from plants (cellulose), animals (gelatin, collagen) or even bacteria (poly(lactic acid)) [1, 2]. Well-known

synthetic polymers are poly(styrene), poly(ethylene), poly(propylene), poly(carbonate), etc.

Polymer based materials can be found in numerous areas given their excellent properties, which can be tailored for each application ranging from building materials through fabrics to medical implants and equipment. One of the most important applications of polymers is the bio-medical application, where more are required from a material compared to everyday usage. In this field a polymer must be biocompatible, which means that upon contact with a body (in the case of implants, drug formulations, etc.) it should not induce any complication, such as inflammation, irritation or foreign body reaction [3]. On the other hand, it is also recommended for a material to be biodegradable, which means that after fulfilling its duty, this material should degrade in the body into small biocompatible molecules, which are either used up as nutrients or are excreted [4]. There are numerous examples for biocompatible but not biodegradable polymers: poly(ethylene glycol), poly(ethylene oxide), poly(vinyl alcohol), poly(vinyl chloride), etc. On the other hand, several natural polymers fulfill the previously mentioned requirements, for instance hyaluronic acid and collagen, etc., although these polymers are expensive, their composition is poorly reproducible and depends on their source. In contrast to this, synthetic polymers of well-defined composition can be produced cost-effectively but in many cases their biocompatibility and/or biodegradability is questionable. Widely studied biocompatible and biodegradable polymers include poly(lactic acid) and poly(caprolactone) [5]. Beside these, poly(amino acids) such as poly(glutamic acid) and poly(aspartic acid) (PASP) and their derivatives are emerging as promising materials for biomedical applications since their chemical structure is based on peptide bonds and amino acids, which are supposedly enzymatically degradable [6].

### 2.1.1 Polysuccinimide and poly(aspartic acid)

Aspartic acid is a non-essential amino acid and as such, a building block of proteins and enzymes. It is synthesized in the human body by the transamination of oxaloacetate and is used as a precursor to some of the essential amino acids such as methionine and lysine [7]. Poly(aspartic acid) is a synthetic polymer composed of aspartic acid molecules attached together by peptide bonds that provides the polymer a

peptide-like chemical structure. Owing to this property poly(aspartic acid) is a biodegradable molecule and gets more and more attention in the past decades [8–25]. There are many different areas where PASP could be used: due to its ability to chelate metal ions it can be used as corrosion inhibitor [9]; as a super-swelling material it could be used as superabsorbent in feminine hygiene and diapers [10]; while owing to its polyanionic structure as biodegradable detergent or dispersant [8].

In the most efficient synthesis route poly(aspartic acid) is synthesized in two steps: first its anhydrous form, polysuccinimide (PSI) is synthesized by the thermal polycondensation of aspartic acid in the presence of phosphoric acid catalyst: either in solvents [11] or in a solvent free method in vacuum [12]. In the second step PSI is transformed into PASP in mild alkali medium (**Figure 1**) [13]. Although there are synthesis routs for the direct preparation of PASP, those result in a much smaller average molecular weight as well as they are more expensive [25]. Whereas the solvent free method in vacuum is cost-effective and yields an average molecular weight for PSI ranging from 10 to 70 kDa [14]. Also, unlike PASP, PSI is a reactive polymer therefore it can be easily modified at room temperature by nucleophilic reagents such as primary amines, which gives PSI a major advantage compared to other synthetic biocompatible and biodegradable polymers. This enables us to synthesize a large variety of PSI or - with its hydrolysis – water soluble PASP derivatives with tunable properties for different applications (**Figure 1**): dopamine conjugation for creating self-healing gels [15] and adhesives for wound dressing [16]; doxorubicin conjugation to poly(aspartamide) for the preparation of pro-drugs for drug delivery [17]; cysteamine (thiol side chains) [18], tercier-amine [19, 20], apolar alkyl group [21] and poly(ethylene glycol) [22] modification for creating poly(aspartic acid) molecules with higher functionalities, etc. [23, 24]. Furthermore, multifunctional amines can be used for the cross-linking of PSI and thus PSI gels (or after hydrolysis hydrophilic PASP hydrogels) can be created [13]. The only drawback of PSI might be the limited availability of solvents to work with which include, but not limited to dimethylformamide (DMF) and dimethylsulfoxide (DMSO). PSI and PASP based gels and their properties will be explained in details in **Section 2.2**.

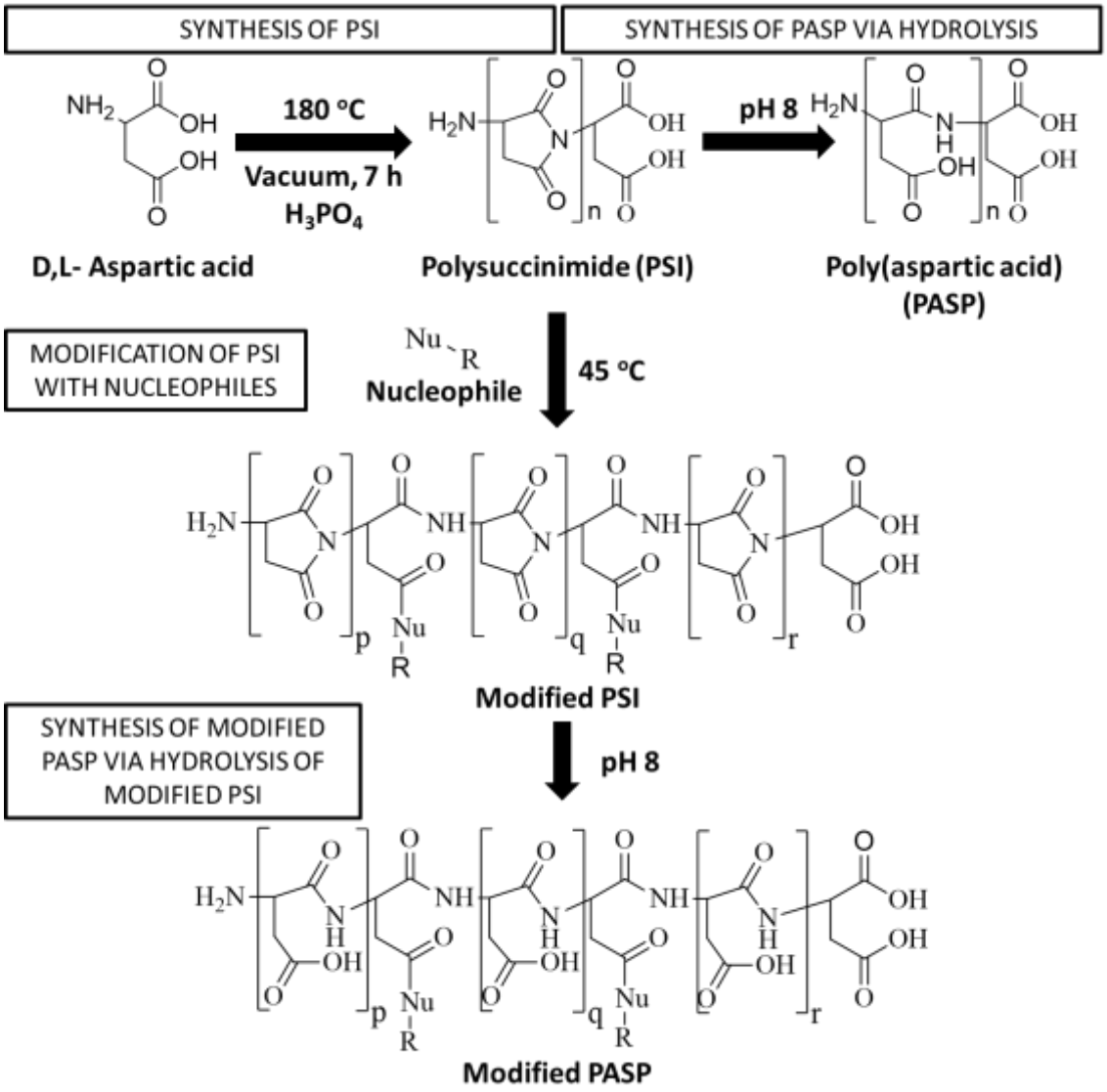


*Figure 1 Synthesis and modification of PSI and hydrolysis of PSI to PASP*

## 2.2 Polymer gels, hydrogels and their properties

Polymer gels are three dimensional polymer networks with a large amount of solvent stored inside them or in other words a solvent distributed in a solid medium. The polymer network creates a sponge like structure that prohibits the solvent from flowing out of it, whereas the solvent stored inside inflates and fills up this network to maintain its shape. Therefore, gels possess the properties of both solid and fluid materials: they maintain their shape after preparation like solids do, but also small molecules like drugs can migrate inside them by diffusion as in fluids. Depending on their chemical structure gels can be soft tissue-like [26] or hard like cartilage [27]. Furthermore, gels can be prepared in a wide variety of forms ranging from slabs, disks

and spheres etc. to nanoparticles, nanofibers and films etc. Special class of gels is hydrogels, in which the solvent filling up the polymer network is water or other aqueous solution (such as biological fluids). These materials are hydrophilic and resemble the soft tissues in living organisms. As a result, hydrogels are commonly used in clinical practice and experimental medicine for a wide range of applications, including drug delivery, tissue engineering, regenerative medicine or diagnostics [28, 29]. Out of the several commercially available products made of hydrogels, the two most common are contact lenses [30] and absorbents in feminine hygiene products [31] and diapers (**Figure 2**).


*Figure 2 Some applications of hydrogels* [32]

The polymer network in hydrogels can be composed of physical and/or chemical interactions [33]. Physical cross-links consist of either entanglement of the polymer chains and/or secondary interactions such as H-bond, ionic bond or hydrophobic associations. Since physical gels are composed of weak interactions, it is possible to dissolve them upon changes in environmental conditions such as temperature, pH, ionic strength, etc. (**Figure 3a**) In contrast, hydrogels prepared by chemically cross-linking polymers cannot be dissolved in such circumstances unless their chemical structure is damaged (**Figure 3b**). However, physical and secondary bonds are always present also in chemically cross-linked hydrogels.

DOI:10.14753/SE.2018.2178

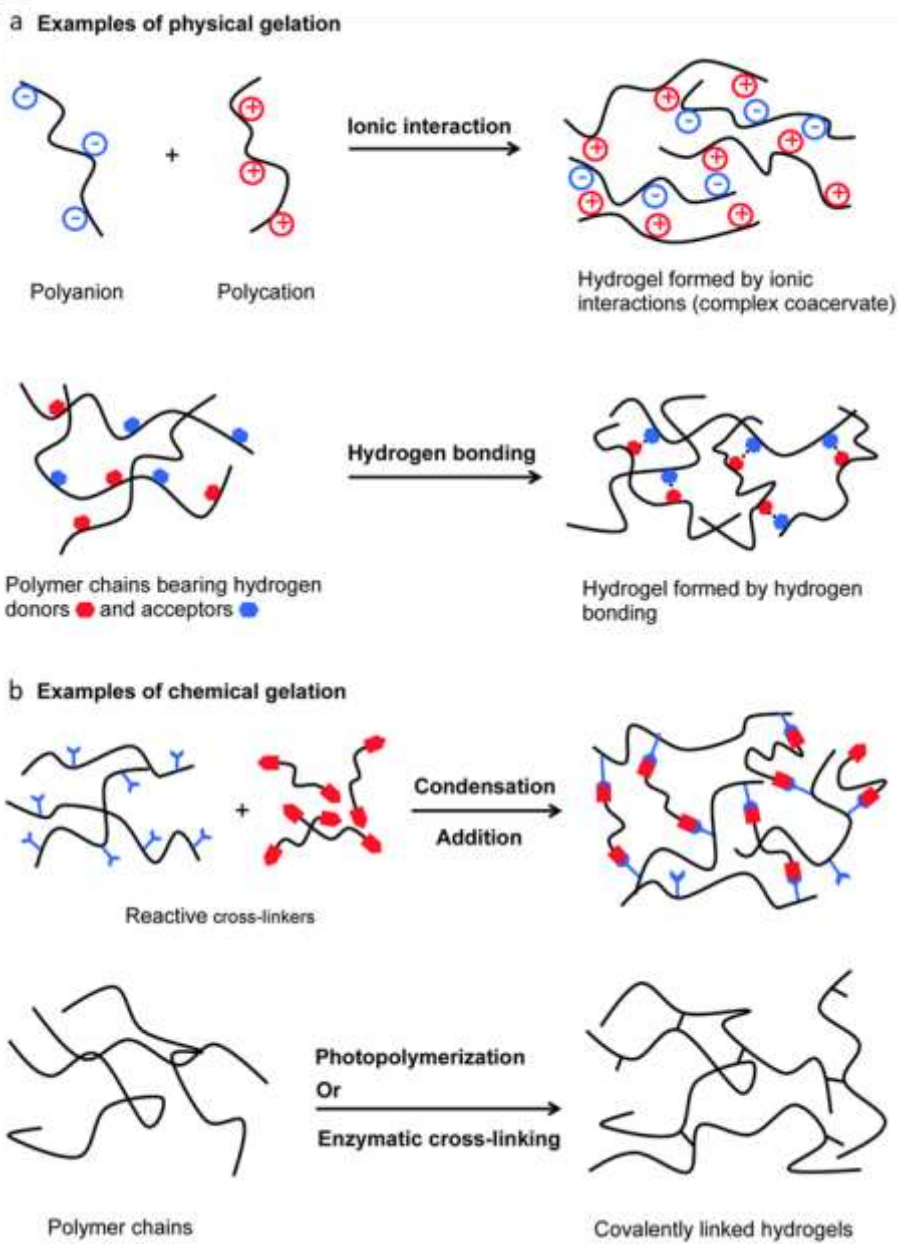


*Figure 3 Examples of physical cross-links in hydrogels (a) and examples of chemical cross-links in hydrogels (b)* [34]

There are two main strategies for the preparation of chemically cross-linked hydrogels [33, 35]. One is the polymerization of molecules in the presence of a cross-linker of functionality higher than 2 where polymerization and cross-linking happens at the same time. However, these types of polymerizations are often prohibited by the presence of water, and thus the use of this route for the preparation of hydrogels is limited. The second strategy is to either cross-link polymers with a cross-linking agent with functionality 2 or higher or implementing reactive side-groups to the polymer and inducing cross-linking between them by external stimuli such as UV light. Some

frequently used cross-linking reactions are the amide formation between amine and carboxylic groups, urethane formation between isocyanate and hydroxyl groups and Schiff base formation. Accordingly, di- and polyaldehydes, -amines, -carboxylic acids and -alcohols are generally used as cross-linker molecules. Hydrogels can be synthesized from both synthetic and natural polymers. Poly(ethylene glycol), poly(vinyl alcohol) or poly(2-hydroxyethyl methacrylate) are one of the most commonly used synthetic polymers whereas agarose, alginate, collagen, chitosan and hyaluronic acid are commonly used naturally occurring ones.

A gel is in equilibrium state when the chemical potential of the solvent stored inside equals to the chemical potential of the surrounding solvent [36, 37]. As a consequence, the cross-linked polymer network swells during solvent uptake until it reaches an equilibrium. The swelling property of a gel can be defined with the absolute swelling degree ($Q_{abs}$) (**Equation 1**) which is the ratio of the volume of the swollen gel in equilibrium ($V_{eq}$) to the dry polymer network ($V_{dry}$) or with the relative swelling degree ($Q_{rel}$) (**Equation 2**), which is the ratio of the volume of the gel in two different states ($V_{eq,1}$, $V_{eq,2}$).

$$\boldsymbol{Q_{abs} = \frac{V_{eq}}{V_{dry}}} \quad \textbf{(1)}$$

$$\boldsymbol{Q_{rel} = \frac{V_{eq,2}}{V_{eq,1}}} \quad \textbf{(2)}$$

Certain hydrogels are called intelligent or smart, if they can respond to one or more environmental stimuli with usually volume change or sol-gel transition [38, 39]. There is a wide variety of physical and chemical stimuli which can induce response: physical stimuli include the change in temperature [40], solvent compound, light [41], electric [42] and magnetic fields [43], whereas chemical or biochemical stimuli [44] include changes in pH, redox potential or the presence of ions and enzymes. Out of these pH and temperature sensitive hydrogels are the most frequently studied in medicine related research, especially in drug delivery, since the gradient of these two parameters are well represented in the human body [38]. Poly(N-isopropylacrylamide) and its derivatives are the most frequently investigated temperature regulated hydrogel, since their lower critical solution temperature (LCST) is close to the temperature of the human body (around 32 °C) [40]. Depending on their molecular structure, hydrogels can be neutral, cationic, anionic or ampholytic. Since the overall charge of the network

in hydrogels depend strongly on the pH of the surrounding medium, most ionic gels exhibit pH dependent swelling behavior [45]. This can be used for controlled drug release in pharmaceutics. For example if administration is planned through the gastro intestinal tract, the drug can be delivered and guarded by a gel which is in shrunken (closed) state in the acidic pH of the stomach (no release) and swollen state (open) in the mild basic pH of the small intestines (drug is released) [46]. Cationic properties arise from pendant amine groups, whereas anionic properties arise from pendant carboxylic acid groups. Poly(aspartic) acid is an anionic polymer which in gel form shows pH dependent swelling properties [47].

There are two main strategies for the preparation of poly(aspartic acid) hydrogels. One is based on the reaction between PSI with molecules having two or more amine groups which is followed by the hydrolysis of the network [6]. Gyenes *et al*. was the first one to synthesize PSI and PASP gels by using 1,4-diaminobuthane, lysine or cystamine as cross-linkers [13, 48], whereas Gyarmati *et al*. synthesized PASP hydrogel with supermacroporous interconnected pore structure by a solid–liquid phase separation technique, cryogelation using 1,4-diaminobuthane as a cross-linker [49]. The second approach is the synthesis of functional PSI molecules, then with their hydrolysis PASP derivatives, which can form cross-links upon physical or chemical stimuli. Gyarmati *et al.* prepared thiolated PASP that showed reversible sol-gel transition upon oxidation and found it a promising candidate for biomedical applications, where *in situ* gelation is beneficial, e.g. drug delivery or implants [50, 51].

PASP hydrogels show abrupt change in their volume around the $pK_a$ values of aspartic acid ($pK_a$=3.25, $pK_a$=4.35) due to the presence of carboxylic groups on the polymer chain [52]. They are in a swollen state in alkali medium, where the hydrophilicity of the polymer is increased due to deprotonation of carboxylic groups, while in acidic environment, below pH=4.2, where carboxylic groups are protonated, they shrink (**Figure 4**) [6, 13, 53–55]. This property is often utilized in drug delivery application, where the release of a drug trapped inside the polymer network is driven by the change in pH [56].

DOI:10.14753/SE.2018.2178

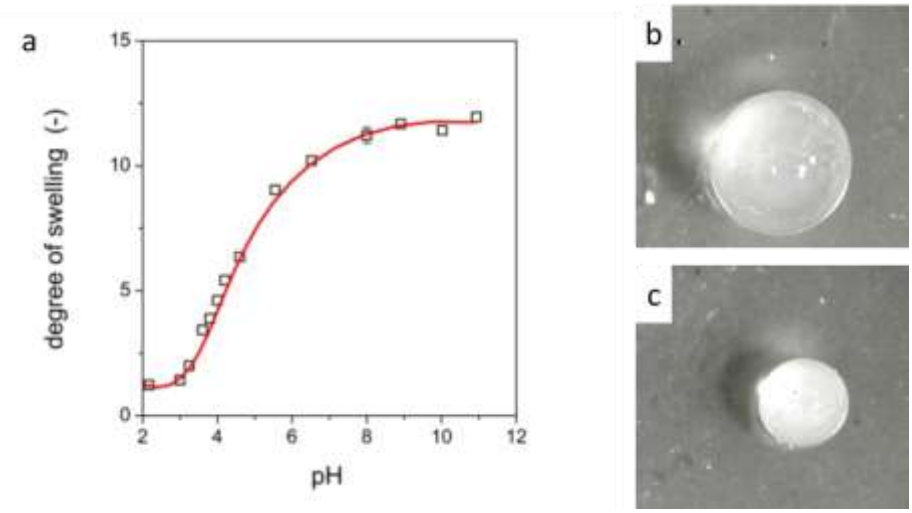


*Figure 4 pH dependent swelling of a PASP based hydrogel cross-linked with 1,4-diaminobutane (a)* [57]*; PASP hydrogel in a swollen state at pH 8 (b) and shrunken state at pH 2 (c) where the volume change was 35 % (part a shows a tendency and not directly related to parts b and c)*

## 2.3 Preparation of polymer fibers – electrospinning

There are many possible ways for creating polymer nano- or microfibers, such as mechanical pulling, electrospinning, melt blowing [58], force spinning [59], etc. Out of these, electrospinning became one of the most widely investigated techniques for preparing such fibers, as it enables the synthesis of fibers with average diameter ranging from tens of nanometers to several micrometers [60].

The basic laboratory setup of single needle electrospinning consists of a DC high voltage power supply, a syringe pump and a grounded (conducting) metal plate (collector) (**Figure 5a**). In principal the positive high voltage (5 – 30 kV) is connected to a syringe with a metal needle filled with a polymer solution, which is pushed out by the syringe pump constantly and the grounded collector is placed in front of it in a well-defined distance (5 cm – 30 cm) [61].

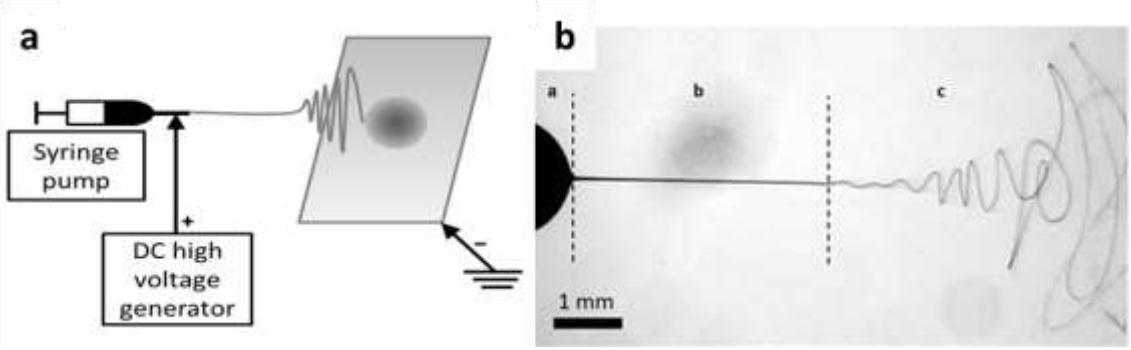


*Figure 5 Basic setup of electrospinning (a)* [62], *picture of the three stages of the electrospun jet (b)* [63] *where part (a) is the Taylor-cone, part (b) is the stable zone and part (c) is the whipping zone*

Upon turning on the power supply the polymer droplet at the tip of the needle is filled with charges due to charge separation. This time two forces awaken: the surface charges repelling each other and the Coulomb force from the electrical field. By raising the applied voltage, due to the forces affecting the droplet, it elongates and shifts its shape to the so-called Taylor-cone (**Figure 5b, part a**). If the applied voltage is high enough, the electrical field strength reaches a critical value (it can overcome the surface tension of the polymer solution) and a thin polymer fiber is ejected in the direction of the grounded collector (**Figure 5b, part b**). After the „linear zone" (due to the electrical field) the jet becomes unstable and starts a whipping motion till it hits the collector where the randomly oriented fibers can be collected (**Figure 5b, part c**). During the flying period the fibers are constantly elongated and thus their diameter constantly reduces till they reach the collector where the polymer fibers create the fibrous non-woven membrane [64]. However, if the jet breaks up into droplets polymer nano- or microparticles can be prepared and the technique is called electrospraying [65, 66], which is also used as an ion source in mass spectrometry [67].

There are several parameters affecting fiber formation (fiber morphology, diameter, and diameter distribution), which can be separated to three main groups [68]:

- solution parameters: viscosity, surface tension, conductivity, dielectric constant;
- process parameters: applied voltage, feed rate of solution, type of collector, type of needle, distance between collector and needle;
- environmental parameters: temperature, pressure, atmosphere, humidity.

All these parameters affect fiber formation in different degrees; however, in most cases they even affect each other. For example, the viscosity of the polymer solution can be adjusted by polymer concentration, polymer molecular weight and ambient temperature. However, if the polymer concentration in the solution is too low, the polymer jet breaks up into small droplets which due to the surface tension will obtain a perfect spherical shape. This can also happen if the molecular weight of the polymer is too low or the polymer-polymer interaction is too weak or simply the surface tension of the solution is too high. However as the polymer concentration is raised the fiber diameter rises too and the correct applied voltage needed for well-balanced feeding-taking ratio has to be raised as well [69].

Almost all the polymers of sufficient molecular weight can be used for electrospinning, so the choice of polymer must be based on the requirements of the field of the targeted application. All fields have their respective requirements of a polymer. For example, water-soluble polymer fibers would not be useful for water filtration but they are very efficient for drug release in the gastrointestinal tract. In biomedical application polymer fibers are required to be biocompatible; in sensory application fibers are required to be conducting, etc. Another aspect in choosing the right polymer for an application is the impact on the environment (green chemistry), since solvents used for electrospinning are volatile, often toxic or even corrosive [70]. Although in laboratory scale those kinds of solvents are acceptable (such as dimethylformamide and dichlormethane), green electrospinning is highly desired for industrial scale fiber preparation [71].

There is a wide variety of fields where electrospun fibrous membranes can be applied. The fibrous structure provides high specific surface area and high porosity to the membranes, which are excellent properties for filtration. Already there are some commercially available air and water filters made of electrospun fibrous membranes for industrial air filtration (eSpin technologies, MANN-HUMMEL, etc.), clean room air filtration (Koken) and even household water filtration system (Coway, Liquidity corporation), facemask (NASK) and fabrics (Revolution Fibers Ltd.), etc. [72]. Electrospun sensors are an emerging field as well even though there are no commercially available products yet [73]. Another important group of possible application for electrospun membranes are biomedical applications, where the two most

developing areas are drug delivery and tissue engineering. For drug delivery, the drug can be directly mixed into the polymer solution to obtain drug loaded fibrous membranes. Depending on the polymer matrix, several different release types can be achieved ranging from immediate release (rapid dissolution of the matrix) [74] to diffusion or dissolution controlled sustained and prolonged release [75]. Another important aspect of electrospinning in drug delivery is the fast solidification of the fibers during preparation process. It is so fast that it can prevent drugs from crystalizing leading to amorphization. Hence electrospinning can enable administration of drugs of poor solubility [76]. Artificial tissues and tissue engineering will be discussed in Section 2.4.

Although a lot can be achieved with a simple, single needle electrospinning setup (**Figure 5a**), there is a wide variety of many different setups for fiber preparation based on electrospinning. Just looking at the needles and nozzles used for electrospinning one can find many articles working on different types either aiming at higher productivity (needleless electrospinning) or complexity in fiber morphology. Recent result in aiming for high productivity have been collected in the review of Yu et al. [77]. For complexity one of the more used setups are based on coaxial or in other terms core/shell or core/sheath nozzles. In coaxial electrospinning a special needle-in-needle is used where a core and a shell solution can be pumped simultaneously (**Figure 6**). The two solutions do not mix in the process and thus, if the processing parameters are set right, special fibers can be prepared such as: fiber-in-fiber [78], hollow [79], loaded with drugs or nanoparticles [80] etc.

DOI:10.14753/SE.2018.2178

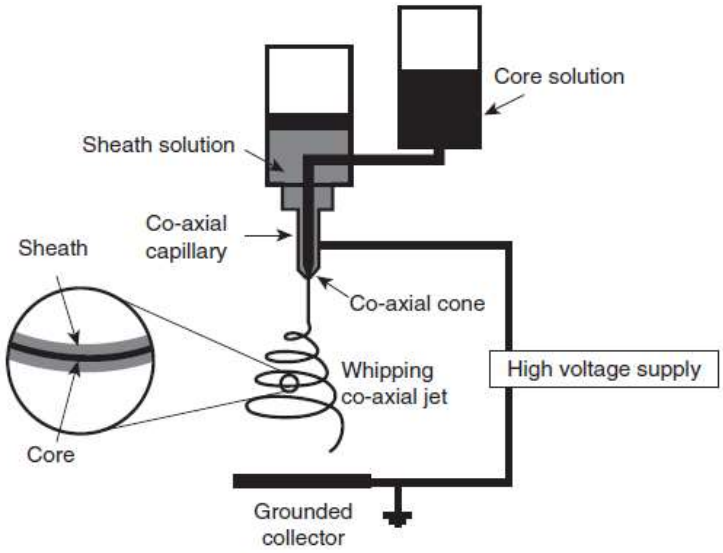


*Figure 6 Schematic of coaxial electrospinning setup* [81]

### 2.3.1 How to cross-link the polymer inside the fibers: reactive electrospinning and post methods

There are many fields where electrospun nanofibers prove to be useful ranging from industrial filtration via protective clothing to biomedical application [82]. However, one must cope with the requirements of each field when choosing the appropriate polymer. For example, in biomedical application the chosen polymer has to be biocompatible and biodegradable. As it will be explained in details later (**Section 2.4**) electrospinning is frequently used technology to build artificial networks for implants. However, in this case it is required from the material to be present without major degradation for days, weeks or even months after implantation. Therefore, in many cases the available polymers are limited to biocompatible, biodegradable and hydrophobic ones as hydrophilic nanofibrous sheets - due to their high surface area - dissolve almost immediately after implantation. Therefore, in many cases the available polymers are limited to hydrophobic ones. On the other hand, dissolution of water soluble polymers in water can be avoided by forming cross-links between polymer chains hence creating hydrogels. By introducing a cross-linking reaction to electrospinning, one can obtain gelfibers that - without chemical or enzymatic degradation - will not dissolve after dipping into a solution, only uptake the surrounding fluid. There are several possible ways to create cross-links between the polymer chains

during electrospinning and in general they can be separated into two main groups: post- and reactive electrospinning.

In post-spinning methods, in general, the fibrous mesh is prepared first and then the cross-links are formed due to a chemical reaction. There are several approaches available in the literature: Zhang *et al*. for example created cross-links inside polysuccinimide fibers by immersing them into the solution of diaminoethane (cross-linker) in methanol [83]. In this case it is hard to control the amount of cross-links, as an excessive amount of cross-linker is present. They also found, that after hydrolysis when the polysuccinimide fibers turned into the water soluble poly(aspartic acid) fibers, they deformed greatly. Gao *et al.* electrospun the mixture of the PVA solution and the cross-linker and used heat to induce cross-linking inside PVA fibers [84], whereas Ding et al. reported a very similar work based on PVA just with another cross-linker [85]. Kim et al. synthesized a modified N-isopropyl-acrylamide and electrospun it to later induce cross-linking between the polymer chains in the fibers also by heat, just without cross-linking agent [86]. It was also shown that gamma radiation can be used after electrospinning to obtain water resistance, even without any cross-linking agent or initiator [87]. Although it is a very efficient method, considering that gamma irradiation is a widely used method for sterilization [88], the chemical reactions are not predictable and it is hard to control the amount of cross-links, not to mention determining their amount. Another often used method is cross-linking fibers by treatment of fibrous membranes in the fumes of cross-linker. Glutaraldehyde is a cross-linker commonly used for post cross-linking hydroxyl group containing polymers such as gelatin [89], collagen [70, 90], PVA [91], etc.

In reactive electrospinning a chemical reaction takes place during the fiber formation. Theoretically this reaction is not limited to cross-linking, however here I will only focus on gelfiber preparation. In reactive electrospinning an obvious method is to directly mix the polymer and the cross-linker in one solution and electrospin it. However, as the cross-linking reaction progresses, due to linking of polymer chains, the viscosity of the solution constantly rises till it gelates and blocks the needle. Therefore, by this method one can only produce a limited amount of fibers/batch resulting in fiber diameters in a wide range due to the constant rise in viscosity of electrospun solution. This time frame, where spinning is possible before the gelated mixture blocks the

nozzle, is called the spinning window. One example of this type is the work of Tang et al. who mixed poly(vinyl alcohol), glutaraldehyde and hydrochloric acid as catalyst for cross-linking [92]. A possible solution for eliminating the spinning window in the case of direct mixing was reported recently by Xu et al. [93]. In their work they used a double barrel syringe (**Figure 7a**) where the two reactive polymers were fed separately and mixed in a special static mixing tube (**Figure 7b**) for a controlled time before electrospinning. This way the properties and compound of the mixture at the tip of the needle was maintained constant.

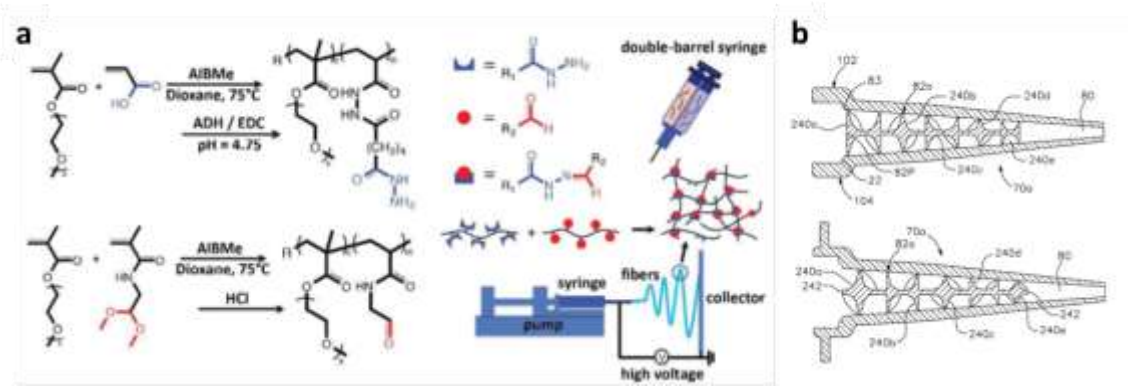


*Figure 7 Solution of Xu et al. for the problem of spinning window in electrospinning of directly mixed polymer and cross-linker (a)* [93] *and an example for the static mixer attached to the double barrel syringe used in their work (b)* [94]

Another method for reactive electrospinning is using UV light induced cross-linking of grafted polymers, where a polymer is grafted with a reactive compound which can create cross-links if treated with UV light during electrospinning. This polymer is stable and maintains its liquid state before spinning, thus a constant cross-linked fiber formation with narrow diameter distribution can be obtained. Another example using poly(vinyl alcohol), is the work of Greiner *et al.* who modified PVA with an UV reactive sidechain to form cross-links during electrospinning [95]. Another approach for UV cross-linking is the electrospinning of the modified polymer and a photo-initiator in the presence of UV light, however the biocompatibility and biodegradability of the photo initiator is always questionable [96]. Similarly to post electrospinning, glutaraldehyde is a common cross-linker in reactive electrospinning as well. In this case the fibers are electrospun in glutaraldehyde fumes directly [91].

Although the immediate dissolution of the previously mentioned fibrous systems were prevented by cross-linking the polymer inside the fibers, in all cases the structure

of the fibrous membranes was still damaged in various extents (fusion and distortion of fibers) upon immersion into water or the original solvent of the polymer. It is still a valid problem to retain the full fibrous form without any fusion and interconnection of fibers in the membranes. However, this is a small price to pay for making membranes of water soluble polymers available for applications where water solubility is a huge drawback. Also with proper control over cross-linking and electrospinning the advantages of fibrous membranes such as high porosity and surface area can still be retained.

## 2.4 Biomedical applicability of polymer matrices – Tissue engineering

There are numerous examples for the application of hydrogels and fibrous tissues in a wide variety of fields ranging from industrial to biomedical. However, the research presented in this thesis is mainly focusing on the biomedical application, especially on regenerative medicine, therefore only that will be discussed in details. One of the most challenging tasks in modern medicine is the regeneration or complete replacement of damaged tissues or organs and the latter is further hindered by the limited availability of donors. Tissue engineering and regenerative medicine are emerging fields aiming to solve this problem. Langer *et al.* defined tissue engineering as "an interdisciplinary field that applies the principles of engineering and life sciences toward the development of biological substitutes that restore, maintain, or improve tissue function" [97]. The size and complexity of these substitutes are ranging from small sheet like scaffolds (for example in wound dressing [98]) to artificial blood vessels and heart valves [99] and functional body parts [100] (**Figure 8**).

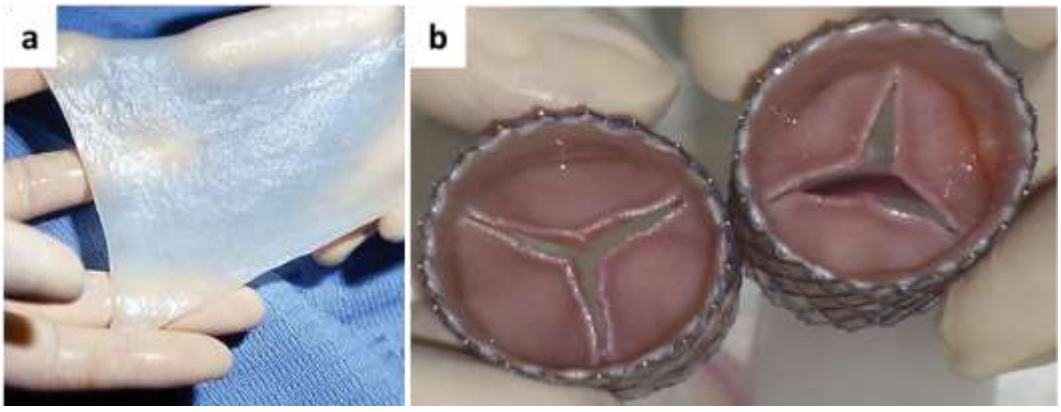


*Figure 8 Matriderm acellular skin graft (a)* [101] *and tissue engineered heart valves (b)* [99]

There are four major synthetic strategies applied in tissue engineering, depending on the aimed type of tissue (such as bone, skin or simply connective tissue) (**Figure 9**) [102]:

- premade porous scaffolds: a synthetic material is developed with different techniques such as 3D printing and electrospinning which can support cell growth and implantation. After seeding cells into the material, it is implanted to the damaged area;
- decellularized extracellular matrix: similar to premade porous scaffolds, however the origin of the scaffold is different. In this case the material is extracted from a donor;
- cell sheets with secreted ECM: in vitro cultivation of cells extracted from a patient enables the preparation of confluent cell layers which tend to excrete ECM for themselves. By generating several layers or cells an artificial tissue can be prepared which supports cell life and implantation;
- cell-encapsulated self-assembled hydrogels: injectable hydrogels which are filled with the cells of the donor can fill holes or replace damaged tissue. Optimally the hydrogel is prepared after injection of the mixture of precursor molecules and cells into the damaged area.

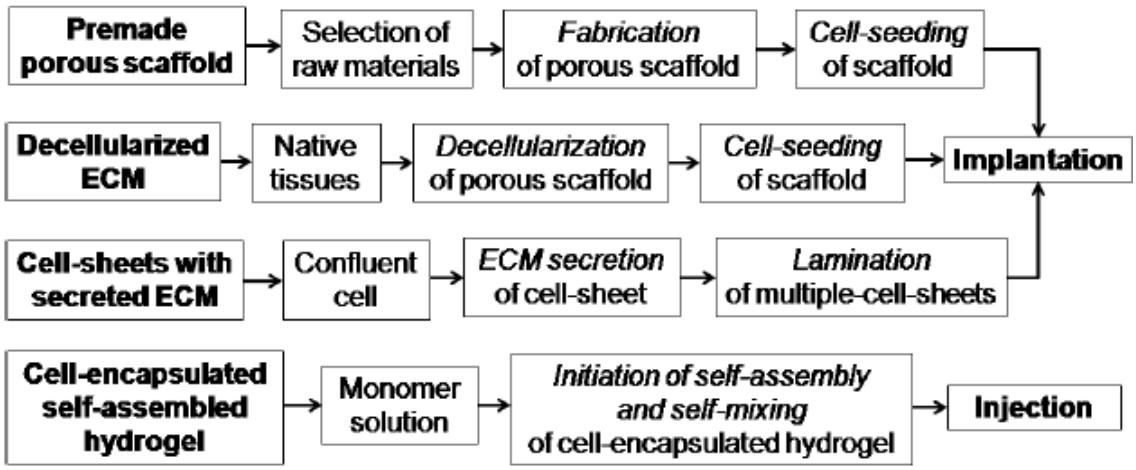


*Figure 9 Different strategies in tissue engineering* [102]

As it was mentioned before premade porous scaffolds can be used as platforms for cell cultivation and later as carriers for those cells/new tissue during implantation. This strategy is often called scaffold-based tissue engineering. This technique can be separated into four distinct steps: first cells from a patient are extracted by biopsy

(**Figure 10 arrow 1**); second they are cultivated/expanded in regular in vitro environment (**Figure 10 arrow 2**); third they are seeded on or into the premade scaffold (**Figure 10 arrow 3**); fourth the scaffold is implanted with the cells to the damaged area (**Figure 10 arrow 4**).

There are numerous requirements of an artificial material necessary to be fulfilled to be appropriate for both cultivation and implantation. The material itself should be biocompatible and biodegradable, have the appropriate mechanical stability for implantation as well as it should mimic the mechanical properties of the native tissue aimed to be repaired or replaced. Also, it should have an appropriate chemical structure that supports cell attachment and ingrowth [103]. Therefore, to create the appropriate matrix for tissue engineering, one must copy the structure and chemical composition of the connective tissue of the area of interest. The most general tissue in the human body is the connective tissue, which consists of the amorphous substance, cells (i.e. fibroblasts), and the extracellular matrix (ECM). The connective tissue is flexible, with a gel-like structure composed of a fibrous backbone of collagen fibers called extracellular matrix with very high fluid content [104].

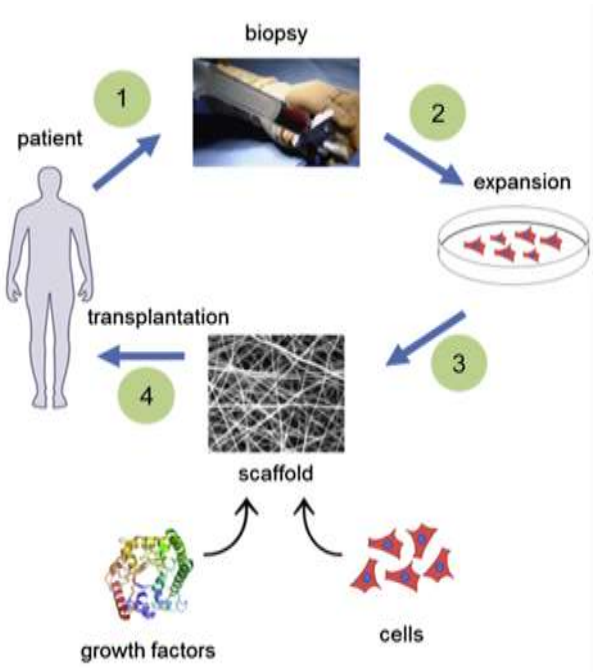


*Figure 10 Schematic representation of scaffold based tissue engineering* [105]

Hydrogels are often in the focus of artificial tissue preparation, given that they resemble a lot to the loose connective tissue owing to their high fluid content and soft

but elastic structure [35]. Furthermore, hydrogels are penetrable for small molecules such as nutrients, growth factors, hormones and other important molecules for cell attachment and proliferation. However, hydrogels mimic only the macroscopic structure of the connective tissue since they do not possess the fibrous structure of ECMs. An elegant technique for reproducing an ECM is electrospinning, which can produce fibrous membranes with fiber diameters in the range of collagen fibers in natural ECM. This is one of the many reasons why electrospinning holds a distinguished position in the preparation of artificial ECMs [56].

Both natural and synthetic materials can be used for matrix preparation, however natural polymers tend to be expensive whereas their quality depends on their source (See **Section 2.1 and Section 2.2**). Water soluble polymers tend to dissolve immediately upon contact with water, and thus their use in pure form is hindered by dissolution. For example, the use of poly(aspartic acid) fibers in biomedical application is prohibited by dissolution. Furthermore polysuccinimide undergoes hydrolysis and turns into poly(aspartic acid) in time, and thus the problem of dissolution remains. However cross-links between the polymer chains inside the fibers inhibit dissolution of the membranes since the fibrous tissue would only uptake the surrounding fluid and swell, eventually forming fibrous hydrogel membranes (See **Section 2.3.1**). These membranes combine the properties of both electrospun fibers and conventional hydrogels eventually getting closer to the physical and partly the chemical structure of the natural connective tissue. The list of commonly used water-soluble and non-water-soluble polymers can be found in numerous reviews with their respective focus areas in tissue engineering [56, 106–109].

DOI:10.14753/SE.2018.2178

# 3 Objectives

The main objective of the research was the development of poly(amino acid) based fibrous membranes, which resemble to the native soft tissue and can be applied in biomedical fields. The development revolved around three major tasks as follows:

- Development of techniques and synthesis routes for the preparation of poly(aspartic acid) based fibrous hydrogel membranes based on electrospinning: it was in our interest to develop methods that can be applied not just in the preparation of cross-linked poly(aspartic acid) fibers but could be used as general strategies for cross-linked fiber preparation;
- Assessment of the physico-chemical properties of the hydrogel membranes: different techniques were developed for the preparation of hydrogel-fibers it was in my aim to compare these techniques and the resulting fibrous membranes. The most important parameters I was interested in were:
    - fibrous structure and fibrous property;
    - productivity and basic characteristics (batch-to-batch or continuous fiber preparation) of the different techniques developed
    - since poly(aspartic acid) hydrogels show pH sensitive swelling properties in bulk forms, the pH sensitivity fibrous membranes was also an important property to be characterized;
- Evaluation of the biocompatibility and biodegradability of the membranes. Although polysuccinimide can be easily turned into poly(aspartic acid) in mild alkali medium, this transformation has never been shown to happen *in vivo* before. Therefore, I wanted to prove the presumed hydrolysis and see the biological response to the polysuccinimide based membranes by implanting them into albino rats.

DOI:10.14753/SE.2018.2178

# 4 Materials and methods

## 4.1 Reagents

L-aspartic acid (Sigma-Aldrich, UK), cysteamine (CYSE) (Sigma-Aldrich, UK), dimethylformamide (DMF) (VWR International, USA), dimethylsulfoxide (DMSO) (Sigma-Aldrich), o-phosphoric acid (VWR), 2,2,4(2,4,4)-trimethyl-1,6-hexanediamine (THD) (Sigma-Aldrich), poly(ethylene oxide) (PEO) (900 kDa) (Sigma-Aldrich), DMSO-d6 (100%, 99.96% atom% D, Aldrich), 1,4-diaminobutane (DAB) (99%, Aldrich), imidazole (ACS reagent, ≥99%, Sigma-Aldrich), citric-acid*H2O (ACS reagent, ≥99.9%, VWR), sodium chloride (99-100.5%, Sigma-Aldrich), phosphate buffer saline (PBS) (Tablet, Sigma), D,L-dithiotreitol (DTT) (Sigma), iron (II) chloride (VWR International,USA), iron (III) chloride (VWR International, USA), oleic acid (VWRInternational, USA), sodium hydroxide (VWR International, USA), acetone (Sigma-Aldrich, UK). Standard pH 9 and pH 4 borax buffer solutions were purchased from Merck. All the chemicals were of analytical grade and used as received. For the aqueous solutions ultrapure water (Human Corporation ZeneerPower I Water Purification System) was used.

For 1 L of imidazole buffer imidazole (pH 8: 12.988 g, pH 3: 4.352 g), citrate (pH 8: 1.728 g, pH 3: 24.96 g), sodium chloride (pH 8-11.466 g, pH 3-10.706 g) and ultrapure water were used. In all cases the exact pH was adjusted by the addition of hydrochloric acid and followed by digital pH meter (Thermo Scientific™ Orion™ 4-Star Plus pH/ISE Benchtop Multiparameter Meter).

Oleic acid stabilized magnetic nanoparticles (OA-Magn) were synthesized in our laboratory by Dr. Angela Jedlovszky-Hajdu and used for the experiments without any further treatment. Synthesis and characterization is described in details in the literature [110–112].

## 4.2 Synthesis of polysuccinimide

Polysuccinimide (PSI) was synthesized by the thermal poly-condensation of L-aspartic acid (**Figure 11**). 20 g L-aspartic acid and 20 g crystalline phosphoric acid was mixed in a 1 L pear shaped glass flask. The mixture was heated up to 180 $^{o}$C under vacuum (4 mBar) using an IKA RV10 digital rotary evaporator (130 rpm) with thermal

feedback and vacuum generator. After the 7 hours long reaction polysuccinimide had a light brown foam-like structure. This product was dissolved in 175 mL dimethylformamide (DMF) while its color changed to dark brown. To remove the unreacted chemicals several washing steps were applied. The PSI solution was dripped into 2 L distilled water and after 10 min of stirring the product was filtered on a G3 type glass filter and washed 3-4 times with distilled water until the pH of the supernatant became neutral. Then PSI was carefully dried at 40 °C for 2 days in an oven [6]. The final product was a white powder (**Figure 12**).

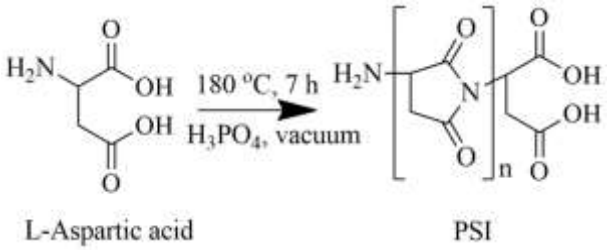


*Figure 11. Synthesis of polysuccinimide*

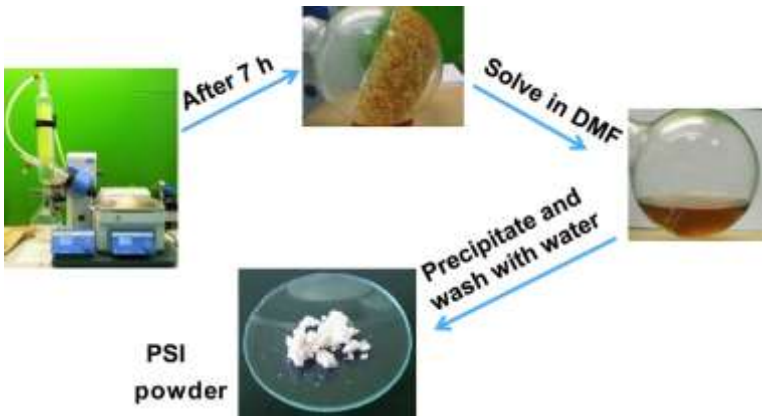


*Figure 12 Different steps in the synthesis of polysuccinimide*

## 4.3 Viscosity of polymer solutions

In electrospinning the viscosity of the solution is a critical parameter that depends on several solution parameters, such as polymer concentration and solvent. The dynamic viscosity of solutions was measured by a vibrational viscometer (Sine-wave Vibro Viscometers (SV-10), A&D Company, Limited, Japan) with a custom made cuvette (inner size 50 x 10 x 36 mm) filled with 13 mL solution (0.625-5 w/w%) for each measurement.

## 4.4 Molecular weight of PSI

Molecular weight of PSI was determined by viscometry using the Kuhn-Mark—Houwink (KMH) equation [113]. PSI was dissolved in 0.1 M LiCl / DMSO at 24 °C [114]. The concentration of the polymer in the solution was varied between 0.625 - 5 w/w%. The Sine-wave Vibro Viscometers provides the dynamic viscosity, $\eta(c_P)$ of the polymer solution at different concentrations, $c_P$. The viscosity of the 0.1 M LiCl / DMSO solution ($\eta_o$) was also measured. The relative viscosity ($\eta_{rel}$) is given by equation 3:

$$\boldsymbol{\eta_{rel} = \frac{\eta}{\eta_0}} \quad \textbf{(3)}$$

From the relative viscosity the specific viscosity ($\eta_{sp}$) can be obtained by equation 4:

$$\boldsymbol{\eta_{sp} = \eta_{rel} - 1} \quad \textbf{(4)}$$

Then, the reduced viscosity ($\eta_{red}$) is calculated by equation 5:

$$\boldsymbol{\eta_{red} = \frac{\eta_{sp}}{c}} \quad \textbf{(5)}$$

From these data the intrinsic viscosity $[\eta]$ was determined by the standard extrapolation method (equation 6):

$$\boldsymbol{[\eta] = \lim_{c \to 0} \left(\frac{\eta_{sp}}{c}\right)} \quad \textbf{(6)}$$

From the intrinsic viscosity data, the polymer molecular mass can be determined by the Kuhn-Mark-Houwink equation:

$$\boldsymbol{[\eta] = K_\eta M^{a_\eta}.} \quad \textbf{(7)}$$

For the calculation the constants of KMH equation was taken from the literature: $K_\eta = 1.32 \cdot 10^{-2}$ and $a_\eta = 0.76$ for PSI [114].

## 4.5 Grafting PSI with cysteamine

The succinimide repeating units of PSI react with primary amines at room temperature without any catalyst. Consequently, PSI chains can be cross-linked by using bi- or multifunctional amines. PSI was grafted with cysteamine (CYSE), which has both amine and thiol functional groups as shown on **Figure 13**.

DOI:10.14753/SE.2018.2178

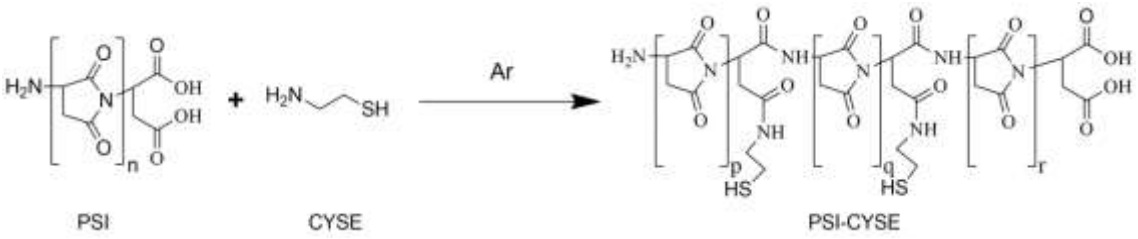


*Figure 13 Grafting polysuccinimide with cysteamine*

In a glass reactor 0.04 g CYSE was dissolved in 1.1 g DMF. Since in the presence of oxygen the thiol groups of cysteamine can react with each other (forming disulfide bonds), the reaction was performed under nitrogen or argon atmosphere. 2 g 25 w/w% PSI-DMF solution was added to the reaction mixture and was stirred for an hour. The molar ratio of succinimide monomer units to moles of cysteamine was 10, which means that - on average – every $10^{th}$ of the PSI monomer units react with cysteamine respectively. And thus in this case the grafting number (GF) is 10, which is the ratio of the number of repeating units to the number of modifier. The mixture was diluted with DMF in order to have a polymer concentration of 10 or 15 w/w%. For the *in vivo* experiments the same procedure was used however the 0.04 g CYSE was dissolved in the mixture of 0.7 g DMSO and 0.4 g DMF.

## 4.6 Electrospinning setups

For the preparation of fibrous membranes a home-made electrospinning instrument was used based on **Figure 5a**. The polymer solutions were filled into a glass syringe (Fortuna Optima 7.140-33) with a metal Hamilton tip (blunt and G21) and placed into a syringe pump (KD Scientific KDS100). The positive electrode was attached to the metal tip whereas the negative electrode (ground) was attached to the collector, made of tinfoil in front of the needle in a well determined distance of 15 cm (**Figure 14**). The voltage applied between 6 and 20 kV was provided by a DC power supply (GENVOLT 73030P).

DOI:10.14753/SE.2018.2178

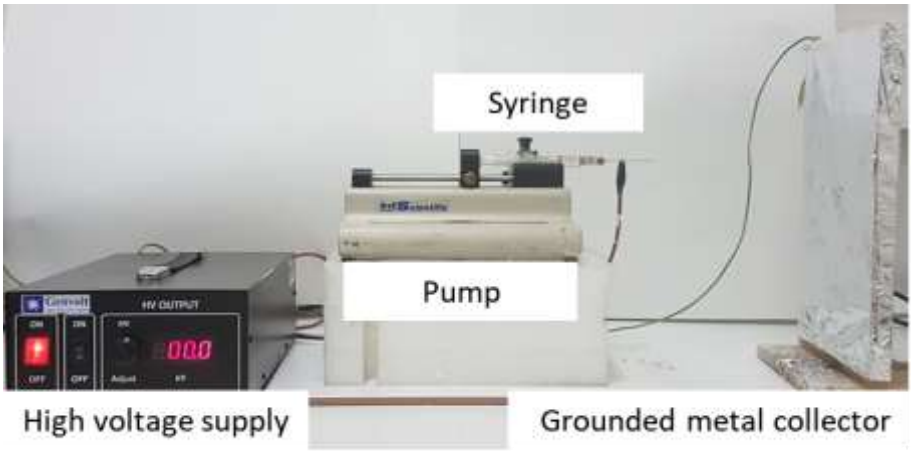


*Figure 14 Setup of electrospinning machine*

The preparation of gelfibers via coaxial reactive electrospinning was carried out under the supervision of Dr. Seema Agarwal, at the Laboratory of Macromolecular Chemistry II, University of Bayreuth, Bayreuth, Germany on a completely custom made electrospinning machine. In coaxial electrospinning, a special needle-in-needle is used where a core solution and a shell solution can be pumped separately and they only meet at the tip of the nozzle. For this technique a home-made nozzle (inner and outer diameter of 0.3 and 1.2 mm, respectively) was used as it can be seen in the **Figure 15a and b**.

Details of samples and processing parameters are presented in the corresponding sections.

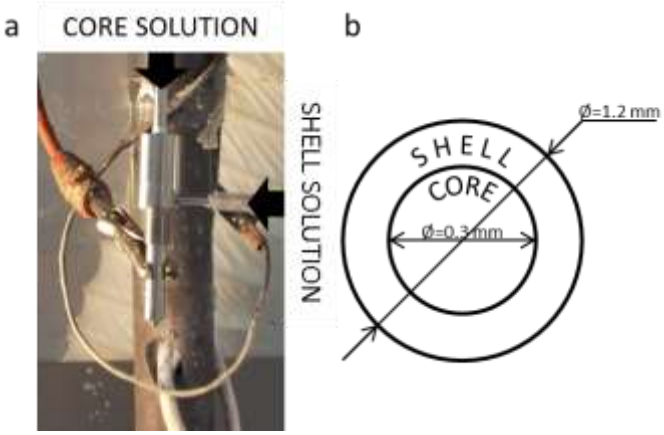


*Figure 15 Coaxial needle used for coaxial reactive electrospinning (a) and schematic of front view of the needle (b)*

### 4.6.1 Preparation of electrospun PSI fibers

Although several trials for the electrospinning of PSI were conducted, only a few relevant will be presented in my thesis. **Table 1** summarizes the technical details of the applied experimental and ambient parameters including the viscosity, the concentration of the polymer solution as well as the humidity of the surrounding air.

*Table 1 Technical parameters of electrospinning of PSI fibers*

| ***Sample*** | ***Concentration w/w% PSI*** | ***Flow rate mL/h*** | ***Voltage kV*** | ***Distance cm*** | ***Humidity %*** | ***Viscosity Pa*s (25 °C)*** |
|---|---|---|---|---|---|---|
| ***PSIsp1*** | *15* | *0.8* | *8* | *15* | *20* | |
| ***PSIsp2*** | *17.5* | *0.8* | *8* | *15* | *20* | |
| ***PSIsp3*** | *20* | *0.8* | *8* | *15* | *20* | |
| ***PSIsp4*** | *22.5* | *0.8* | *8* | *15* | *20* | |
| ***PSIsp5*** | *25* | *0.4* | *8* | *10* | *20* | *1.8* |
| ***PSIsp6*** | *25* | *0.4* | *8* | *15* | *20* | *1.8* |
| ***PSIsp7*** | *25* | *0.4* | *8* | *20* | *20* | *1.8* |
| ***PSIsp8*** | *25* | *0.8* | *8* | *5* | *20* | *1.8* |
| ***PSIsp9*** | *25* | *0.8* | *8* | *10* | *20* | *1.8* |
| ***PSIsp10*** | *25* | *0.8* | *8* | *15* | *20* | *1.8* |
| ***PSIsp11*** | *25* | *0.8* | *8* | *20* | *20* | *1.8* |

### 4.6.2 Polysuccinimide cross-linked by DAB post electrospinning

If suitable chemistry is available, electrospun fibers can be cross-linked by post spinning methods (after electrospinning) as it was described in **Section 2.3.1**. In order to investigate the possibility of cross-linking PSI fibers with DAB, 1 x 1 cm square samples were cut from sample PSIsp10 and placed into 0.5 M DAB/EtOH solution for different time intervals (1 min, 5 min, 10 min, 20 min, 30 min, 60 min, 120 min, 180 min, 1 day) at room temperature. After the supposed reaction (**Figure 16**), samples were washed thoroughly in DMF and dried carefully on microscope cover glasses and investigated by AFM and SEM.

DOI:10.14753/SE.2018.2178

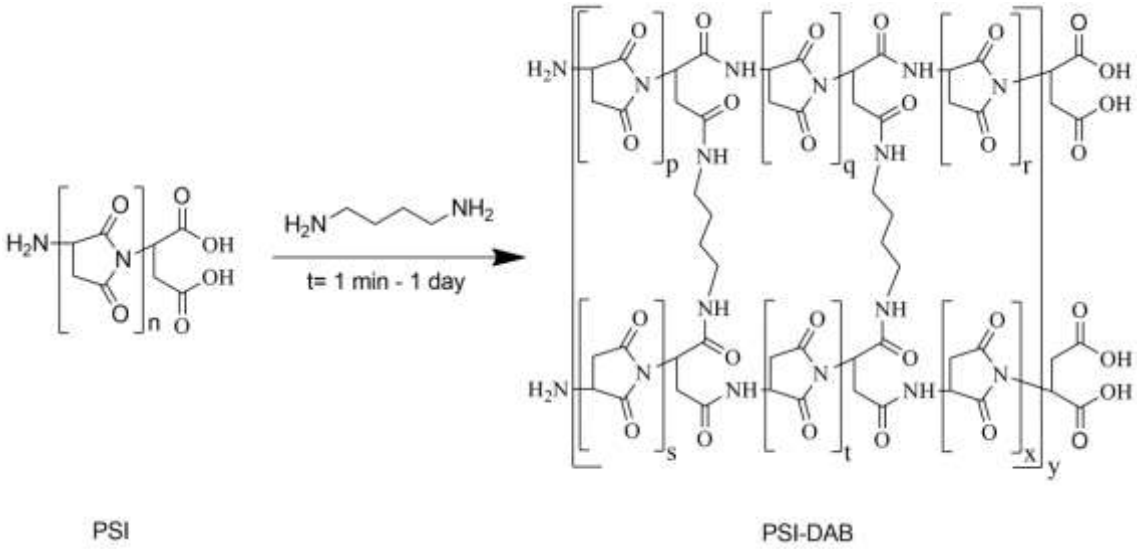


*Figure 16 Chemical reaction of cross-linking PSI with 1,4-diaminobuthane*

### 4.6.3 Reactive electrospinning of PSI-CYSE

Reactive electrospinning is a special class of electrospinning technique where chemical reaction takes place during the fiber formation as it was mentioned in **Section 2.3.1**. In order to induce cross-linking reaction during electrospinning process PSI was primarily modified with cysteamine (PSI-CYSE). The thiol groups on the side chains can react with each other in the presence of oxygen creating disulfide bonds between the PSI chains as shown on **Figure 17**. This reaction takes place during the electrospinning process, thus the resulting fibers are composed of a cross-linked polymer matrix. The disulfide bridges provide cross-links between the polymer chains (PSI-CYS). Electrospinning of PSI-CYS was carried out with a 0.4 mL/h flow rate, 10 kV applied voltage at 15 cm distance whereas humidity was 20% and the solutions viscosity after synthesis was 84 mPas.

DOI:10.14753/SE.2018.2178

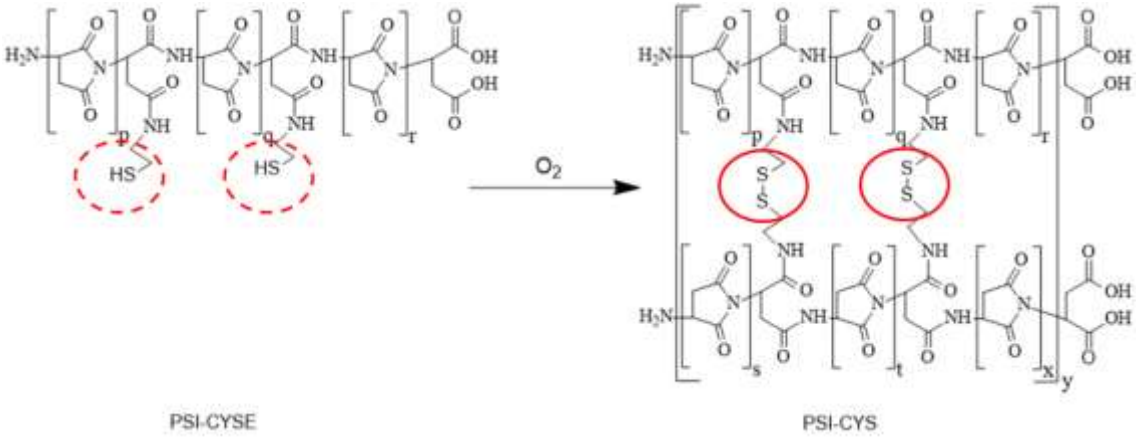


*Figure 17 Cross-linking reaction of cysteamine modified PSI in air*

The reaction mixture of PSI and CYSE was electrospun after different reaction times and samples were collected for investigation by light microscopy to investigate how the reaction time in the synthesis of PSI-CYSE affects electrospinning and fiber morphology. Since there is no difference whether the reaction takes place in the reactor or in the syringe after homogenization, instead of preparing several reactions for different reaction times, one solution was prepared and electrospun continuously. For this PSI and CYSE was homogenized for 10 minutes in nitrogenous atmosphere than poured into a syringe and electrospun. Samples were collected during electrospinning at 0, 20, 40 and 70 minutes which represented 10, 30, 50, and 80 minutes of reaction times respectively.

### 4.6.4 Electrospinning of magnetite doped PSI (PSI-OAMagn) and PSI-CYS fibers (PSI-CYS-OAMagn)

For the preparation of magnetite containing PSI fibers, the surface modified magnetite particles were directly dispersed into the PSI (25 w/w% PSI/DMF) solution in different concentrations prior to electrospinning. These samples are denoted as PSI-OAMagn-x where x refers to the number of the sample in the series. In all cases the distance between the collector and the needle was set to 15 cm. Samples and processing parameters are listed in **Table 2**.

*Table 2 Technical parameters of electrospinning of PSI-OAMagn.*

| *Sample* | *Magnetite concentration, w/w%* | *Flow rate, ml/h* | *Voltage, kV* |
|---|---|---|---|
| ***PSI-OAMagn 1*** | *2.5* | *0.4* | *6* |
| ***PSI-OAMagn 2*** | *5* | *1.2* | *8-7* |
| ***PSI-OAMagn 3*** | *10* | *1.2* | *8-8.5* |

Cross-linked samples were prepared by mixing different amounts of magnetite into the cysteamine grafted PSI solution (PSI-CYSE) right after the polymer modification, stirred further for 5 minutes and then this mixture was electrospun. All the ratios and processing parameters can be found in **Table 3**.

*Table 3 Technical parameters of reactive electrospinning of PSI-CYS-OAMagn*

| *Sample* | *PSI, w/w% / Grafting number* | *Magnetite concentration, w/w%* | *Flow rate, ml/h* | *Voltage, kV* |
|---|---|---|---|---|
| ***PSI-CYS-OAMagn 1*** | *15/10* | *2* | *-* | *-* |
| ***PSI-CYS-OAMagn 2*** | *15/10* | *4.6* | *-* | *-* |
| ***PSI-CYS-OAMagn 3*** | *15/15* | *2* | *1.2* | *8* |
| ***PSI-CYS-OAMagn 4*** | *15/15* | *4* | *1.2* | *10* |
| ***PSI-CYS-OAMagn 5*** | *15/15* | *5* | *1.2* | *6.5-7* |

### 4.6.5 PSI-CYS fibers cross-linked with DAB (PSI-CYS-DAB)

Double cross-linked (two different cross-linkers in one system) PSI based membranes were prepared by immersing PSI-CYS electrospun fibrous membranes into 0.5 M DAB/EtOH solution. In the first step disks (diameter: 16 mm) were cut from PSI-CYS then immersed into the DAB solution for 3 hours. The chemical reaction can be seen on **Figure 18**. After cross-linking all the samples were washed thoroughly with ultrapure water and separated into different vials for further treatments (described later): hydrolysis (described in **Section 4.7.1**) and cleavage of disulfide bonds (described in **Section 4.7.3**).

DOI:10.14753/SE.2018.2178

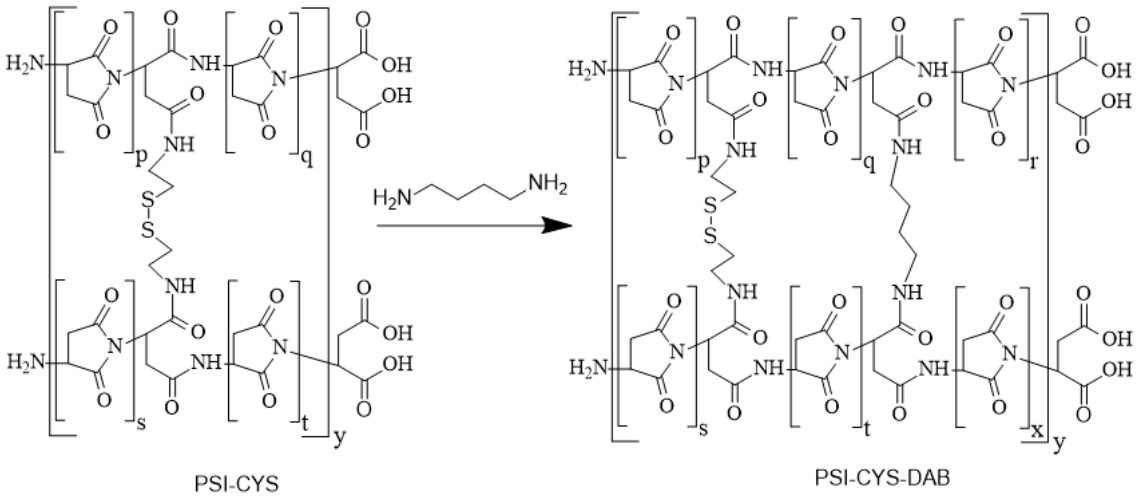


*Figure 18 Crosslinking of PSI-CYS with 1,4-diaminobuthane*

### 4.6.6 Coaxial electrospinning of PSI and THD

As a pre-test to see, whether THD can cross-link PSI, 0.5 M THD/DMF solution was mixed with 25 w/w% PSI/DMF solution, in the ration of PSI-THD2 in a glass vial (**Table 4**). For coaxial electrospinning a coaxial nozzle (details can be found in **Section 4.6, Figure 15**) was utilized where the cross-linker (THD) solution and polymer solution (PSI) were fed in the core and shell, respectively (**Figure 19a**). The reaction between PSI and THD at room temperature is shown on **Figure 19b**. The parameters for coaxial electrospinning are listed in **Table 4**. Solubility test in DMF was applied to check the cross-linking of the fibrous samples.

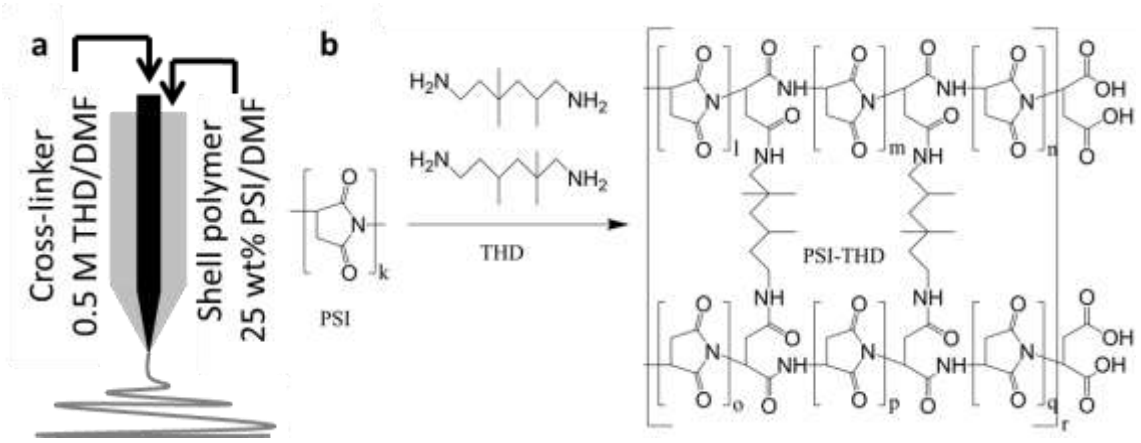


*Figure 19 Schematic of the co-axial setup in our experiments (a), and the preparation of PSI gels by crosslinking with THD (b)*

*Table 4. Conducted experiments with co-axial electrospinning setup.*

| ***Sample name*** | ***Voltage (kV)*** | ***Target distance (cm)*** | ***Feeding rate (ml/h) Core/Shell*** | ***Cross-links*** | ***Comment*** |
|---|---|---|---|---|---|
| ***Shell: 25 w/w% PSI/DMF; Core: -*** | | | | | |
| ***PSI*** | *16* | *18* | *0 / 2* | *No* | *Smooth fibers* |
| ***Shell: 25 w/w% PSI/DMF; Core: 0.5 M THD/DMF*** | | | | | |
| ***PSI-THD1*** | *19* | *18* | *0.12 / 2* | *No* | *Smooth fibers* |
| ***PSI-THD2*** | *19* | *18* | *0.37 / 2* | *Yes* | *Beads and fibers* |
| ***PSI-THD3*** | *19* | *18* | *0.74 / 2* | *Yes* | *Alternating spinning and spraying* |
| ***Shell: 25 w/w% PSI/DMF; Core: 0.5 M THD/DMF + 2 w/w% PEO*** | | | | | |
| ***PSI-THD-PEO*** | *19* | *18* | *0.37 / 2* | *Yes* | *Smooth fibers* |

## 4.7 Preparation of PASP based fibrous networks and their pH responsivity

### 4.7.1 Hydrolysis of electrospun PSI based fibrous networks

Poly(aspartic acid) based nanofibers were prepared by the mild alkaline hydrolysis of the PSI based fibers in imidazole based buffer solution of pH 8 (I=250mM). The chemical reaction of PSI turning into poly(aspartic acid) (PASP) can be seen on **Figure 20**. In order to ensure 100 % conversion, samples were kept in the buffer for 24 hours [53]. After the hydrolysis, samples were washed with ultrapure water to get rid of unnecessary salts and either used in their swollen state in further experiments (pH responsivity) or freeze-dried for SEM and ATR-FTIR. PASP based networks are denoted by changing the PSI part in the original sample name to PASP. For example PSI-CYS after hydrolysis is denoted as PASP-CYS etc.

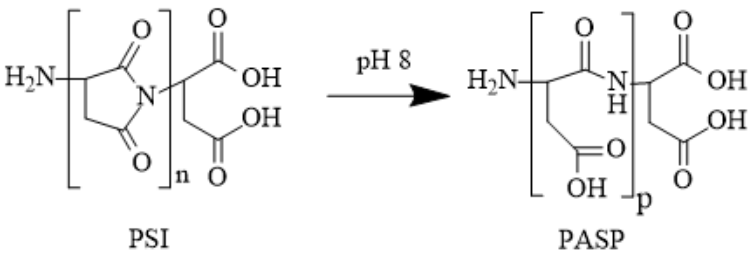


*Figure 20 Hydrolysis of polysuccinimide in pH 8 results in poly(aspartic acid)*

### 4.7.2 Preparation of PASP-DAB samples

For the preparation of PASP-DAB samples first PSI-DAB samples were prepared as described in **Section 4.6.2** then treated in 2 separate groups as summarized on **Figure 21**:

a) Route A: Washing with ultrapure water → pH 8 (hydrolysis for 1 day) → washing with ultrapure water thoroughly => PASP-DAB (**Figure 21** route a, red);
b) Route B: Washing with DMF → pH 8 (hydrolysis for 1 day) → washing with ultrapure water thoroughly => PASP-DAB (**Figure 21** route b, blue);

Obtained samples were dried carefully on microscope cover glasses and investigated by AFM (details explained **Section 4.9.2**).

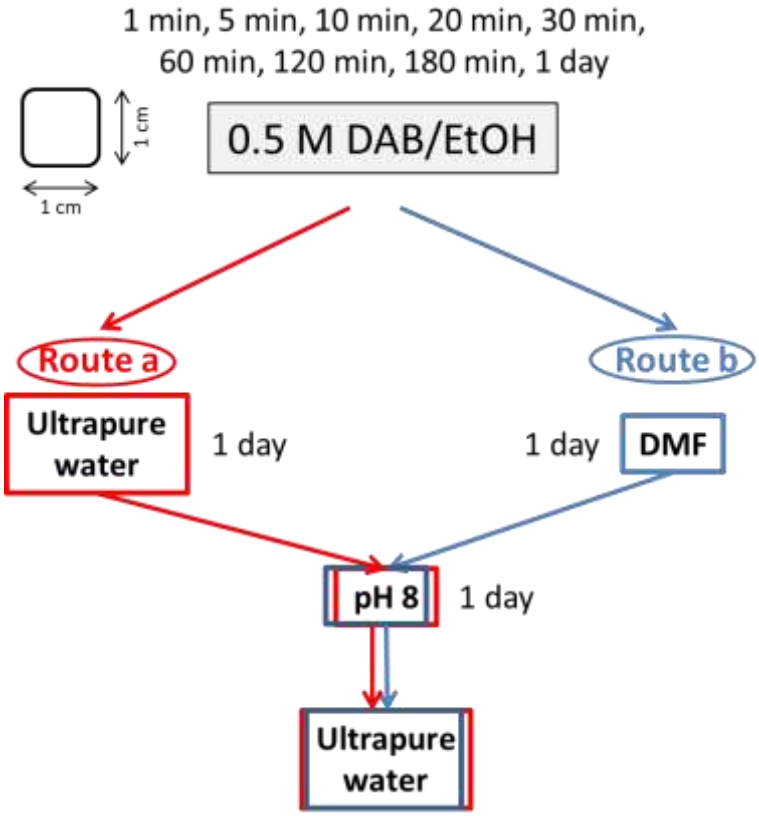


*Figure 21 Schematic reaction routes of cross-linking of PSI based fibrous networks by immersion into DAB solution for different times and further treatments*

### 4.7.3 Cleavage of disulfide bond in PASP-CYS-DAB

Disulfide bonds can be cleaved in a red-ox reaction by for example D,L-dithiotreitol (DTT) [53]. Reaction for the cleavage of disulfide bonds in PASP-

CYS-DAB can be seen on **Figure 22**. In the reaction thiol side-chains are obtained on the polymer backbone which is denoted as PASP-CYSE-DAB. For the reaction 0.1 M DTT/pH 8 imidazole buffer solution was used.

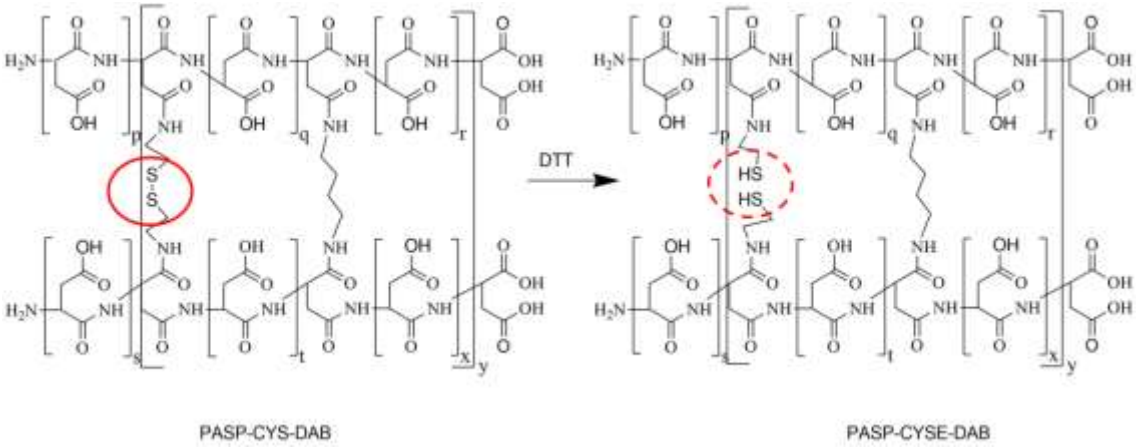


*Figure 22 Chemical reaction of cleavage of disulfide bonds in PASP-CYS-DAB*

### 4.7.4 Preparation of PASP-THD samples by immersion of PSI membranes into THD solutions then hydrolysis

For cross-linking the PSI membrane after electrospinning with THD, first 1 x 1 cm square samples were cut from PSIsp10 then one set of samples were immersed into 0.5 M THD/EtOH solution for 5, 10, 30 and 60 minutes while the other into pure THD for 1, 2 and 3 hours respectively. Chemical reaction between PSI and THD can be seen on **Figure 19b**. After cross-linking samples were transformed into PASP basis by immersing them into pH 9 buffer solution. After treatment samples were washed with ultrapure water and freeze-dried for SEM investigations.

### 4.7.5 pH responsivity of PASP-DAB

To investigate the pH responsivity of DAB cross-linked PASP fibrous membranes first PSIsp10 disk (diameters of: 16, 25 and 50 mm) were cut out and immersed in 0.5 M DAB/EtOH solution for 10 minutes. After thorough washing with ultrapure water 3 parallel samples from each size were chosen and placed into separate vials of pH 8 buffer solution. After the hydrolysis the size of the samples were measured by a caliper inside the buffer then the solution was changed to pH 3. Samples were left in each buffer for 1 day to reach equilibrium then their size was measured with a caliper again. In four cycles sample sizes were measured 4 times in pH 3 and 4 times in pH 8

(Dry → DAB/EtOH → pH 8 → pH 3 → pH 8 → pH 3 → etc.) (**Figure 23**). For the pH sensitivity measurements pH 8 and pH 3 imidazole buffers were used. Average of sizes was calculated with standard error (confidence of 95%) using standard procedure. For calculating the relative swelling degrees ($Q_{rel}$ See **Section 2.2**) of membrane disks first the area of disks were calculated from the average diameters in different pHs, than they were all divided by the first average area in pH 8. In the calculations the area of disks were used based on the assumption that the diameter of the disks did not change significantly during swelling. Thus $Q_{rel}$ is 1 in pH 8 if the size of the disk is the same in pH 8 throughout the four cycles.


*Figure 23 Schematic of pH responsivity test of PASP-DAB*

### 4.7.6 pH responsivity of PASP-THD-PEO

To determine the pH responsivity of PASP-THD-PEO, fiber membranes (1.5 × 2 cm square) were placed into standard alkaline (pH 9) and acidic (pH 4) borax buffer solutions. The diameter change of the wet nanofiber membranes were determined with a caliper consecutively after incubation of the membrane in pH 4 and pH 9 buffers for 1 day. These pH 4 and pH 9 cycles were repeated 3 more times (**Figure 24**). The average size of membranes was calculated from surfaces of three parallel samples. Ionic strength of buffers used in these experiments was kept constant (I = 0.15) by the addition of potassium chloride (KCl) to exclude volume change caused by ionic strength.

DOI:10.14753/SE.2018.2178

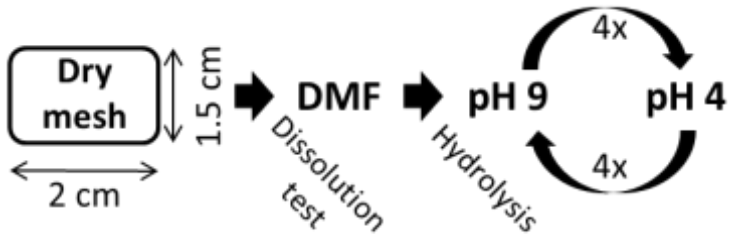


*Figure 24 Schemeof pH responsivity test of PASP-THD-PEO*

## 4.8 Chemical analysis

### 4.8.1 Attenuated Total Reflectance Fourier Transform Infrared Spectroscopy (ATR-FTIR)

To confirm the chemical structure of PSI and its derivative's after modification Attenuated Total Reflectance Fourier Transform Infrared (ATR-FTIR) spectroscopy measurements were carried out with a Brucker IFS 55 instrument with a Deuterated triglycine sulfate detector (DTGS) and a diamond ATR head (PIKE technology). All infrared spectra were collected over the range of 4000 – 550 $cm^{-1}$ at a resolution of 0.5 $cm^{-1}$ and the number of scans was accumulated at 128. The background spectra were measured on clean and dry diamond crystal.

In coaxial electrospinning ATR-FTIR measurements were carried out using an Excalibur FT-IR-Spektrometer (Digilab) instrument with diamond ATR head (PIK Miracle). All spectra were collected over the range 550–4000 $cm^{-1}$ at a resolution of 0.5 $cm^{-1}$. The background spectra were measured on clean and dry diamond crystal. A DTGS detector was used, and the number of scans accumulated was 128. Electrospun dried PSI, PSI-THD2, PSI-THD-PEO and PASP-THD-PEO membranes were measured after the electrospinning procedure.

### 4.8.2 Nuclear Magnetic Resonance (NMR)

All NMR spectra were obtained using a JEOL SC400 spectrometer (JEOL Ltd., USA) operating at 400 MHz for the $^{1}H$ nucleus. Sample solutions were prepared by dissolving 15 mg of PSI fibers in 0.6 mL of DMSO-d6 in 5 mm NMR tubes. All spectra were recorded at 23.5 ± 0.5 °C and tetramethylsilane (TMS) was used as the internal

standard. The pulse angle was 45º, 2 sec delay was used with 8 spectral widths, 16 K data points and 16 scans were done in every measurement.

### 4.8.3 Thermal gravimetric analysis (TGA) and differential thermal analysis (DTA)

Thermal gravimetric analysis measurements were performed to study the thermal stability of the fibrous polymer samples. TGA and DTA curves were recorded with Derivatograph-C System (MOM, Hungary) under dynamic air-flow at a heating rate of 6 °C $min^{-1}$ on crushed bulk specimens from room temperature to 1000-1500 °C.

For investigating the effect of dry heat sterilization on fibrous PSI and PSI-CYS, small samples were heated up in a Q500 (TA Instruments) at maximum heating rate to 160 °C and kept at that temperature for 2 hours.

## 4.9 Microscopy

Different microscopic techniques were used in order to ensure the presence of fibers in samples and to characterize the fiber morphology and the average fiber diameter in samples. In every case average fiber diameters were determined from the diameter of 50 individual fibers at least. Each case standard error was calculated assuming that fiber diameter had normal distribution.

### 4.9.1 Light microscopy

In order to determine the diameter of the dry polymer fibers and their surface characteristics a HUND-WETZLAR H500 light microscope with a Sony Hyper HAD CCD-IRIS/RGB Color Video Camera was used. Samples were gathered on microscope slides by holding them in front of the electrospinning jet for 1 second. For the diameter measurements Scope Photo software was used. Every diameter distribution was made from 50 fibers.

For following the dissolution of electrospun PSI and hydrolysis of electrospun PSI-CYS 1 x 1 cm square samples were cut out and placed into pH 8 imidazole buffer solution under an ALPHA STO-3 microscope. Photos were taken every hour by ScopeTek DCM 130 till complete dissolution or conversion.

DOI:10.14753/SE.2018.2178

### 4.9.2 Atomic Force Microscope (AFM)

The diameter and surface properties of the polymer fibers were imaged with Molecular Force Probe 3D (MFP3D) and a Cypher Atomic Force Microscope Instrument (Asylum Research, Santa Barbara, CA, USA). In the case of MFP3D an OlympusIX81 invert microscope was used to fix the target under the AFM tip and oscillation mode was used during the measurements. The sample preparation and the experimental setup was the same as it was described in the Light microscopy (**Section 4.9.1**), except for the AFM measurement a special glue to fix the polymer fibers to a microscope slide was used to avoid fiber removal during the interaction between the AFM needle and the fibers. The dried polymer fibers were measured in air at oscillation mode with resonance frequencies of about 0.2-1 Hz and 0.3-0.5 V target value. For the topography pictures 512 x 512 pixel magnification was used. The axial height distribution along the PSI and PSI-CYS samples was obtained by manually tracking and then the size distribution was plotted using IgorPro 6 software (Wavemetrics, Lake Oswego, OR). Every diameter distribution was made from 75 fibers.

For the AFM imaging of PASP-CYS bulk membrane, a small sample was placed on a microscope coverslip. To fix the sample onto the surface of the slide, a drop of water was placed on it than slowly evaporated in an oven at 45 $^{0}$C.

For the measurement of all the other samples a Cypher AFM (Asylum Research, Santa Barbara, CA, USA) was used with an IgorPro 6 software. All set parameters were the same as previously described for MFP3D.

### 4.9.3 Scanning Electron Microscope (SEM)

For SEM studies samples were treated different ways depending on their origin:

- PSI based membranes: a small part of the membrane was cut out and placed on conductive tape for coating and microscopy;
- PASP based membranes: samples were washed thoroughly with ultrapure water and freeze-dried, then a small portion was placed on conductive tape for coating and microscopy
- Samples from *in vivo* experiment: a small portion of membranes extracted from *in vivo* measurement was washed in an excessive amount of 100 mM Na-cacodylate pH 7.2 solution, then stored in 1 V/V% glutaraldehyde solution in 100 mM Na- cacodylate pH 7.2. For drying, samples were placed for 5 mins in a series of ethanol solution: 20, 50, 70, 85, 96 V/V% (diluted with water) than 1:1 ethanol (96 V/V%) and acetone mixture, finally in pure acetone placed in a porous container. In a slow process acetone was replaced with supercritical $CO_2$ and slowly heated till complete evaporation. The dry samples then were placed on conductive tape for coating and microscopy.

Micrographs were taken using a ZEISS EVO 40 XVP scanning electron microscope equipped with an Oxford INCA X-ray spectrometer (EDS). The accelerating voltage of 20 kV was applied. Samples were fixed on a special conductive sticker with tweezers. For the measurements samples were sputter coated with gold in 20-30 nm thickness with a 2SPI Sputter Coating System.

In the case of coaxial electrospinning small fragments of all 5 samples in **Table 4** were mounted on a standard sample holder by conductive adhesion graphite-pad (Plano) and examined with a Zeiss LEO 1530 (FE-SEM with Schottky-field-emission cathode; in-lens detector, SE2 detector or Back Scattered Detector) using an accelerating voltage of 2 kV. The samples were sputtered with platinum (1.3 - 2 nm using a Cressington HR208 sputter coater and a Cressington mtm20 thickness controller). For calculating the average fiber diameter 50 fibers of each sample were measured using ImageJ software.

DOI:10.14753/SE.2018.2178

### 4.9.4 Multiphoton microscopy

Multiphoton microscopy enables the in-depth investigation of samples (similarly to confocal microscopy) which have either auto fluorescent properties or have been labeled with fluorescent dyes prior to the investigation. For the examination of PSI and PASP based membranes a two photon microscope (Femto2d, Femtonics, Hungary) with a Spectra Physics Deep See laser was used at 800 nm wavelength to induce the auto fluorescence of PSI and PASP [53]. The emitted photons were detected parallel in the green and red channels. Images were taken with 10x objective by the MES4.4v program.

## 4.10 In Vivo biocompatibility and biodegradability of PSI-CYS and PSI-DAB fibrous membranes

### 4.10.1 Reinforcement of membranes for implantation

Since a single layer of an electrospun membrane cannot withstand standard procedures in surgery (handling, suturing) samples were reinforced by folding them into ~4 x 4 cm squares (6-8 layers) and pressed with a GS25011 Atlas Manual 25T Hydraulic Press (generally used in the preparation of KBr pastilles for IR) (**Figure 25a**). To ensure that the pressure is evenly distributed on the whole surface of the samples without damaging them a sandwich of wooden pressure plates, paper and alumina foil layers and the sample was used (**Figure 25b**). In every case a pressure equal to roughly 5 tons was applied.

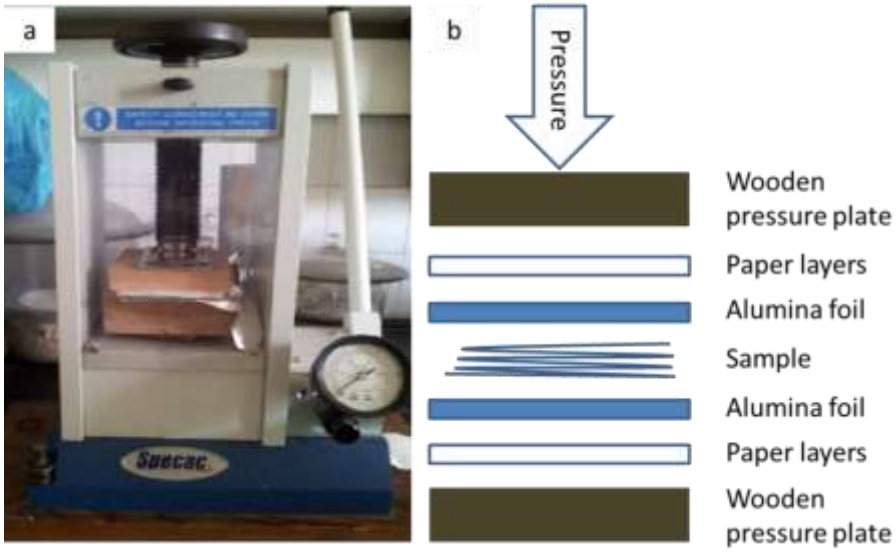


*Figure 25 Hydraulic press used for pressing the samples (a) and schematic of the applied pressure sandwich (b)*

### 4.10.2 Preparation and sterilization of PSI-CYS and PSI-DAB samples

For the *in vivo* evaluation standard PSI-CYS samples were electrospun from 1 mL solution each case, then folded and pressed as described in **Section 4.10.1**. Prior to implantation disks of an average diameter of 16 mm were cut and sterilized (according to the Guideline for Disinfection and Sterilization in Healthcare Facilities, 2008 [115]) by dry heat sterilization in a Memmert SLP 500 oven at 160 $^{o}$C for 2 hours.

For the preparation of PSI-DAB standard PSIsp10 was electrospun from 1 ml solution then folded and pressed as described in **Section 4.10.1**. For cross-linking samples were stored in 0.5 M DAB/EtOH solution for 3 hours then washed with ultrapure water. After the treatment these samples were stored in ultrapure water, sterilized by adding $ClO_2$ solution and kept in a well-sealed container till surgery [116–118].

### 4.10.3 In vivo animal model

Biocompatibility and biodegradability of electrospun PSI-CYS and PSI-DAB samples were investigated on 24 male Wistar rats (250 g), 12 for each sample type. In each case, prior to implantation, the PSI-CYS and PSI-DAB samples were soaked in sterile physiological saline (0.9%) for 10 minutes, so that hydration would cause them to assume full size. Sedation of animals was performed with a mixture of ketamine and xylazine (~0.8 ml/animal) than samples were implanted in the nuchal region. After a 1-

2 cm long incision along the Nuchal Ligament (**Figure 26a**) the samples were placed and fixed on the paramedian line via a single interrupted suture using Atramat 2-0 Polyglycolic acid absorbable suture material. (**Figure 26b, c**). Skin closure was performed with 3-4 simple interrupted stitches using the same suture material. Post-operatively for both PSI-CYS and PSI-DAB animals were randomly divided into two groups of 6 animals each. Animals were kept in individual cages, and observed daily for evidence of wound complications, such as infection, seroma, abscess, hematoma, or skin dehiscence. The experimental protocol adhered to rules laid down by the Directive of the European Parliament and of the Council on the protection of animals used for scientific purposes and was approved by the Semmelweis University's Institutional Animal Care and Use Committee. The accreditation number of the laboratory is 22.1/1244/3/2011. Termination and sample retrieval was performed after 3 days (Group A) and 7 days (Group B). Samples were then preserved in formaldehyde and sent off for histological evaluation, whereas in the case of PSI-DAB, SEM micrographs were taken from retrieved and freeze-dried samples (Pretreatment of *in vivo* samples for SEM investigation is described in **Section 0**).

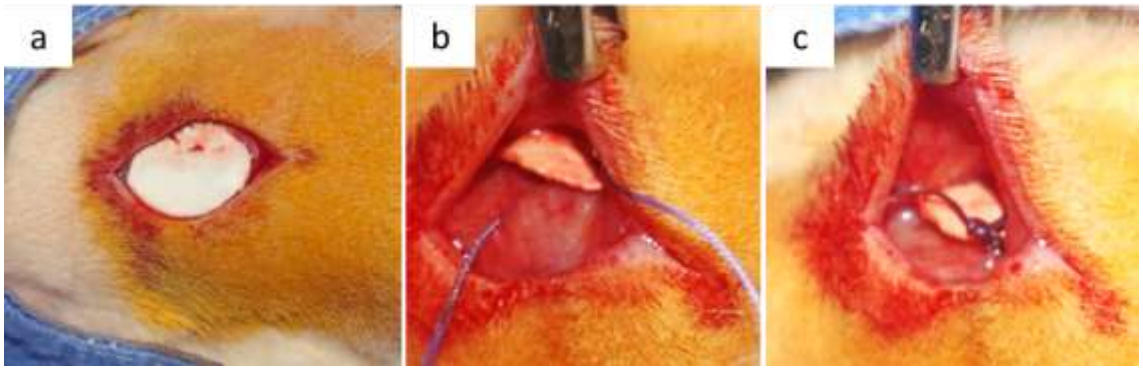


*Figure 26 Incision on the skin and sample in implantation area (a), inserted sample with suture line (b) and implanted sample with suture (c)*

### 4.10.4 Histology and microscopy

Samples were gathered for both PSI-DAB and PSI-CYS at 3 and 7 days after implantation. In general, skin tissue was separated and the samples were cut out around the stitch including the muscle tissue and placed in 4 V/V% formaldehyde solution. After fixation water was eliminated according to a standard protocol in a Leica ASP300 enclosed tissue processor then fixed in paraffin and slices of 4 µm thickness were cut (Leica microtome). After the paraffin was removed slices were stained by standard

DOI:10.14753/SE.2018.2178

hematoxylin-eozin staining protocol. All slides were digitalized with Pannoramic 250 Flash Scanner (3DHISTECH Ltd.). All the above mentioned protocols can be found in the supplementary (**Section 11**).

Small sample of PSI-DAB at 7 days was gathered with a tweezer and investigated by multiphoton microscope without any staining and after freeze-drying with SEM.

DOI:10.14753/SE.2018.2178

# 5 Results

## 5.1 Polysuccinimide

### 5.1.1 Molecular weight of PSI

The molecular weight of the polymer directly influences its properties as well as the electrospinnability, and thus it is a key information and necessary to be determined [119]. The reduced viscosity of a PSI solution as a function of concentration is shown on **Figure 27**. The intercept on the reduced viscosity axis provides the intrinsic viscosity, which was found to be $[\eta] = 32.4 \pm 1.5$ ml/g. On the basis Kuhn-Mark-Houwink equation (**Equation 3**), the viscosity average molecular mass for this batch of PSI was found to be $M_\eta = 28500 \pm 3000$ g/mol. Average molecular masses ranged from 23000 to 31000 g/mol depending on their batch.

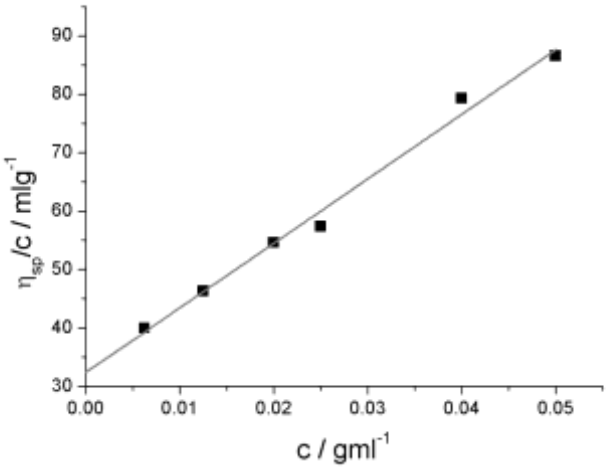


*Figure 27 The reduced viscosity of the PSI solution as a function of polymer concentration*

### 5.1.2 PSI fibers by electrospinning technique

In the first step PSI solution of different concentrations were electrospun (PSIsp1-4 and PSIsp10 in **Table 1**). As it can be seen on **Figure 28,** at lower concentrations than 20 w/w% only electrospraying occurred resulting in PSI particles of different sizes. At 20 w/w% a mixture of fibers and particles, while at 22.5 w/w% fibers with beads were prepared.

DOI:10.14753/SE.2018.2178

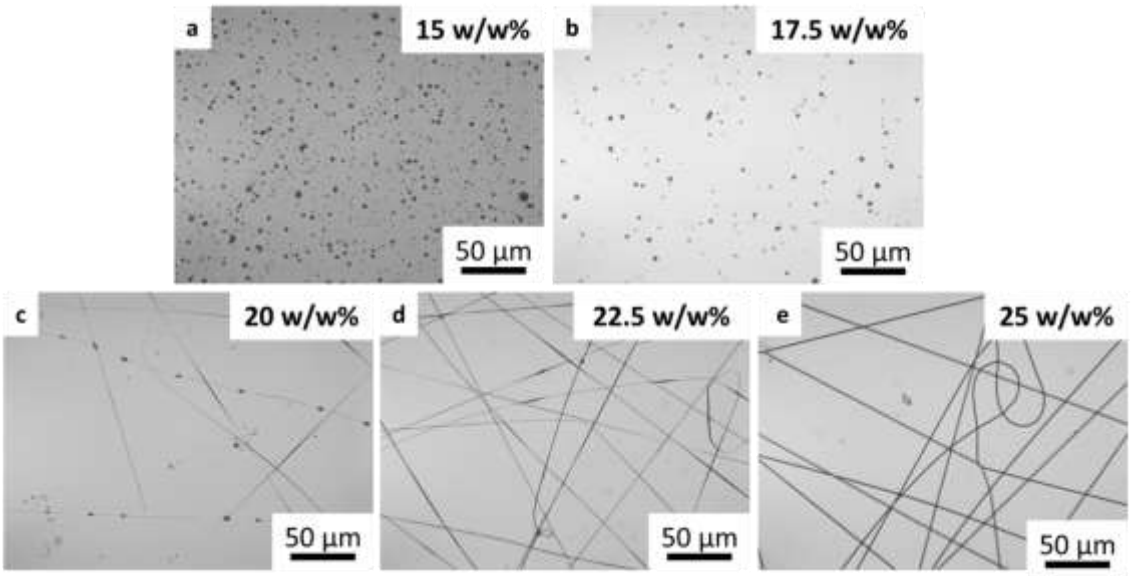


*Figure 28 Light microscopic pictures taken from PSI fibers electrospun from 15 w/w% (a), 17.5 % (b), 20 w/w% (c), 22.5 w/w% (d) and 25 w/w% (e) DMF solutions.*

Electrospinning of PSI from 25 w/w% in DMF solution resulted in a white web of nanofibers. As a typical sample, PSIsp10 fibrous membranes can be seen on **Figure 29a**. Since the electrospinning jet is concentrated at the center of the aluminum collector, the samples were thick in the center and thin at the sides (showing a bell-curve in cross-section). This is represented on **Figure 29a** where the thickness gets smaller to the edge of the membrane and also whiter as more light is transmitted. The distribution of fibers on the collector and the overall average thickness of fiber membrane can be controlled by the collector distance. As it can be seen on **Figure 29b**, where collection of fibers was conducted for 5 minutes under same circumstances (flow rate, polymer concentration, humidity and so on), the size of the membrane increased with the collector distance while the thickness of the membrane reduced. The average fiber diameters for 3 different distances and 2 different volume rates measured by light microscopy are collected in **Table 5**.

DOI:10.14753/SE.2018.2178

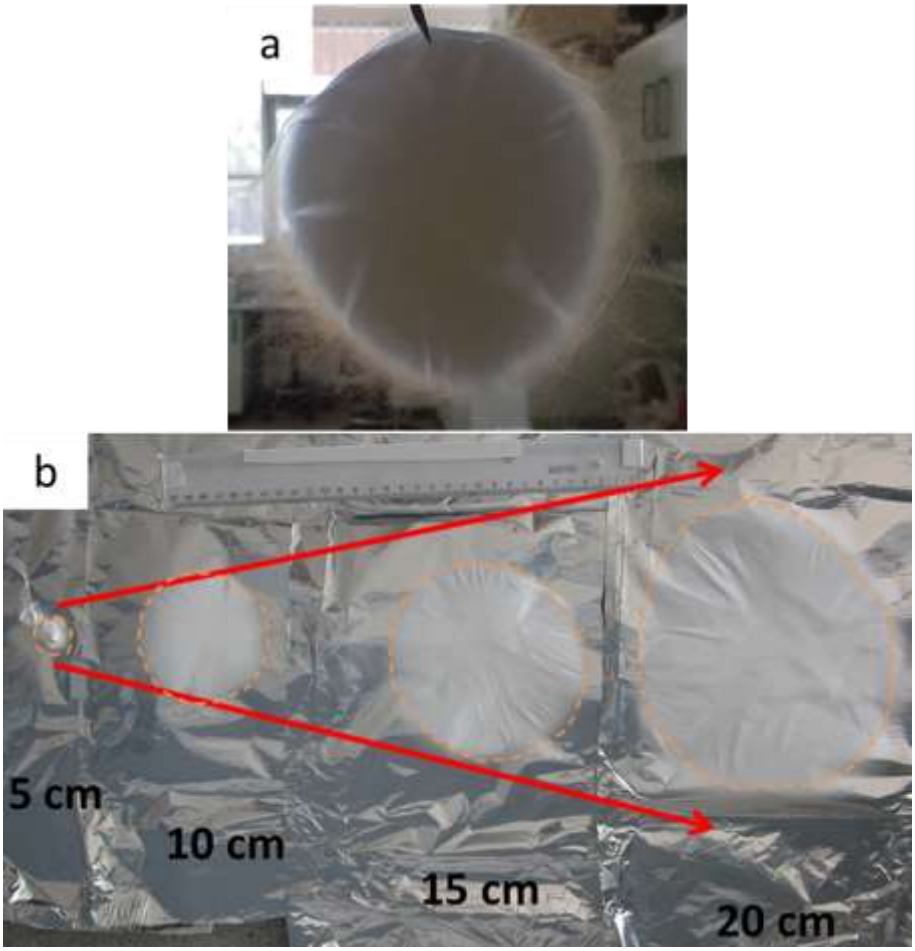


*Figure 29 PSI membrane held with a tweezer (a) and PSI membranes prepared from the same solution with the same parameters except collector distance (b)*

*Table 5 Average fiber diameters of PSI membranes prepared at different collector distances with 2 volume rates*

| Distance | Volume rate 0.4 ml/h Average fiber diameter | Volume rate 0.8 ml/h Average fiber diameter |
|---|---|---|
| **10 cm** | 1.47 ± 0.03 µm | 1.53 ± 0.07 µm |
| **15 cm** | 1.48 ± 0.03 µm | 1.28 ± 0.06 µm |
| **20 cm** | 1.39 ± 0.03 µm | 1.35 ± 0.08 µm |

### 5.1.3 Characterization of electrospun PSI fibers by different microscopic techniques

Light microscopy, AFM and SEM micrographs were taken of PSI fibers to investigate fiber morphology and diameter distribution. Light microscopic pictures shown on **Figure 30** suggest, that the PSIsp10 fibers are uniformly thick without any defects.

DOI:10.14753/SE.2018.2178

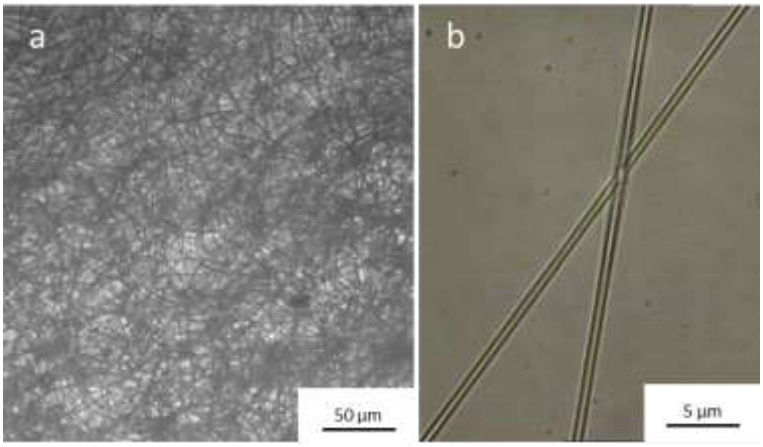


*Figure 30 PSIsp10 fibers seen by light microscope at two magnifications (a, b)*

The average diameter of the PSI fibers was found to be 500 ± 60 nm (**Figure 31a**). It is worth mentioning that along the axis of fibers the diameter was constant. This was supported by several AFM investigations. **Figure 31c** shows a representative fiber from the same sample studied by atomic force microscopy.

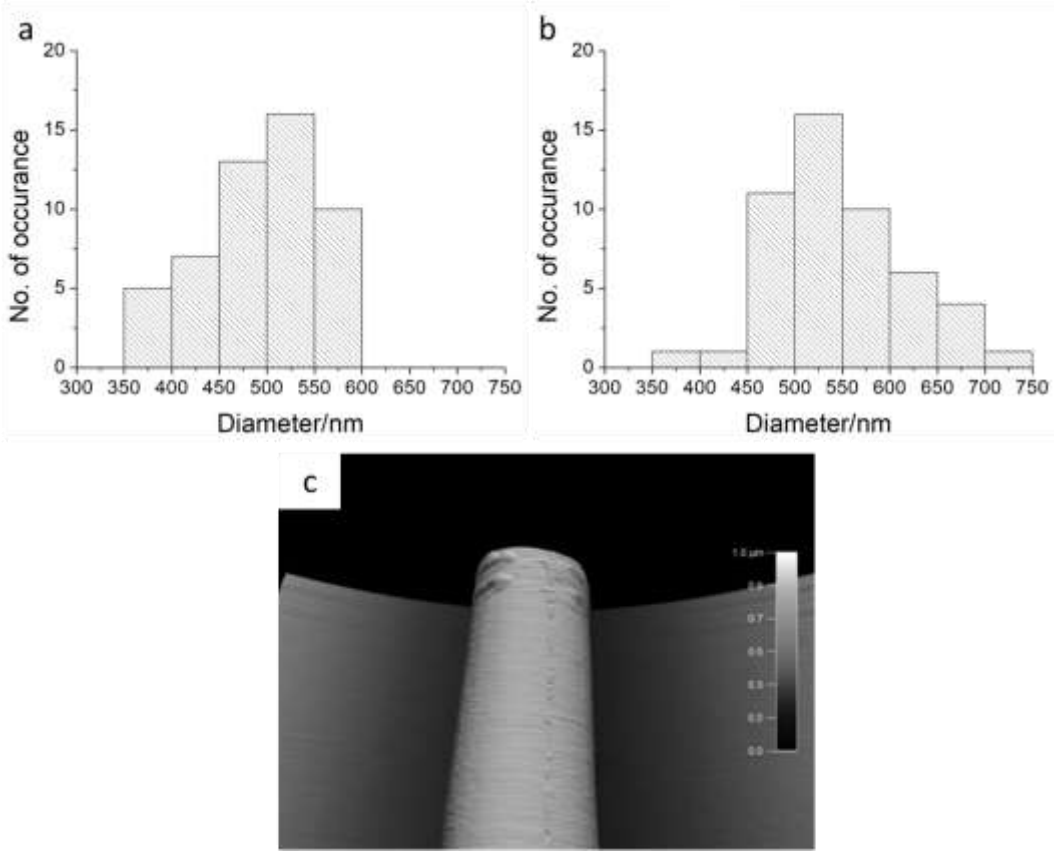


*Figure 31 Size distribution of PSIsp10 fibers by light microscope (a), AFM (b) and an AFM micrograph of a PSIsp10 fiber (c)*

DOI:10.14753/SE.2018.2178

All the fibers had smooth surface and uniform diameter along the fibers. The distribution of fiber diameter was also evaluated using AFM height data and it was found, that the average diameter was 550 ± 70 nm which is in line with the data obtained from light microscopy (**Figure 31a and b**).

SEM images further proved the quality of the PSIsp10 fibers (**Figure 32**). Similar smooth surface and uniform fiber width can be seen on the pictures as seen on the light microscopic and AFM figures as well. The high order of orientation on the picture (**Figure 32a**) is due to the sampling process, where a small portion was pulled out from the scaffold.

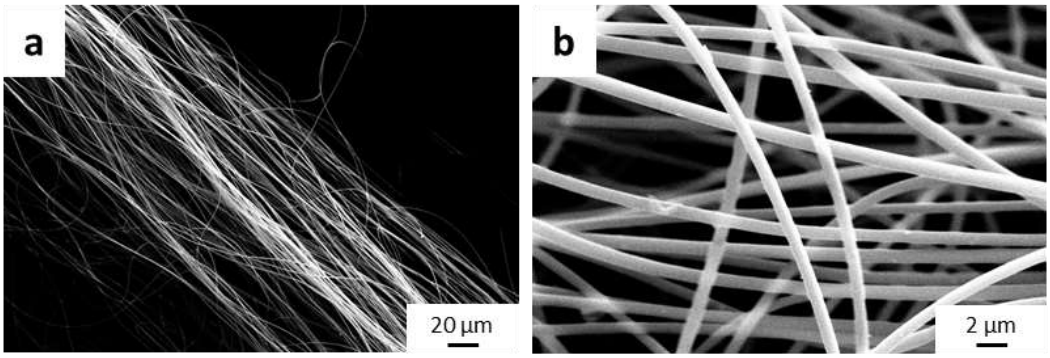


*Figure 32 SEM pictures of PSIsp10*

### 5.1.4 Chemical analysis of PSI powder and PSI fibers

To ensure that the high electric field does not alter the chemical structure of the polymer, analytical evaluation was carried out. In every case as reference material dry PSI powder was used. ATR-FTIR spectra of PSI powder and electrospun PSIsp10 can be seen on **Figure 33a**. This figure evidences that during electrospinning the chemical structure of PSI did not change. The characteristic absorption bands of imide rings in the polysuccinimide can be seen at 1709 $cm^{-1}$ (asymmetric stretching vibration is attributed to the $\nu_{CO}$ of $–(OC)_2N–$), 1391 $cm^{-1}$ (C–O bending vibration, δ) and 1355 $cm^{-1}$ (stretching vibration, $\nu_{C–N}$ of $–(OC)_2N–$) are retained after the electrospinning procedures.

DOI:10.14753/SE.2018.2178

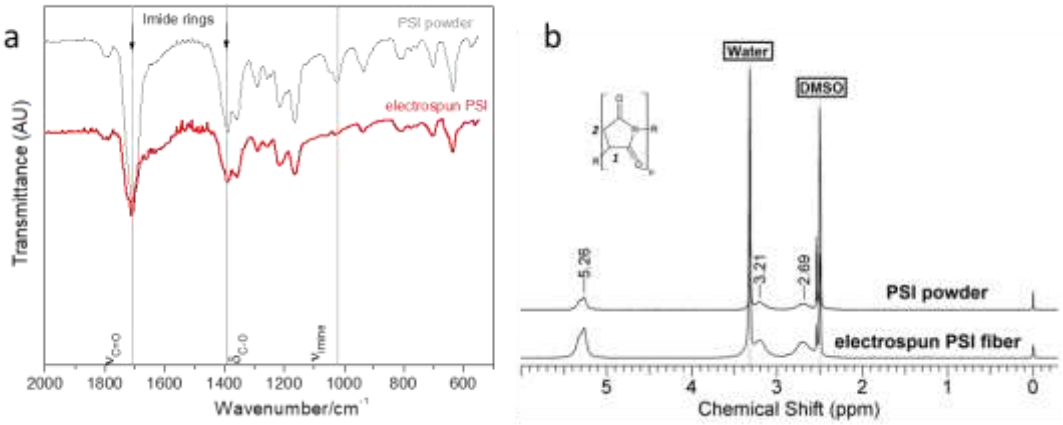


*Figure 33 ATR-FTIR spectra (a) and NMR spectra (b) of PSI powder and electrospun fibers*

The $^{1}$H NMR of electrospun PSI fiber is shown on **Figure 33b**. The peak at 5.3 ppm is the hydrogen connected to the methyl group marked with 1 on the molecule (**Figure 33b**). The hydrogens on the methylene group (marked with 2) appeared at 2.7 and 3.2 ppm [15]. The chiral methyl group is responsible for the separation of the peaks. These spectra also supports that the high electric field intensity during the electrospinning process does not alter the chemical structure of PSI fibers.

### 5.1.5 PSI fibers doped with magnetite (PSI-OaMagn)

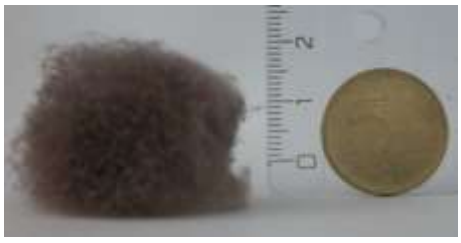

*Figure 34 3D structure of magnetite loaded PSI fibers*

In the presence of magnetic particles, not only the polymer solution but also the fibers become dark as shown on **Figure 34** whereas the electrospinning procedure resulted in either a flat 2D or a fluffy 3D structure. The fiber membrane shown on **Figure 34** has macroscopic extent in 3 dimensions in contrast to that shown on **Figure 29**, where the polymer fibers do not contain magnetic particles. As it is summarized in **Table 6**, at low magnetite content (PSI-OAMagn1) the produced scaffold is a thin film (**Figure 35)**. Upon increasing the magnetite concentration (PSI-OAMagn 2 and 3 in) 3D macrostructures develop as shown on **Figure 34** and **Figure 35**.

DOI:10.14753/SE.2018.2178

*Table 6 The influence of solution viscosity on the morphology of electrospun fibers.*

| Sample | Magnetite concentration, w/w % | Morphology | Viscosity (at 25°C), Pas |
|---|---|---|---|
| **PSI-OAMagn 1** | 2.5 | 2D thin film | 1.79 ± 0.0051 |
| **PSI-OAMagn 2** | 5 | 3D spiderweb like structure | 2.92 ± 0.0047 |
| **PSI-OAMagn 3** | 10 | 3D spiderweb like structure | 7.35 ± 0.0143 |

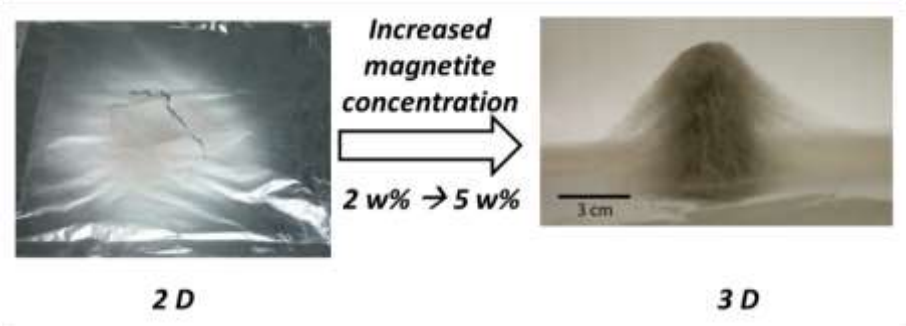


*Figure 35 Structural changes of the PSI fiber membrane loaded with different amounts of magnetic nanoparticles*

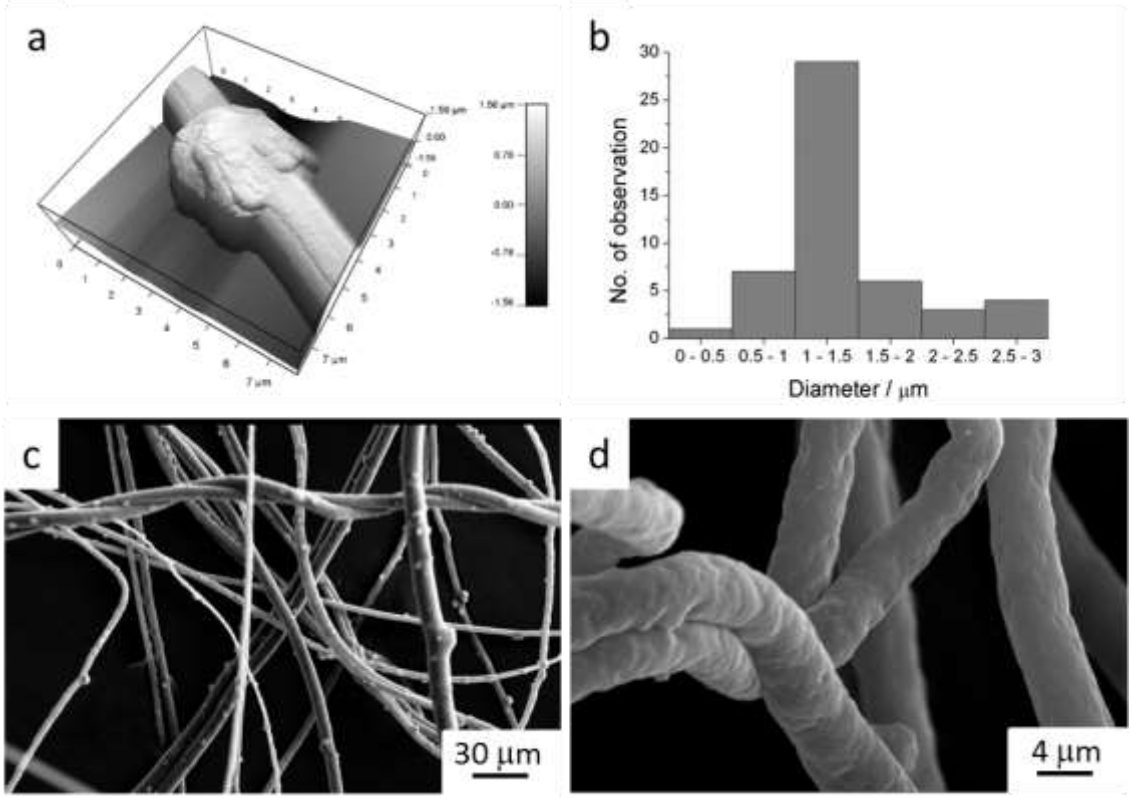


*Figure 36 AFM micrograph (a); diameter distribution measured by AFM (b) and SEM pictures of the PSI nanofibers loaded with magnetic nanoparticles (c, d)*

DOI:10.14753/SE.2018.2178

AFM showed that the fibers have a rough surface raising the surface area while there are clots along the fibers (**Figure 36a**). The average diameter of the fibers was found to be 1.43 ± 0.5 μm measured by AFM (**Figure 36b**). SEM also showed clots along the fibers as well as a rough surface of the fibers (**Figure 36a, c and d**).

## 5.2 Preparation of PSI based cross-linked fibers by reactive elctrospinning and post-spinning methods

As it was described in **Section 2.3.1** cross-links can be created inside the fiber either during (so called reactive electrospinning) or after electrospinning (post-spinning method). In this part of the thesis, both methods and related results are described based on different PSI systems. Reactive electrospinning was carried out by using thiol side-group modified PSI (**Section 5.2.1**) and its mixture with oleic acid modified magnetite nanoparticles (**Section 5.2.2**) as well as using a core-shell nozzle where the cross-linker and the polymer are delivered in the nozzle separately (**Section 5.2.4**). In post-spinning method PSI based fibrous membranes were simply dipped into the solution of cross-linker to prepare the cross-linked membranes in a heterogeneous reaction (**Section 5.2.3**).

### 5.2.1 Reactive electrospinning with PSI-CYSE

The reaction time for the preparation of PSI-CYSE was optimized by electrospinning the reaction mixture after the start of the synthesis at different times. The light microscopy results can be seen on **Figure 37**, where samples were collected during electrospinning after 10, 30, 50 and 80 minutes of reaction times respectively. It was found that at the $10^{th}$ minute the electrospinning resulted in spheres, at $30^{th}$ minute in a mixture of spheres and fibers, at the $50^{th}$ less spheres and incorporated into the fibers and finally at $80^{th}$ smooth fibers.

DOI:10.14753/SE.2018.2178

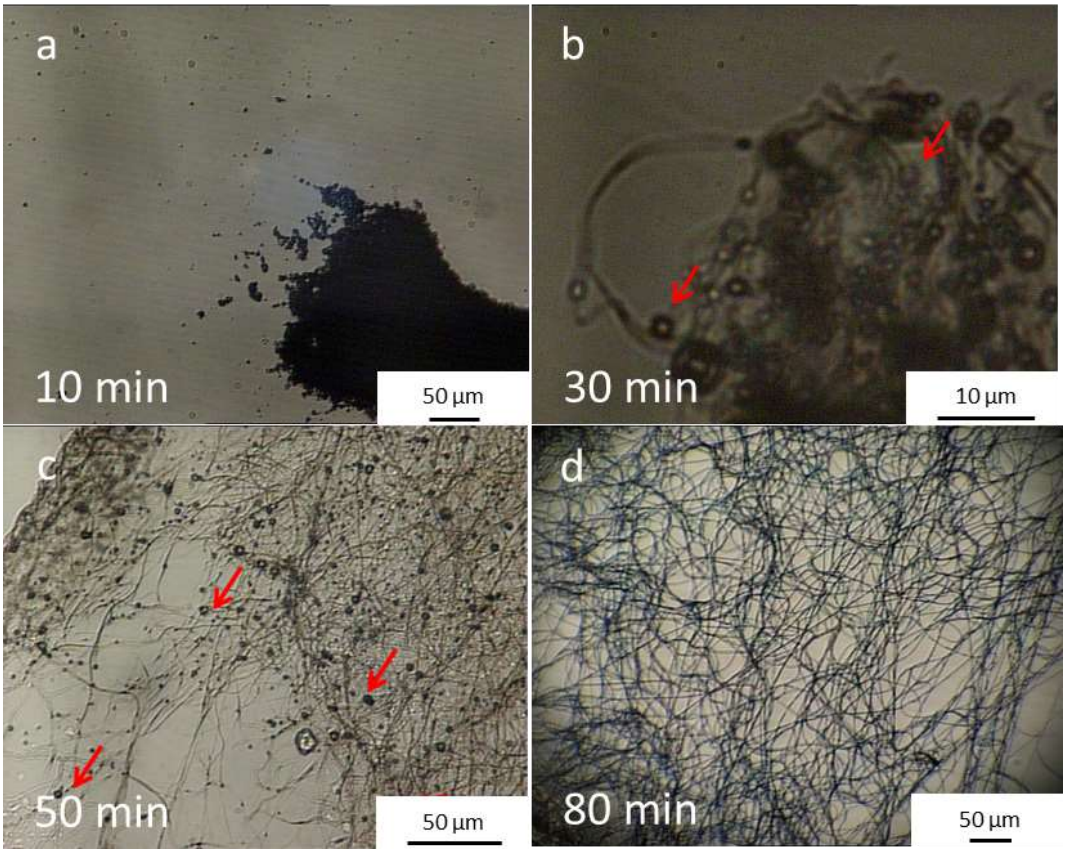


*Figure 37 Light microscopic pictures taken of PSI-CYS collected at 10 (a), 30 (b), 50 (c), 80 (d) minutes after the start of electrospinning, where red arrows indicate beads on fibers*

For the preparation of high quality PSI-CYS fibers the optimal reaction time was found to be 50 minutes, whereas the so called spinning window, where spinning and fiber formation were possible varied with each batch and was at least 1 hour.

#### 5.2.1.1 Characterization of PSI-CYS fibers by AFM and SEM

Reactive electrospinning of PSI-CYSE had two outcomes depending on the synthesized PSI batch used for thiol modification. As it can be seen on **Figure 38a, b and c** either fibers with beads or smooth fibers were obtained. A typical PSI-CYS fiber can be seen on **Figure 38d**. According to AFM the average diameter of PSI-CYS fibers was 90 ± 30 nm (**Figure 38e**) while according to SEM it was 850 ± 40 nm (**Figure 38f**).

DOI:10.14753/SE.2018.2178

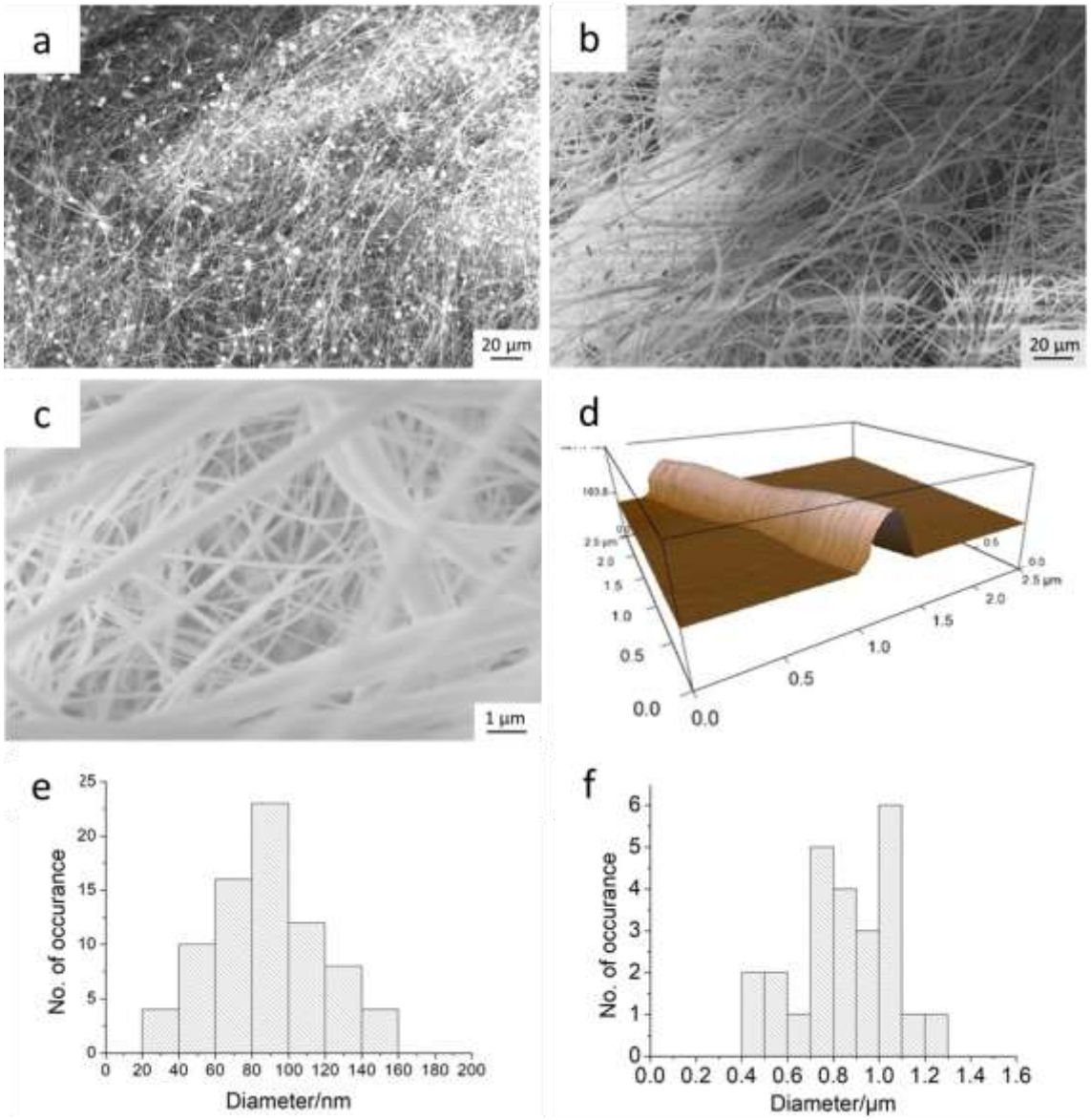


*Figure 38 SEM micrographs of PSI-CYS fibers with incorporated beads (a) and smooth fibers (b, c); AFM image of a piece of PSI-CYS fiber (d) and fiber diameter distribution according to AFM from fibers at the beginning of electrospinning (e) and according to SEM of fibers at the end of electrospinning process (f)*

### 5.2.1.2 Thermal analysis of electrospun membranes

According to the thermoanalytical curves, the mass loss of both samples (PSI, PSI-CYS) occurs in two main steps (**Figure 39a and b**). The difference between the two samples is more significant when comparing the DTA and TGA curves. As seen on the DTA curve the PSI fibers can be decomposed only in endothermic reaction and the PSI-CYS fibers show complicated endothermic and exothermic reactions. This difference is related to the difference in the chemical structure of samples, e.g. disulphide bonds. The exothermic peaks on DTA curve is the consequence of

combustion of fibers. It is important to emphasize that none of the sample showed structure changes or any reaction at the sterilization temperature (160 ºC). The slight decrease of mass below 80 ºC may be due to either the evaporation of remnant DMF or the absorbed water in the fibers (**Figure 39c**).

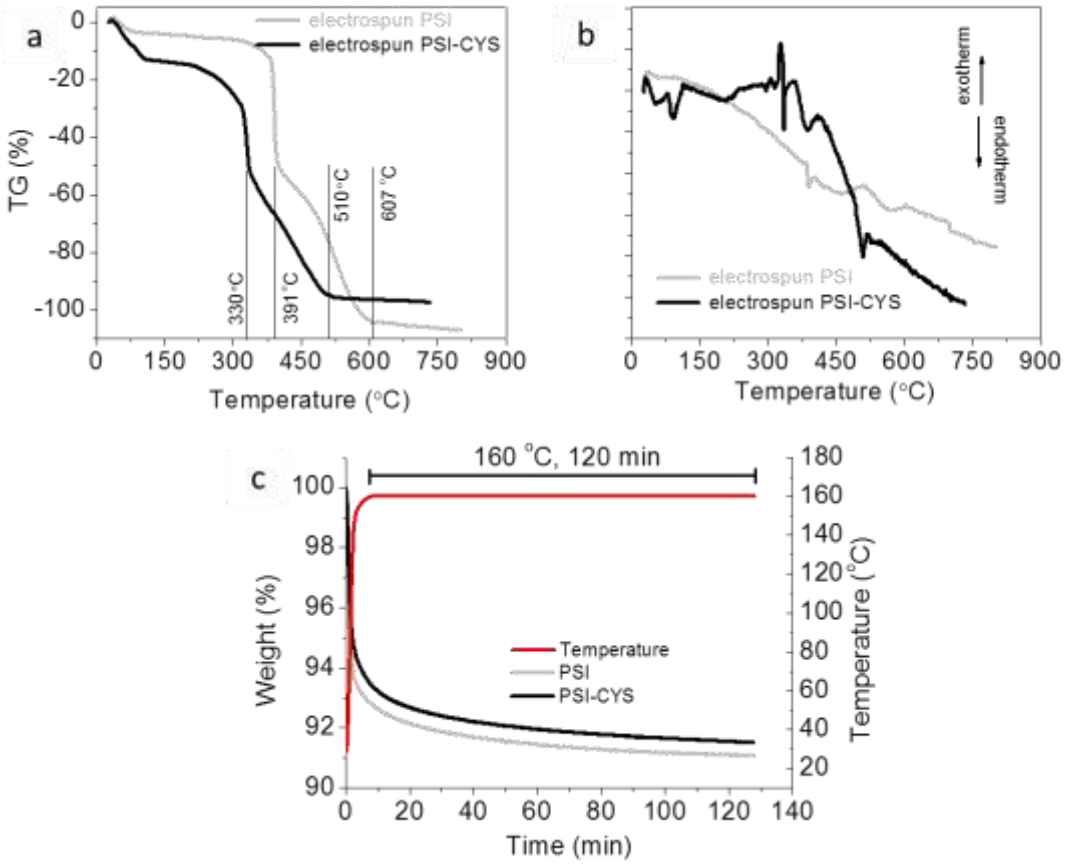


*Figure 39 Results of thermal gravimetric (a), differential thermal analysis (b) and thermal gravimetric analysis of sample held for 120 mins at 160 ºC (c)*

### 5.2.1.3 Chemical analysis of PSI-CYS fibers

The FTIR spectra for electrospun PSI and PSI-CYS are very similar to each other (**Figure 40**). The characteristic absorption bands of imide rings (at 1709 and 1391 $cm^{-1}$) were not altered by the cross-linking procedure. Free thiol groups or disulfide bonds cannot be seen in these spectra. The FTIR curve of electrospun PSI-CYS fibers heated at 160 ºC is the same as the not heat treated one's.

DOI:10.14753/SE.2018.2178

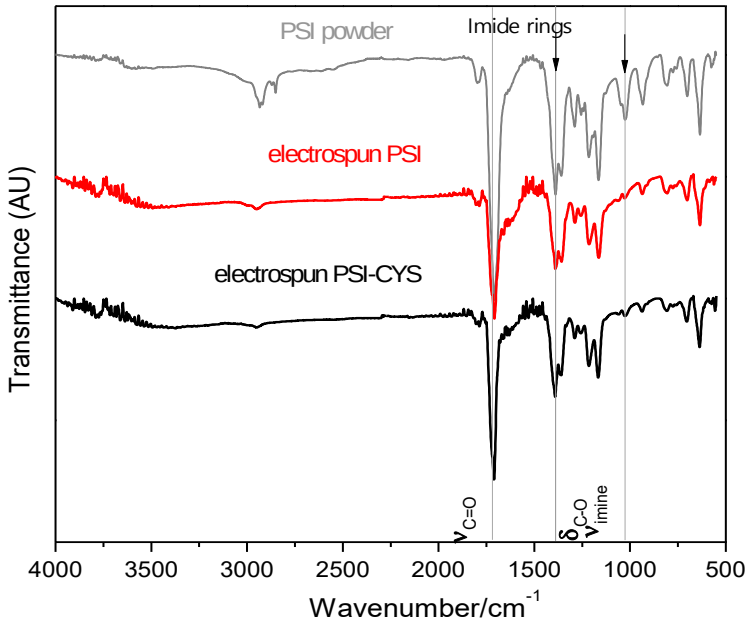


*Figure 40 ATR-FTIR spectra of dried PSI powder (reference) and electrospun PSI fibers.*

### 5.2.2 PSI-CYS-OAMagn

**Table 7** summarizes the impact of grafting number and magnetite concentration in the electrospinning of the mixture of PSI-CYSE and magnetite. When the cross-linking density was relatively high e.g. every 10$^{th}$ succinimid monomer was cross-linked by cystamine, even a small amount of particles (2 w/w%) induced gelation, which hindered electrospinning. When decreasing the amount of cysteamine cross-links (every 15$^{th}$) a flat 2D fiber membrane was obtained even in the presence of both 2 and 4 w/w% of magnetite concentration. Further increasing the magnetite concentration up to 5 w/w%, resulted in 3D structure. According to AFM the magnetite loaded PSI-CYS fibers had a fairly rough surface and a small average diameter without clots or broadening of fibers (**Figure 41a, b**).The average diameter of the fibers was found to be 500 ± 100 nm (**Figure 41c**). Since fiber membranes contained magnetic particles, in non-uniform external magnetic field they could be attracted and deformed as shown on **Figure 42**.

DOI:10.14753/SE.2018.2178

*Table 7 Macroscopic changes of PSI-CYSE system at different magnetite and cysteamine concentrations.*

| **PSI w/w% / Grafting number** | **Magnetite concentration, w/w %** | **Notes** |
|---|---|---|
| **15/10** | 2 | Gel formation in the presence of MPs |
| **15/10** | 4.6 | Gel formation in the presence of MPs |
| **15/15** | 2 | Homogenous 2D thin film |
| **15/15** | 4 | Homogenous 2D thin film |
| **15/15** | **5** | **Fluffy 3D structure** |

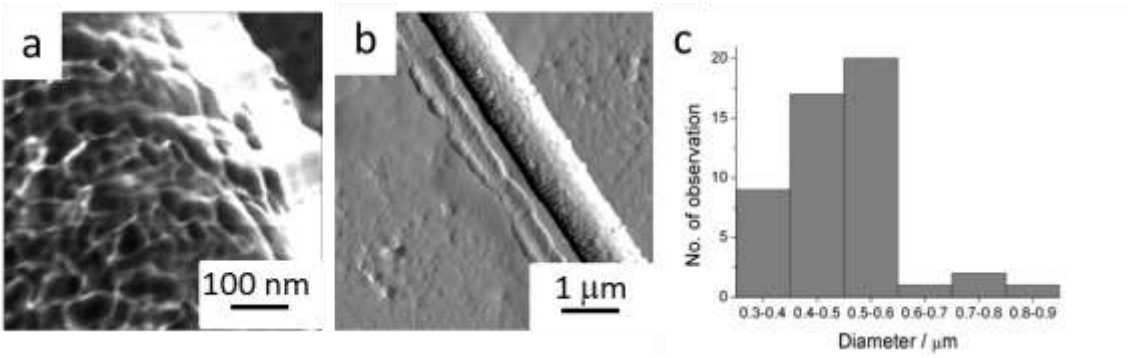


*Figure 41 AFM micrographs (a, b) and the size distribution of PSI-CYSE fibers loaded with magnetic nanoparticles.*

*Figure 42 Attraction of electrospun fiber membrane loaded with magnetic particles by non-uniform magnetic field.*

DOI:10.14753/SE.2018.2178

### 5.2.3 Preparation of PSI-DAB and PSI-CYS-DAB fibers

Post-electrospinning of PSI and PSI-CYS fibers were carried out by immersion of the membranes into the solution of 0.5 M 1,4-diaminobuthane in 96 % ethanol.

#### 5.2.3.1 Modification of PSI with DAB (PSI-DAB)

PSIsp10 fibers (average diameter determined by SEM: 911 ± 41 nm) were immersed into the solution of DAB for different amounts of times. If there were enough cross-links inside the fibers the membrane did not dissolve in DMF. Although, 10 minutes was enough to have the proper amount of cross-links for the samples to not dissolve, samples were very weak and misshaped after washing comparing with the original 1 x 1 cm square samples (**Figure 43a, b**). There was no visible difference between keeping the samples in the cross-linker for 20 minutes or 1 day since macroscopically they all looked the same with a retained shape (**Figure 43c**)

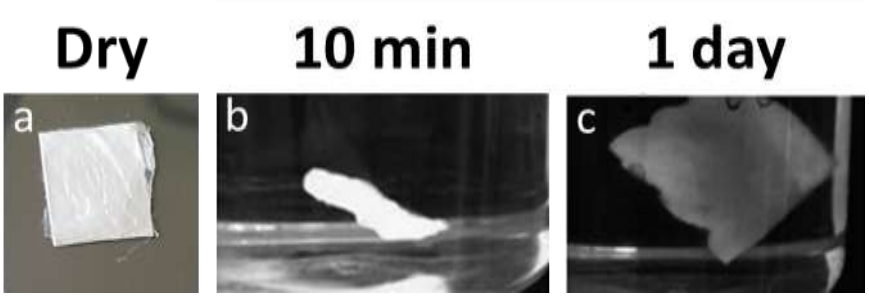


*Figure 43 Dry PSIsp10 sample before cross-linking (a); PSI-DAB samples in DMF prepared from PSIsp10 with cross-linking times 10 minutes (b) and 1 day (c)*

DOI:10.14753/SE.2018.2178

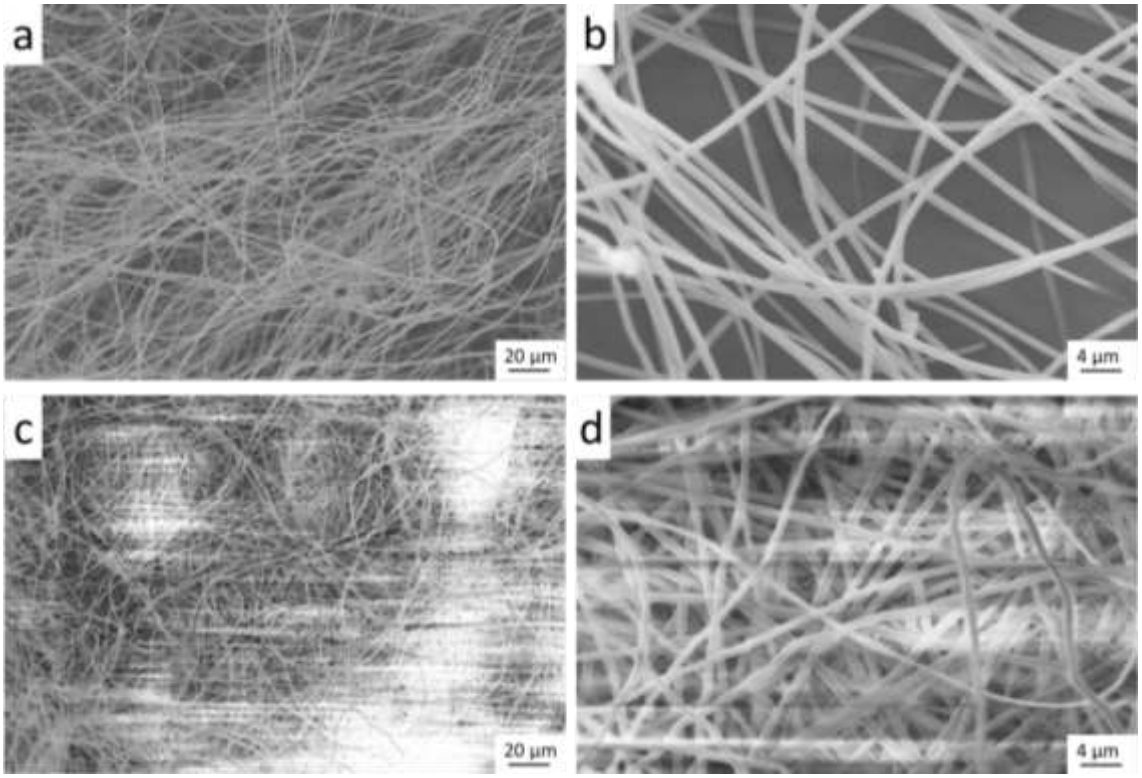


*Figure 44 SEM micrographs of freeze-dried PSI-DAB samples: without pressing (a, b) and pressing (c, d)*

A PSI-DAB sample can be seen on **Figure 44a and b** which was cross-linked for 3 hours then washed with ultrapure water and freeze-dried. The membrane maintained its fibrous structure and fused or damaged fibers were not found. Average diameter of PSI-DAB fibers was 800 ± 30 nm (determined with SEM). There was a difference between the resulting PSI-DAB samples depending on whether an un-pressed or a pressed sample was treated with the cross-linker. Compared to the standard as-spun membrane (**Figure 44a, b**) when a pressed PSI sample was treated the resulting membranes had higher fiber density (**Figure 44c, d**). The results of the FT-IR analysis of PSI-DAB will be presented in **Section 5.3.7**.

#### 5.2.3.2 Modification of PSI-CYS with DAB (PSI-CYS-DAB)

In the same procedure as in the case of PSI-DAB, a PSI-CYS sample was treated with DAB solution for 3 hours than washed with ultrapure water and freeze-dried. The resulting fibers (called PSI-CYS-DAB) can be seen on the SEM micrographs on **Figure 45a and b**.

DOI:10.14753/SE.2018.2178

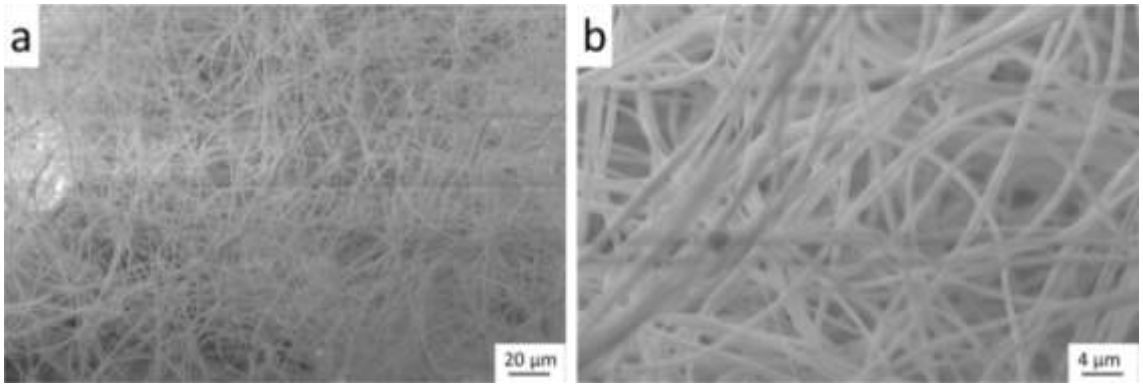


*Figure 45 SEM micrograph of a PSI-CYS-DAB samples (a, b)*

The sample maintained its fibrous structure, fused or damaged fibers were not found. According to SEM the average diameter of non-fused fibers was 760 ± 44 nm.

FT-IR showed the successful modification of PSI-CYS membranes to form PSI-CYS-DAB membranes. The results of the FT-IR analysis of PSI-CYS-DAB will be presented in **Section 5.3.7**.

### 5.2.4 Coaxial electrospinning of PSI and THD (PSI-THD and PSI-THD-PEO)

As a pre-test to see, whether THD can gelate PSI, the solutions used for coaxial electrospinning were mixed. The mixture gelated in about 1 minute (**Figure 46a**).

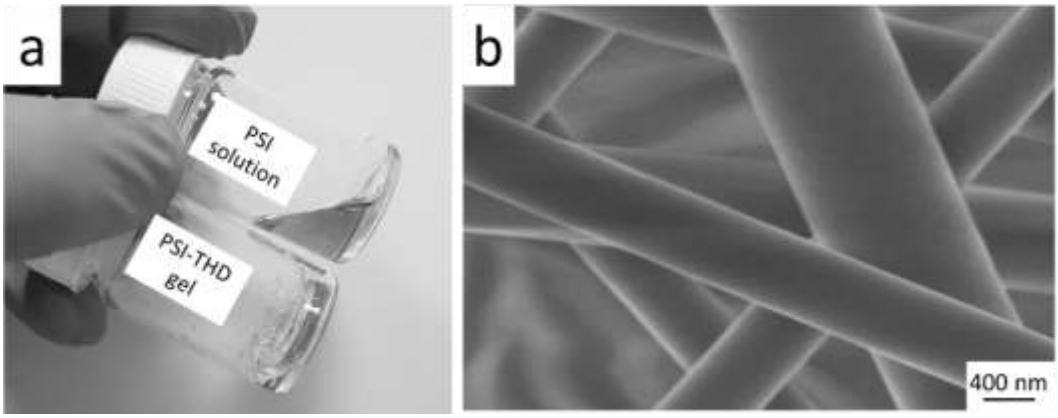


*Figure 46 PSI solution and a PSI based gel cross-linked with THD (a), reference PSI fibers (b)*

All the compositions and set parameters can be found in **Table 4**. SEM micrograph of the reference PSI fibers can be seen on **Figure 46b**. The average diameter of PSI fibers was 595 ± 44 nm (determined with SEM). When both the core and shell were fed, smooth fibers were obtained with low feeding rate (0.12 ml/h) of

core solution (**Figure 47a**). However, due to the insufficient amount of cross-links, these fibers (PSI-THD1) could be dissolved in DMF (**Table 4**). At higher feeding rate (0.74 ml/h) of core solution the core and shell solutions broke up at the tip of the nozzle and the spinning of shell and the spraying of core took place alternately, resulting in deformed but cross-linked membrane containing spheres and fibers (PSI-THD3) (**Figure 47b**). At 0.5 ml/h of core feeding rate (PSI-THD2) a stable fiber formation could be observed and fairly smooth fibers with beads could be found (**Figure 47c and d**). However, there were lot of beads and droplets in all fibrous samples containing THD. The average fiber diameter for PSI-THD2 was found to be 305 ± 41 nm according to SEM.

In PSI-THD-PEO 2 w/w% PEO was added to the core solution to raise its viscosity (~60 mPas). This case the electrospinning resulted in fibers without beads (**Figure 47e and f**). In addition, PEO also made the spinning process easier to control with less occasions of gelation caused blockage of the nozzle. The resultant PSI-THD-PEO fibers had an average fiber diameter of 320 ± 42 nm and did not dissolve in DMF (**Table 4**). Fiber diameter distribution of PSI, PSI-THD2 and PSI-THD-PEO can be seen on **Figure 47g**

DOI:10.14753/SE.2018.2178

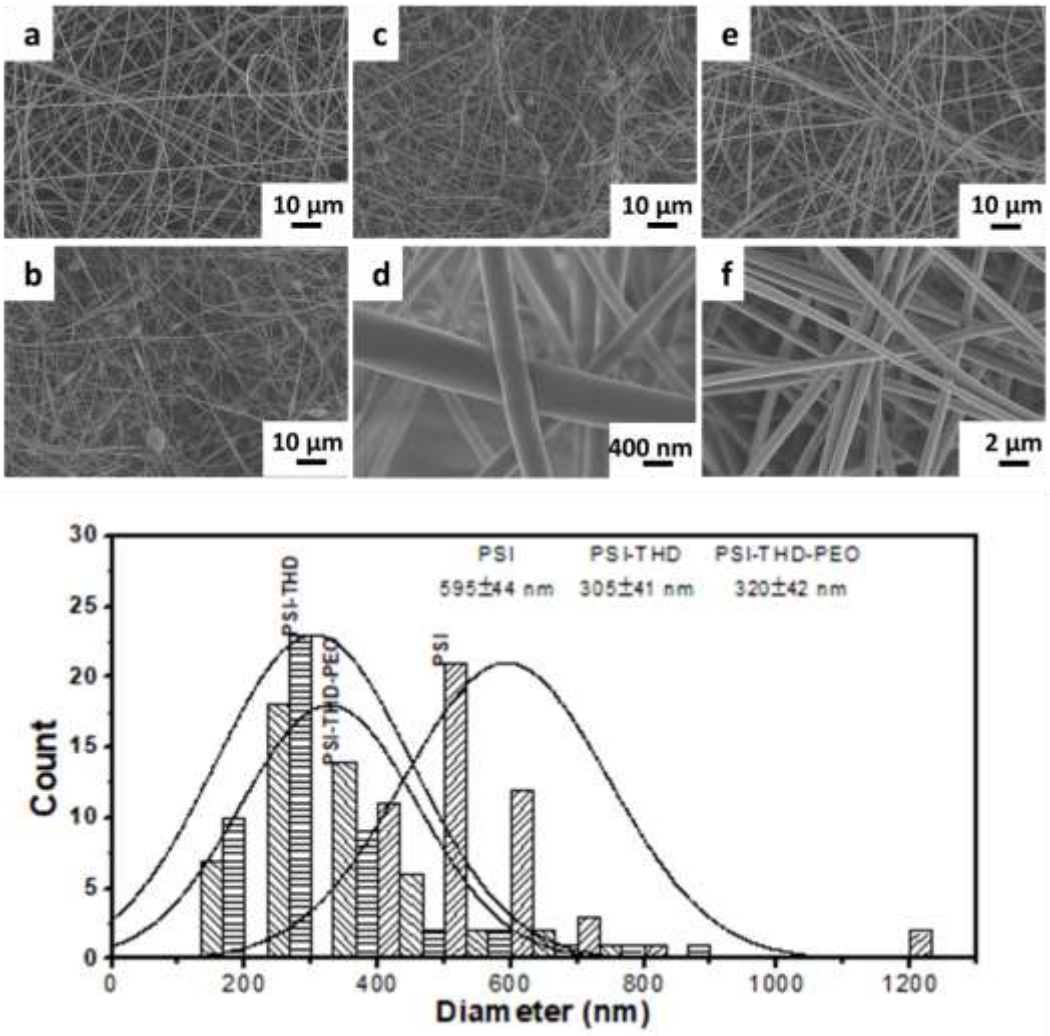


*Figure 47 SEM images of electrospun fibers of PSI-THD1 (a), PSI-THD3 (b), PSI-THD2 (c, d), PSI-THD-PEO (e, f), diameter distribution of PSI, PSI-THD2 and PSI-THD-PEO fibers*

The characteristic absorption bands of imide rings in PSI can be seen at 1709 $cm^{-1}$ (C=O of $–(OC)_2N–$, asymmetric stretching vibration of C=O), 1391 $cm^{-1}$ (C–O, bending vibration) and 1355 $cm^{-1}$ (C-N of $–(OC)_2N–$, stretching vibration). These characteristic bands are presented in both PSI-THD2 and PSI-THD-PEO samples. The appearance of vibration of >N-C=O bond at 1662 $cm^{-1}$ shows opened rings caused by cross-linking.

DOI:10.14753/SE.2018.2178

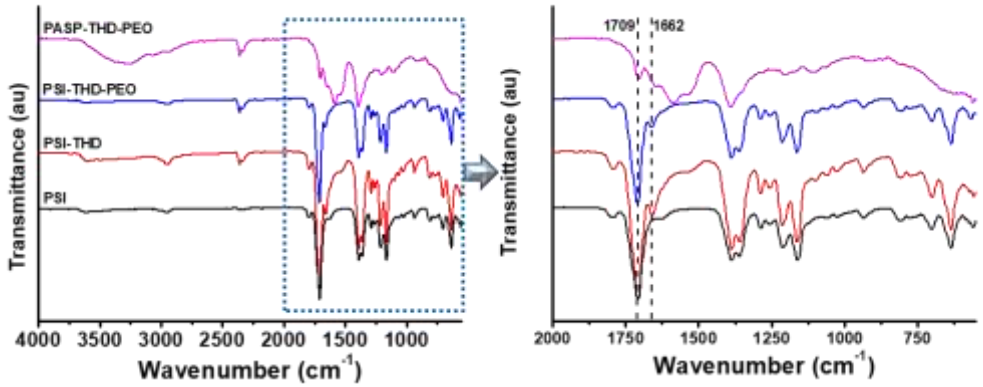


*Figure 48 FT-IR spectra of reference PSI, PSI-THD2, PSI-THD-PEO and PASP-THD-PEO*

## 5.3 Preparation and investigation of PASP based gelfibers

In this section the results of the hydrolysis of PSI based membranes, the poly(aspartic acid) based membranes (note the change in sample names to PASP): PASP-CYS, PASP-DAB, PASP-CYS-DAB and regarding the coaxial spinning the PASP-THD and PASP-THD-PEO are described. Their pH dependent properties will also be described based on PASP-DAB and PASP-THD-PEO.

### 5.3.1 Hydrolysis of PSI and PSI-CYS fibers

PSI turns into poly(aspartic acid) upon hydrolysis in mild alkaline aqueous solutions and dissolves [48]. The same phenomenon can be observed with a PSI based fibrous membrane without any cross-links as it dissolves in pH 8 imidazole buffer in 15 hours (**Figure 49)**.

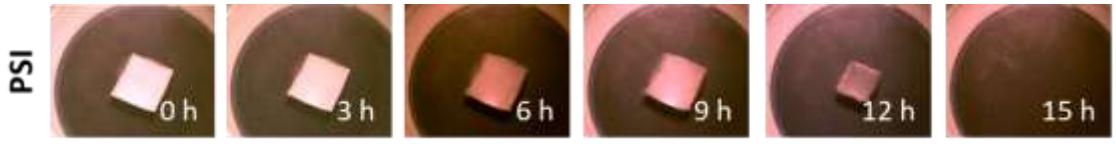


*Figure 49 Hydrolysis of electrospun PSI fiber membrane in pH 8 buffer solution*

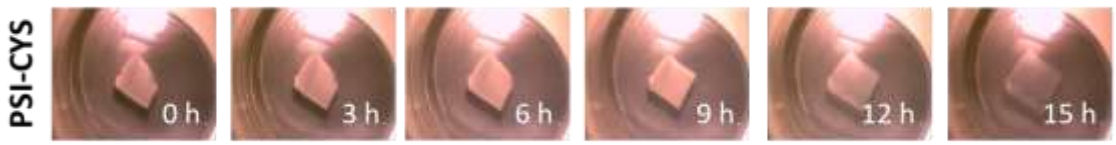


*Figure 50 PSI-CYS fibrous membrane in pH 8 buffer solution during hydrolysis*

In the case of PSI-CYS, as there are cross-links between the polymer chains, the fibrous membrane did not dissolve, only took up the buffer and turned into an opaque

gel membrane (denoted as PASP-CYS). As it can be seen on **Figure 50** the membrane obtained its equilibrium state in 15 hours. During this chemical transformation, the volume of the gel changed slightly. It is also important to note, that opposed to bulk PASP gels these fibrous membranes are very flexible and rubberlike, withstanding bending without any damage, however, their transparency is worse due to the fibrous structure. For comparison a PASP-CYS hydrogel membrane and a PASP-CYS bulk gel film can be seen on **Figure 51**.

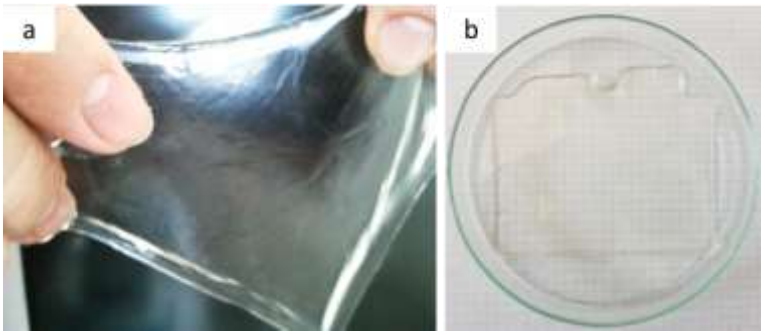


*Figure 51 PASP-CYS fibrous gel membrane (a) and a PASP-CYS bulk gel film (b)*

Hydrolysis caused a significant change in the structure of gelfibers. According to the AFM pictures (**Figure 52**) the PASP-CYS membrane is a highly dense matrix with fiber bundles, however it is impossible to tell if these bundles are really fused and/or connected or simply aggregated to each other during the drying process (AFM sample preparations is described in **Section 4.9.2**) .

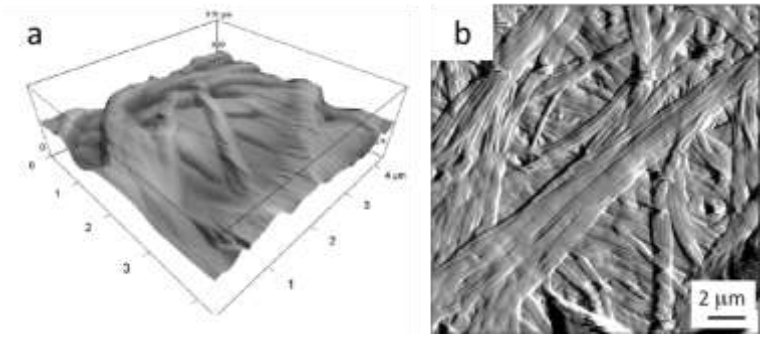


*Figure 52 AFM images of dried chemically cross-linked PASP fibers (a, b)*

To investigate the original fiber structure of the swollen gel membrane (**Figure 51a**) SEM micrographs were taken from two freeze-dried PASP-CYS samples (**Figure 53**).

DOI:10.14753/SE.2018.2178

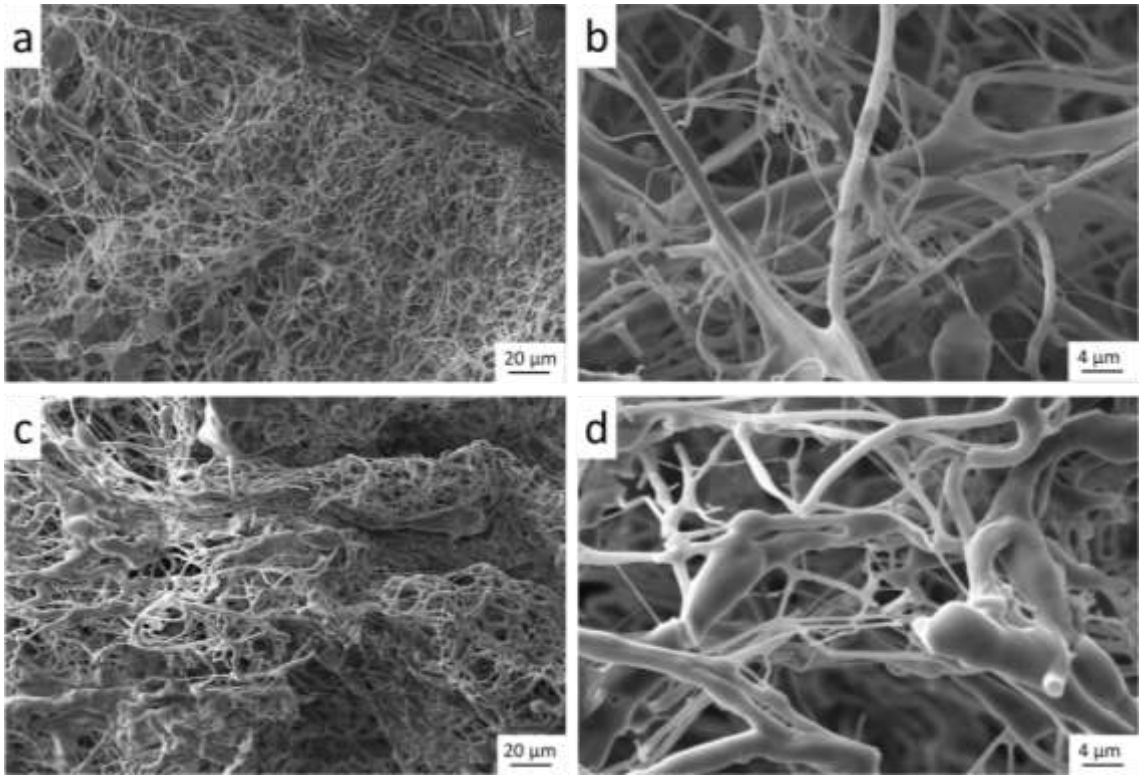


*Figure 53 SEM micrographs of two PASP-CYS samples of the same type but different batch: first (a, b), second (c, d)*

It can be clearly seen that the fibers in PASP-CYS fused together forming an interconnected web. Determining the fiber diameter distribution was not possible; however, it seemed that it increased during the deformation of the fibrous structure. There was no significant difference between the two samples represented on the figure.

### 5.3.2 Hydrolysis of PSI-DAB fibers (PASP-DAB)

Preparation of PASP-DAB samples were carried out in two ways and the only difference was in the washing step between cross-linking and hydrolysis (**Figure 21**). As it was expected in both routes the necessary cross-linking time for the samples to maintain their integrity after hydrolysis was 10 minutes (**Figure 54a and b**). The difference in results was that in "route b" the resulting membrane was smaller and clearly deformed compared to "route a". However, this difference diminished when cross-linking was 1 day, as both routes resulted in swollen whitish fibrous membranes (**Figure 54c and d**). Another important thing to note is that higher reaction times resulted in whiter samples compared to the 10 minutes reaction time, when slightly opaque ones were obtained. All the samples with reaction times longer than 1 hour were about equally easy to handle and strong, meaning that they were not torn by the tweezer.

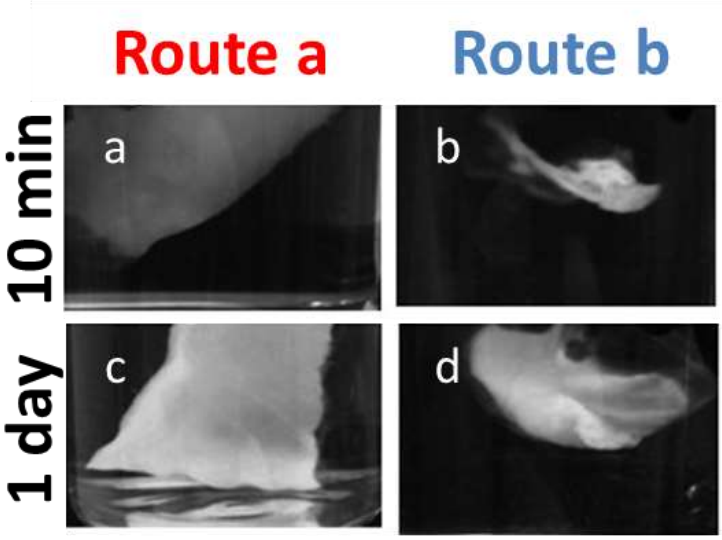


*Figure 54 PASP-DAB samples in ultrapure water after treatments according to* ***Figure 21*** *where, 10 min immersion (a, c) and 1 day immersion in DAB solution (b, d) corresponds to the different routes*

AFM analysis on dry matrices from both "route a and b" showed that after immersion for 10 minutes in the solution of the cross-linker, samples could maintain their fibrous structure. Since all the samples looked very similar under the microscope only samples with 3 hours reaction time is represented on **Figure 55a and b**.

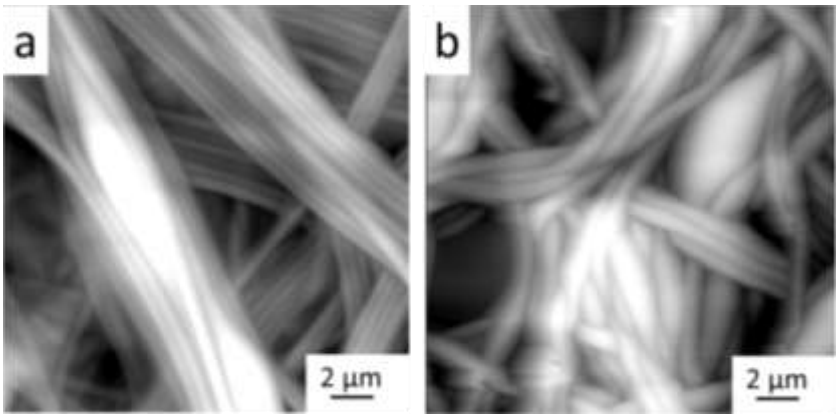


*Figure 55 AFM height picture taken of a PASP-DAB with 3 hours reaction time from „route a" (a) and from „route b" (b)*

**Figure 56a and b** show the SEM micrographs of a PASP-DAB sample from "route a" (cross-linking for 3 hours then hydrolysis). The chemical transformation slightly changed the fibrous structure: the fibers were loosely interconnected and few narrow and flat sheets were found. This was also evidenced by multiphoton microscopy presented on **Figure 56c**. According to SEM the average diameter of non-fused PASP-DAB fibers was 940 ±60 nm.

DOI:10.14753/SE.2018.2178

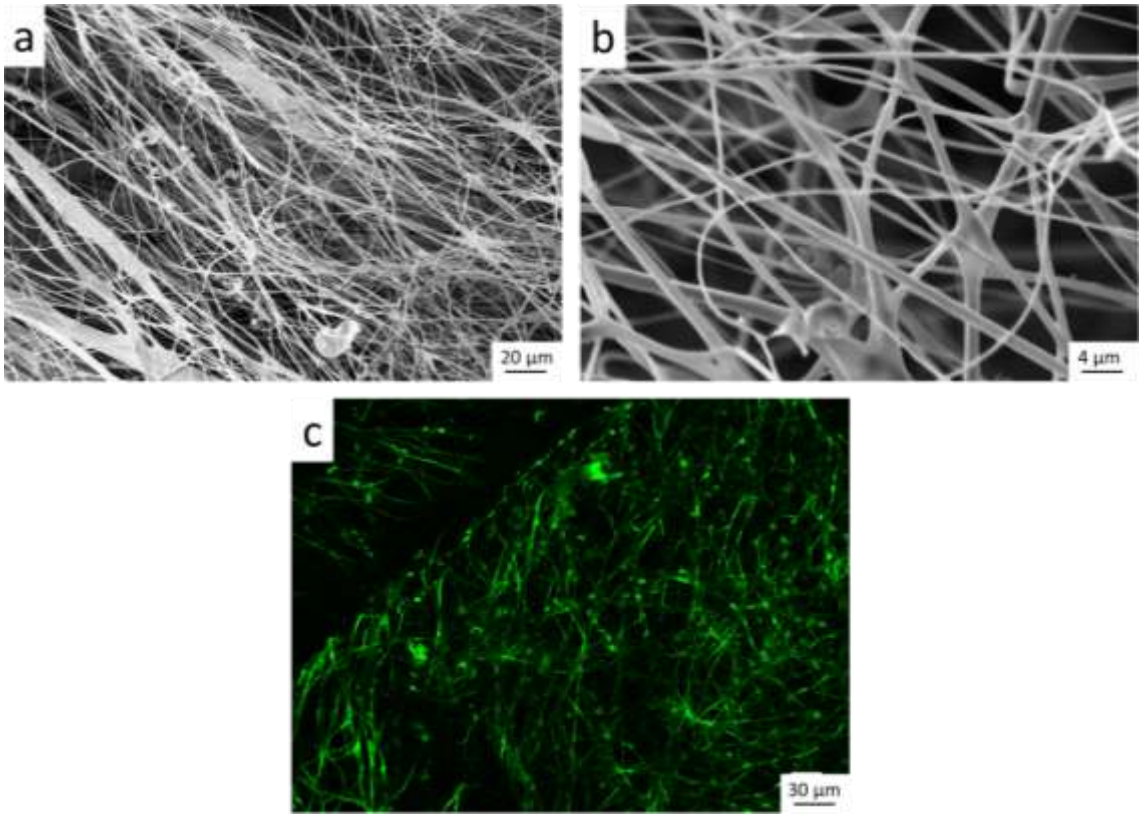


*Figure 56 SEM micrographs of a typical PASP-DAB sample (a, b) and a multiphoton micrograph of the same sample showing the autofluorescence of PASP (c)*

### 5.3.3 Hydrolysis of PSI-CYS-DAB fibers (PASP-CYS-DAB)

The hydrolysis of PSI-CYS-DAB changed the samples into slightly opaque, very soft gel sheets (**Figure 57a**). According the SEM (**Figure 57b, c**) the chemical transformation did not change the fibrous structure and the average fiber diameter was 725 ± 40 nm.

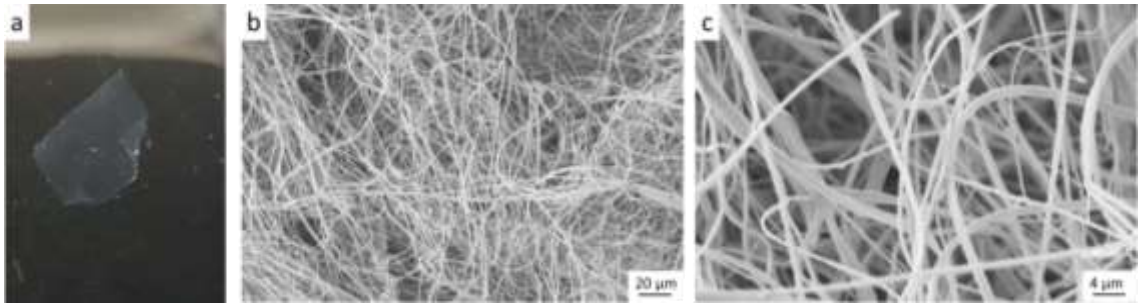


*Figure 57 Macroscopic picture (1x1cm square) (a) and SEM micrograph of a PASP-CYS-DAB sample in two magnifications (b, c)*

### 5.3.4 Cleavage of disulfide bond in PASP-CYS-DAB (PASP-CYSE-DAB)

As a result of the cleavage of the disulfide bonds in PASP-CYS-DAB (**Figure** 22) the membrane became transparent and very weak. Samples were easily torn and hard to pick up with a tweezer. SEM micrographs of PASP-CYSE-DAB are shown on **Figure 58**. According to these results the membrane maintained its fibrous structure, however, in some parts fused or bundled fibers were found. According to SEM the average diameter of non-fused fibers was 680 ± 40 nm.

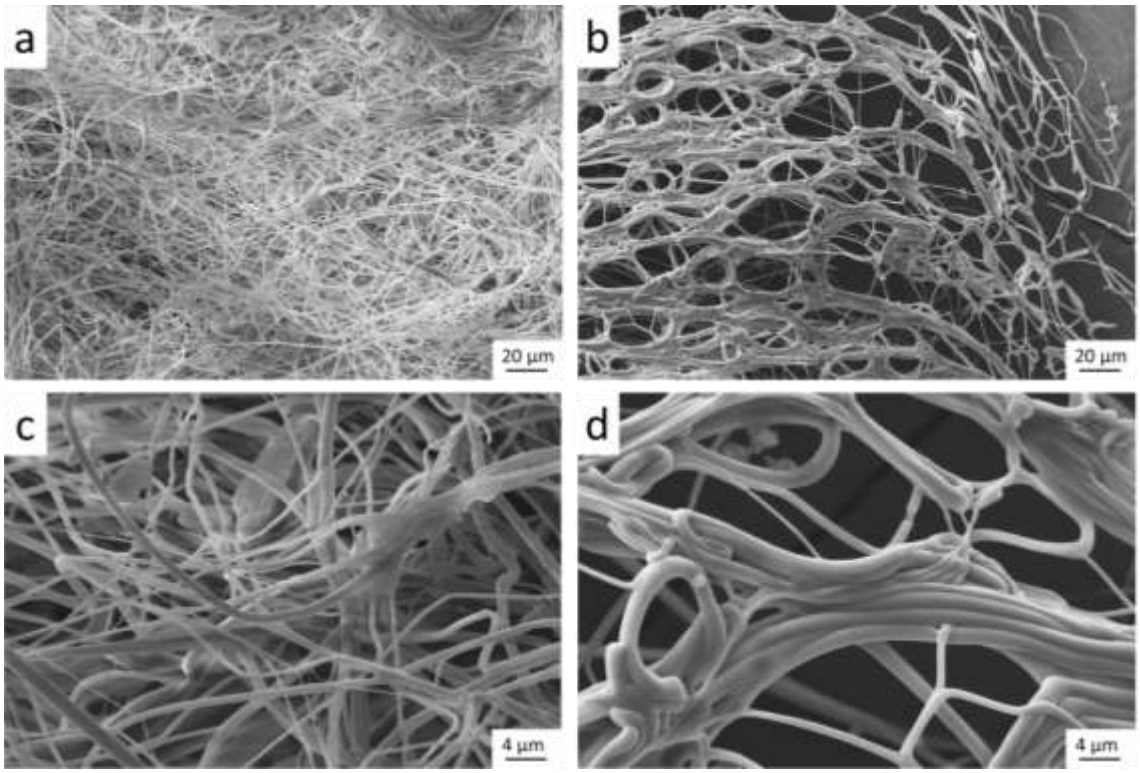


*Figure 58 SEM micrographs of two different parts of the same PASP-CYSE-DAB sample (a, c, corresponds to one part while b, d, to the other)*

### 5.3.5 PASP-THD samples by post spinning method

PSI samples treated in 0.5 M THD/EtOH solution (similarly to the preparation of PSI-DAB samples after either 5, 10, 20 and 60 minutes) dissolved after hydrolysis proving that not enough cross-links were established during treatment to prohibit dissolution. On the contrary, after treatment in pure THD for 1, 2 and 3 hours, respectively, none of the samples dissolved after hydrolysis. SEM on the freeze-dried PASP-THD samples showed that although 1 h in pure THD was enough for the samples not to dissolve, the fibrous structure diminished due to the fusion of the fibers (**Figure**

**59a**). 2 h proved to be better, however there were still many fused and damaged fibers (**Figure 59b**), while 3 h resulted in misshaped but pure fibers (**Figure 59c**).

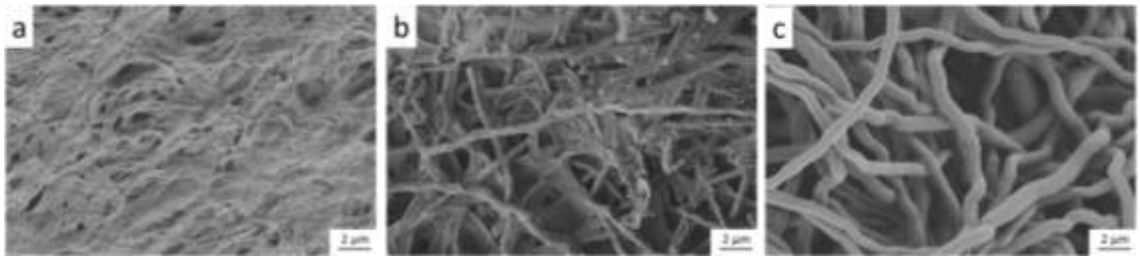


*Figure 59 SEM micrographs of PASP-THD samples prepared by immersion into pure THD for 1 h (a), 2 h (b) and 3 h (c) and finally hydrolysis in pH 9 buffer solution*

### 5.3.6 PASP-THD samples by the hydrolysis of PSI-THD membrane

Hydrolysis of PSI-THD2 resulted in soft, mildly opaque sheets similar to PASP-CYS-DAB (**Figure 57a**). SEM on the washed and freeze-dried samples showed that fibers fused together or there were sheets between them, while the pore size between fibers got bigger (**Figure 60**).

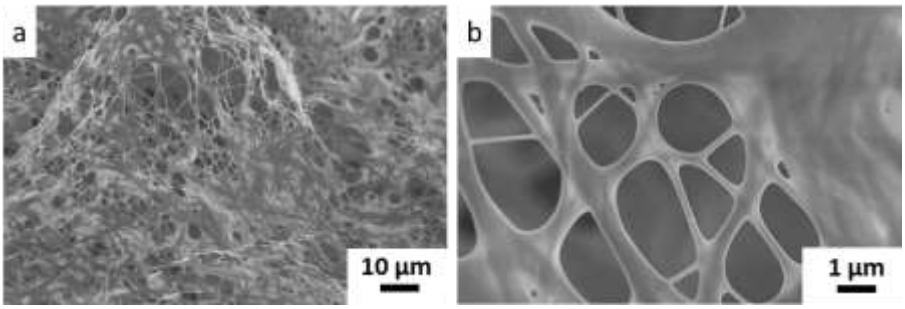


*Figure 60 SEM micrographs of PASP-THD2 in two magnifications*

### 5.3.7 FT-IR analysis of PASP based fiber membranes and their precursors

For the FT-IR analysis of PASP based membranes, their precursor molecules were measured as references for comparison. Both in PSI-DAB and PSI-CYS-DAB the peak emerging at 1662 $cm^{-1}$ indicates the opening of the succinimide rings, marking the success of modification. Otherwise the spectra of both molecular structures resemble to the original PSI and PSI-CYS respectively.

Compared to their precursor polymers in both PASP-DAB, PASP-CYS-DAB and PASP-CYSE-DAB there was a new wide peak at around 3250 $cm^{-1}$ indicating new –OH groups on the polymer. Furthermore, the reduction of the peak at 1709 $cm^{-1}$ and the raise in the peak at 1662 $cm^{-1}$ refers to the opening of succinimide rings. The change

in those three peaks indicates the hydrolysis of the molecules (**Figure 61a and b**). Unfortunately FT-IR dose not enable the observation of the opening of disulfide bridges, therefore no change can be seen on the spectrum of PASP-CYSE-DAB compared to PASP-CYS-DAB (**Figure 61b**).

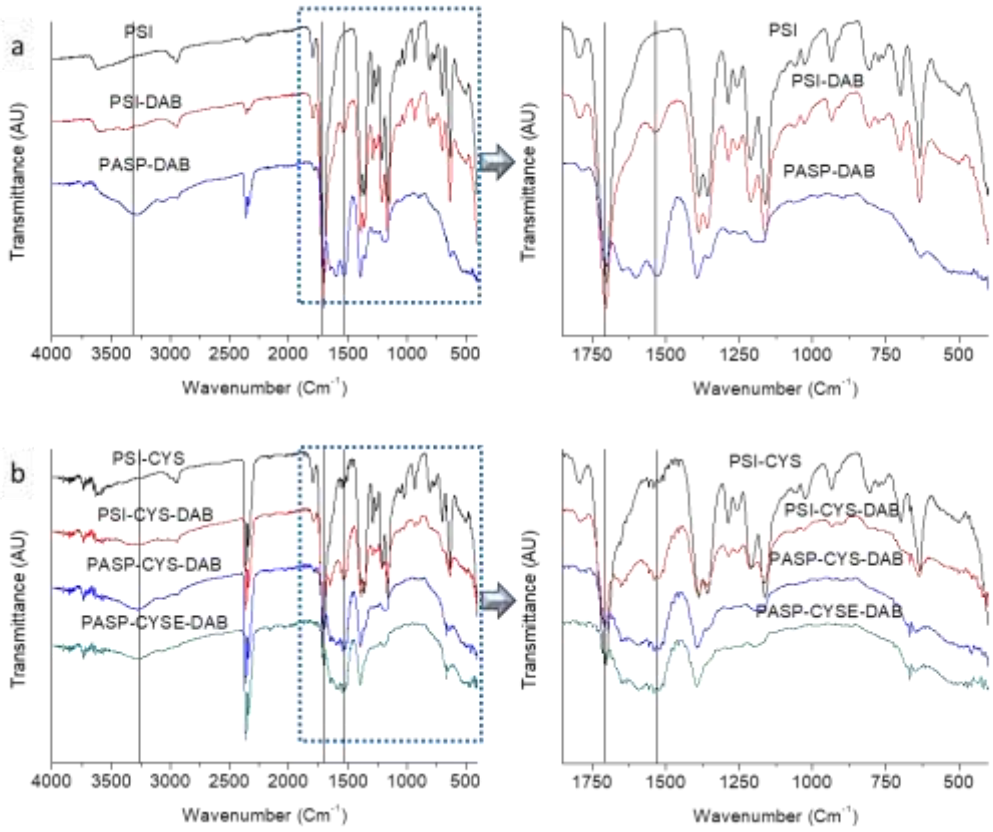


*Figure 61 FT-IR spectra of PSI, PSI-DAB, PASP-DAB (a) and FT-IR spectra of PSI-CYS, PSI-CYS-DAB, PASP-CYS-DAB, PASP-CYSE-DAB (b)*

### 5.3.8 pH responsivity of PASP based membranes

In this section results related to the pH responsivity of PASP based fibrous membranes are presented. Although the pH induced swelling and shrinking of PASP based bulk gels have been studied extensively [6], there are no articles describing it on fibrous membranes.

#### 5.3.8.1 pH sensitivity of PASP-DAB membrane

The pH responsive properties of PASP-DAB samples were investigated by measuring the size of the fiber membrane disk in different buffers. It can be seen on **Figure 62** that compared to the dry disks the samples in pH 8 swelled significantly

DOI:10.14753/SE.2018.2178

whereas in pH 3 their size decreased to about their initial sizes before modification and hydrolysis. Compared to their original sizes in pH 8 and pH 3, samples reached the same sizes with only a small error throughout the 4 cycles in pH 8 and pH 3 (**Table 8, Figure 63a**).

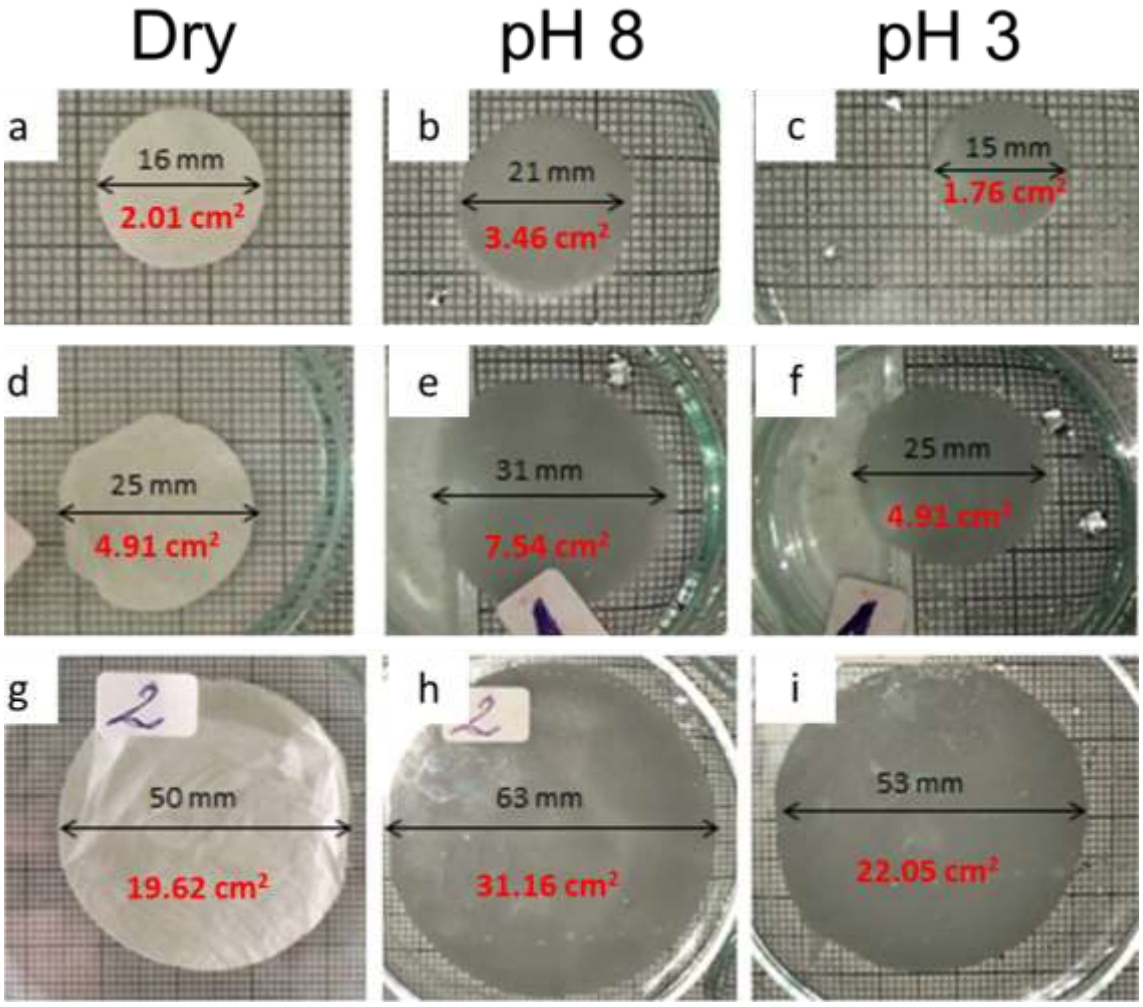


*Figure 62 Dry PSI fibrous membranes of different sizes (a, b, c), same membranes after cross-linking with DAB in pH 8 buffer solution (b, e, h respectively) and as next treatment in pH 3 (c, f, i respectively) where red numbers are the area of samples (the grid in the background is not calibrated, it is only for creating contrast between the samples and background)*

*Table 8 Relative size changes of PASP-DAB fibrous disks in pH 3 and pH 8 solutions in 4 cycles respectively*

| | pH3/pH8 | pH8/pH8 | pH3/pH8 | pH8/pH8 | pH3/pH8 | pH8/pH8 | pH3/pH8 |
|---|---|---|---|---|---|---|---|
| $Q_{rel,h}$ **16** | 0,588 | 1,068 | 0,614 | 1,068 | 0,640 | 1,103 | 0,640 |
| $Q_{rel,h}$ **25** | 0,630 | 1,000 | 0,682 | 1,022 | 0,682 | 1,066 | 0,719 |
| $Q_{rel,h}$ **50** | 0,711 | 1,033 | 0,757 | 1,044 | 0,729 | 1,055 | 0,757 |

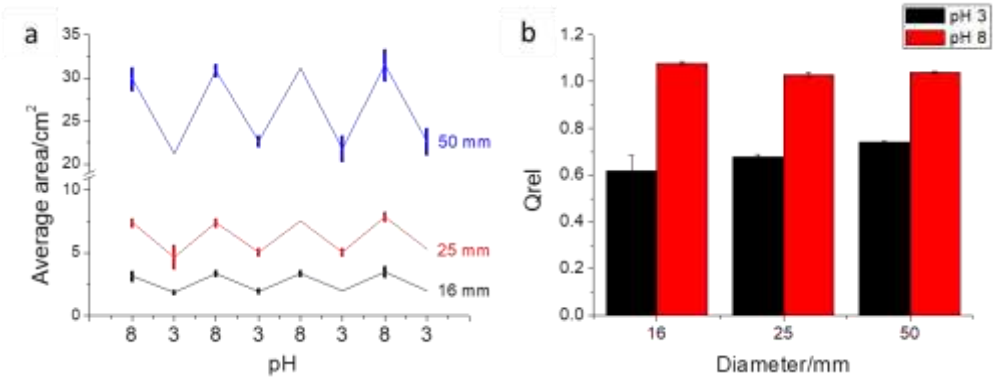


*Figure 63 Average area of PASP-DAB disks of different initial sizes in pH 8 and pH 3 buffer solutions in 4 cycles (vertical line indicate standard error) (a), relative degree of swelling of PASP-DAB disks in pH 3 and pH 8 (b)*

**Figure 63b** shows the difference in relative swelling degrees of PASP-DAB disks of different initial sizes. The figure suggests that the bigger the initial size is the smaller the relative change is due to the change in pH.

### 5.3.8.2 Preparation and pH responsivity of PASP-THD-PEO

After merging dry electrospun PSI-THD-PEO samples (3.03 ± 0.13 $cm^2$) (**Figure 64a**) in DMF, membranes shrunk (1.28 ± 0.05 $cm^2$) (**Figure 64b**). Then, in pH 9 buffer solution, the same membranes swelled significantly (~39% area change) and became transparent (**Figure 64c**). After washing with ultrapure water and freeze-drying of a PASP-THD-PEO sample, a web of connected fibers were found in SEM (**Figure 64e, f**). It was found that the samples are in a swollen state (in the maximum size of 7.37 ± 0.11 $cm^2$) in alkali medium (pH 9, **Figure 64c**), while in acidic environment they shrank (5.04 ± 0.07 $cm^2$, pH 4, **Figure 64d**). Average area of samples through the 4 cycles of buffer change can be seen on (**Figure 64g**).

DOI:10.14753/SE.2018.2178

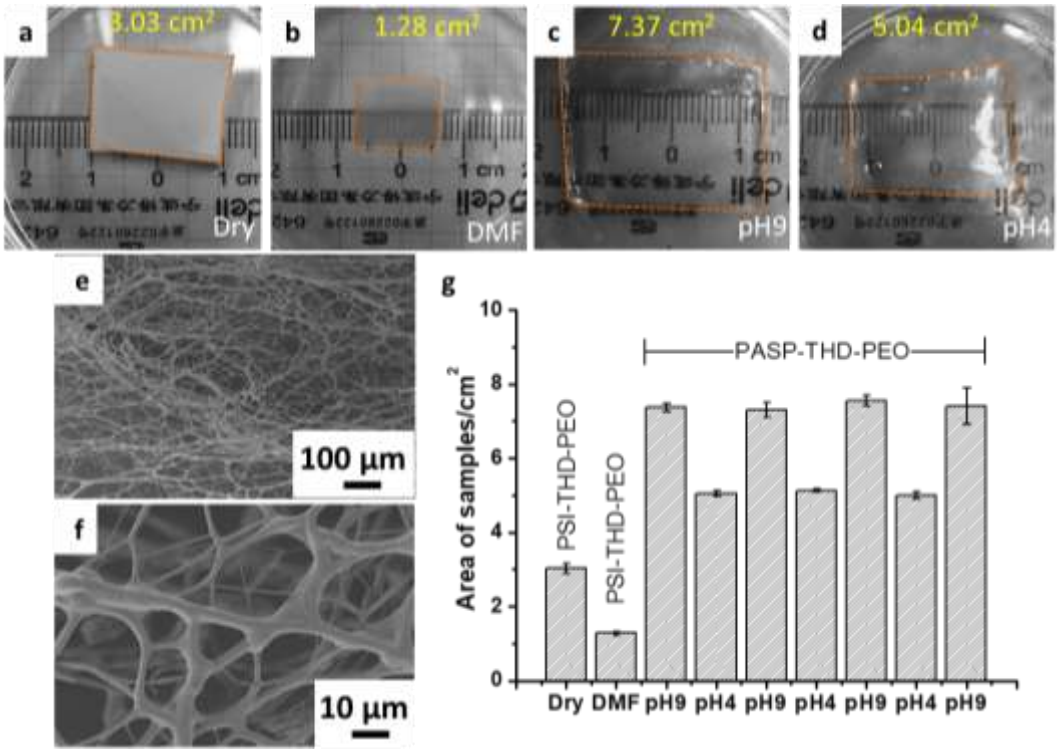


*Figure 64 Macroscopic picture of a PSI-THD-PEO fiber membrane in dry state (a) in DMF (b) and after hydrolysis the same fiber membrane in pH 9 (c) and in pH 4 (d), SEM micrograph of a washed and freeze-dried PASP-THD-PEO membrane (e, f) and pH induced area changes of PASP-THD-PEO samples (g)*

## 5.4 In vivo biocompatibility and biodegradability of electrospun samples

During implantation, both PSI-CYS and PSI-DAB samples were easy to handle and suture. Although in a few cases sample layers got slightly separated due the handling, the suture held it together. Upon regular inspection, none of the animals showed any signs of irritation, infection or any other adverse reaction until the day of termination.

### 5.4.1 Implantation of PSI-CYS membranes

In Group A, where termination was performed 3 days post implantation, skin closure was intact with physiologic wound edge healing. After dissection, the samples were easily located between the skin and the underlying muscle and easily moved (**Figure 65a**). Consistency of samples changed from paper-like, to soft and gelatinous while their size increased by approximately ~40 % in diameter. There was no visible

DOI:10.14753/SE.2018.2178

irritation, infection or foreign body reaction observable at the implantation area only a small amount of fibrinous material.

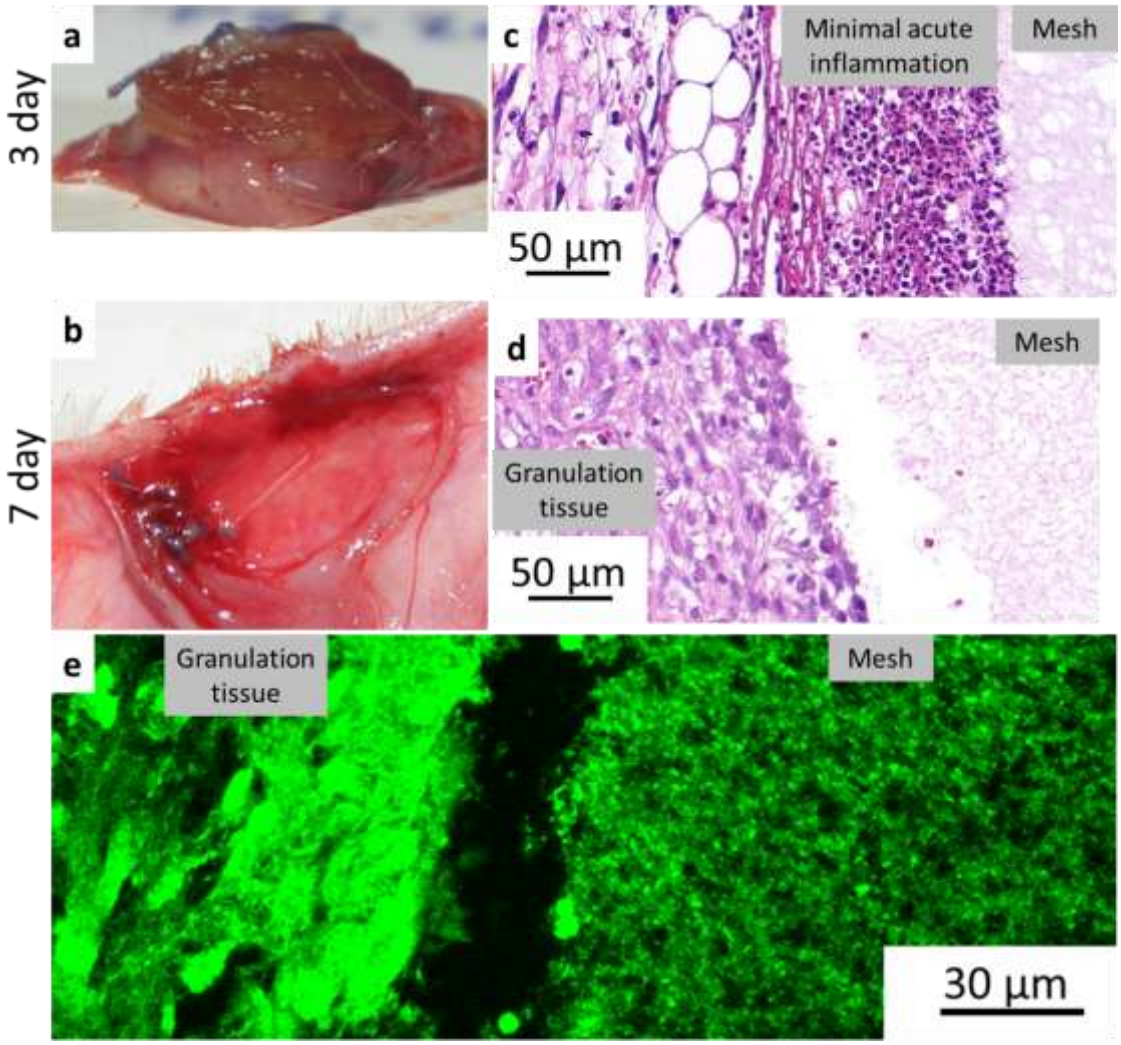


*Figure 65 PASP-CYS sample extracted 3 days after implantation (a) and a representative image from histopathology (c); implantation area without sample after 7 days after implantation (b), a representative image from histopathology (d) and multiphoton micrograph of the same slide (e)*

**Figure 65b** represents results at termination on the 7$^{th}$ day (Group B), where membranes were either not found or were replaced by a soft new tissue. This very soft granulation tissue grew around the stitch used for positioning of the implant however it was easily deformed and removed. Upon cutting it half, there was no evidence for the presence of any remnants of PASP-CYS observable with the naked eye. Furthermore, there were no signs of irritation, infection or foreign body reaction neither on, nor around the samples.

During the histopathology analysis in all cases the central part of the membrane floated off the slide during the staining process, however it was visible and intact near the tissue. The suture material hallmarked the fixation point upon the underlying muscle. In all cases, foreign body type reaction could only be observed around the suture, but not in relation to the membranes. Histology of Group A revealed that there was a thin rim of acute inflammation composed of neutrophil granulocytes and some fibrin in the tissue surrounding the membrane (**Figure 65c**). Scattered histiocytes were also observed in the near tissue. Although membranes were either not visible macroscopically or were diminished in size and covered in new tissue after 7 days post implantation (Group B), they were still visible under a microscope (**Figure 65d**). Granulation tissue composed of fibroblasts and newly formed vessels had developed surrounding the membrane with numerous histocytes present in the close vicinity without any sign of acute inflammation proving the incorporation of the membrane into the native tissue. Also the membranes could be observed with multiphoton microscopy without any special staining (**Figure 65e**). However, native tissue also has autofluorescent property with similar intensity.

### 5.4.2 Implantation of PSI-DAB membranes

In Group A skin closure was intact 3 days post implantation with physiologic wound edge healing. After dissection the samples were easily located between the skin and the underlying muscle and easily moved. Sample consistency changed from paper-like to soft and gelatinous, while their size grew by approximately ~40 % (from the original 16 mm to 21 mm) (**Figure 66a, b**). No visible irritation, infection or foreign body reaction could be observed at the implantation area except only a small amount of fibrinous material.

Samples still maintained their integrity after 7 days post implantation however they were easily torn and dissected into separate layers or truncated by tweezers (**Figure 66c**). Due to the deformation of the samples it was hard to distinguish the samples from the granulation tissue macroscopically. Furthermore, there were no signs of irritation, infection or foreign body reaction.

Histopathology, as in the case of PSI-CYS, foreign body type reaction could only be observed around the suture, but not in relation to the membranes. Group A

showed a more excessive inflammation compared to PSI-CYS samples with a mixture of neutrophil granulocytes, lymphocytes and histiocytes surrounding and invading the membrane (**Figure 66d**). There was also a fibroblastic reaction in the near tissue. In Group B (**Figure 66e**) the acute inflammation is largely reduced and granulation tissue surrounds and grows into the periphery of the membrane. Within the membrane, scattered red blood cells, neutrophil granulocytes, lymphocytes, histiocytes and fibroblasts were also detected. Thanks to the autofluorescent property of poly(aspartic acid) the membranes could be found on the slides from histopathology without any staining (**Figure 66f**). However only separated layers or layers which drifted away from the tissue could be observed since the rest incorporated too much into the new grown tissue.

DOI:10.14753/SE.2018.2178

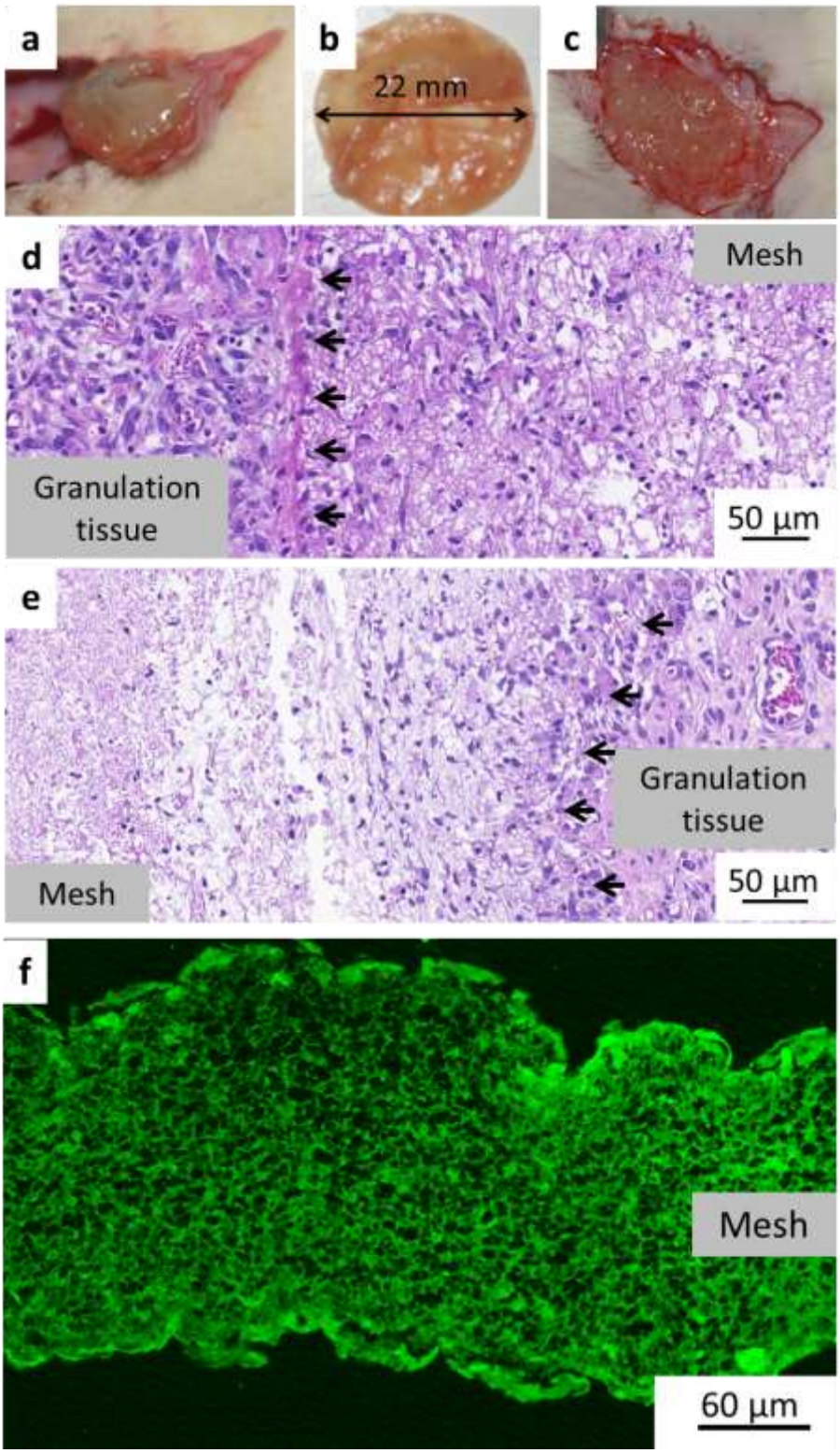


*Figure 66 PSI-DAB sample 3 days after implantation (a), extracted sample grew in size and changed consistency (b), 7 days after implantation (c); representation of histopathology of a sample at day 3 (d) and day 7 (e); slide from histopathology from day 7 under multiphoton microscope. Black arrows indicate the boundary between the sample and the tissue.*

DOI:10.14753/SE.2018.2178

#### 5.4.2.1 Microscopic analysis of PSI-DAB samples 7 days after implantation

To see the exact composition of the PSI-DAB matrix after 7 days, a small sample was taken with a tweezer and investigated by multiphoton microscope without any treatment (**Figure 67a**). Both the fibrous sample and the cells surrounding it were visibly under the microscope glowing in green with similar intensities. Anyhow it is still observable that the fibrous structure of the DAB cross-linked sample was retained.

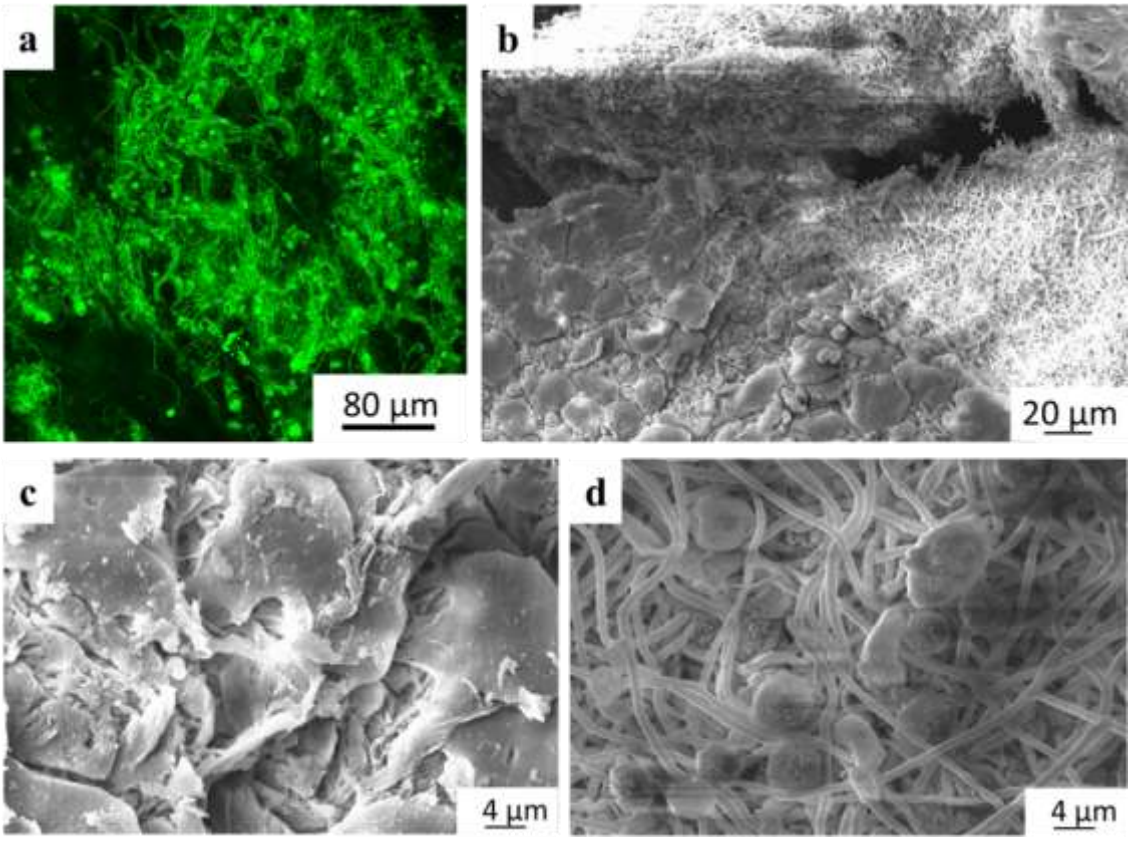


*Figure 67 Multiphoton (a) and SEM (b, c, d) micrographs of PSI-DAB sample from group B*

SEM showed that the sample was covered with flattened cells (**Figure 67b, c**). **Figure 67b** shows an area where the "cellular shell" was discontinued and the fibrous network under became observable. In higher magnification (**Figure 67d**) it can be clearly seen that the fibrous structure was almost intact. Also many spheres were found with 6-8 µm in diameter.

DOI:10.14753/SE.2018.2178

# 6 Discussion

Electrospinning and properties regulating fiber formation have been studied for decades now, thus the general rules that apply to the vast majority of polymer systems have been already established [68]. Therefore, finding all the relations between fiber qualities and processing parameters were not the subject of the research presented in the thesis. The intention was to develop new methods based on electrospinning for the preparation of gelfibers containing cross-linked polymer chains as well as to investigate the responsivity of such hydrogelfiber membranes to external stimuli and the biological reaction upon introduction into small animal models.

As it was described in **Section 2.1** polysuccinimide is a very good candidate both from a chemist's point of view (easy chemical modification) and a biologist's point of view (possible biodegradability). The white powder of PSI used for the experiments was synthesized by the thermal polycondensation of L-aspartic acid. The average molecular weight of the polymer ranged from 22000 to 31000 g/mol (**Section 5.1.1**) and the chemical structure of the final product was proven by both FTIR and NMR (**Figure 33, Section 5.1.4**). Although the molecular weight of PSI may seem low compared to commercially available poly(ethylene oxide), poly(lactic acid), poly(ethylene glycol), etc. as it will be shown in the thesis it is high enough for the preparation of fibers. It is also important to note that the availability of PSI in the market is very limited. For example Shandong Yuanlian Chemical Co., Ltd sells 1 metric ton of PSI for about 4000 USD, which is a good price however their product's quality for biomedical application is questionable.

## 6.1 Preparation of PSI fibers by electrospinning

All the most important setups and compounds for the electrospinning of PSI can be found in **Table 1**. PSI has only 3 known solvents, such as DMF, DMSO and n-methylpyrrolidone [57, 62]. Although several trials were made, electrospinning PSI from DMSO was not successful, only electrospraying, thus particle formation could be achieved. On the other hand, even though DMF has a high boiling point and low vapor pressure, it proved to be a good solvent for fiber formation from PSI. Polymer concentration highly affects electrospinning and fiber properties [120], thus it was

necessary to investigate the optimal polymer concentration for the PSI/DMF system. In line with data available of other polymers/solvent systems in the literature [121], at low polymer concentration (15 w/w% and 17.5 w/w%) only electrospraying occurred while at 22.5 w/w% fibers with beads and finally at 25 w/w% smooth fibers could be prepared (**Figure 28, Table 1**).

PSIsp10 membrane and its fibers were chosen as reference for most of the comparisons of different setups, therefore it was thoroughly investigated by different microscopic techniques. Both light microscope (**Figure 30**), AFM (**Figure 31c**) and SEM (**Figure 32**) showed that the fibers have clean and smooth surface and according to light microscopy have an average fiber diameter of 500 ± 60 nm (**Figure 31a**), which was confirmed by AFM height data as well (550 ± 70 nm) (**Figure 31b**) for samples originated from the same batch of PSI. However, PSI fibers prepared with the same parameters yielded fibers with different average diameters depending on the PSI batch used for preparation. For example the average diameter of PSI fibers used for post electrospinning cross-linking (PSI-DAB) was 911 ± 41 nm, whereas in the experiments related to the effect of collector distance on fiber preparation it was 1.28 ± 0.06 μm (**Table 5**). Since the only difference in the preparation of these samples was in the molecular mass of PSI batches, one can conclude that the reason behind the variety of fiber diameters is the molecular mass of PSI This is supported by the fact that polymer molecular mass affects solution viscosity, polymer-polymer interactions hence electrospinnability and fiber properties [122, 123]. In general, the longer the polymer chains are in a solution, the higher the viscosity which affects electrospinnability similarly to polymer concentration (**Figure 28**). Macroscopically the distance between the collector and needle had impact on overall fiber distribution on collector (**Figure 29**), however its effect on average fiber diameter was not significant for the PSI/DMF system (**Table 5**). With high collector distance the jet has a longer flying time to the collector thus longer time for elongation and solvent evaporation, which leads to thinner fibers [124]. While lower distance leads to higher electric field strength and thus faster jet movement and lower time for the jet to reach the collector which can result in fused fibers due to partial evaporation of the solvents [125]. It seems that the larger the collector distance, the thinner the PSI fibers are which is in a good agreement with the study of Ayutsede *et al*. [124] however the experimental data available for the PSI/DMF

system is not enough for proper justification. As it was expected, both FT-IR and NMR analysis showed that electrospinning did not alter the chemical structure of the polymer (**Figure 33**).

## 6.2 Cross-linked fibers by electrospinning

Electrospun fibrous membranes dissolve rapidly in their solvents due to their high surface area, thus in most of the cases in biomedical application suitable polymers are limited to non-water soluble but biocompatible and biodegradable ones. Therefore, it is necessary to develop techniques by which water soluble polymers can be made available in fibrous forms for this field. One possible way to prevent the fast dissolution of such polymer fibers is to create cross-links between the polymer chains, thus creating a polymer network inside the fibers [109]. Such systems would not dissolve upon immersion into their solution, but uptake the surrounding fluid and swell, hence forming a gel [48]. As it was described in **Section 2.2** hydrogels are very similar to the soft tissue in general, which resemblance could be further enhanced by preparing hydrogels out of hydrogelfibers.

An obvious method for cross-linking during electrospinning (reactive electrospinning) would be to directly mix the cross-linker and polymer in one solution and electrospin it [92]. However as the cross-linking goes on, the viscosity of the solution is continuously rises till it solidifies (gelates) and inevitable blocks the nozzle used for electrospinning [62]. This way only a batch-to-batch electrospinning can be achieved which seriously limits productivity and due to the change in viscosity –as it is important parameter affecting fiber morphology- fiber morphology would be very diverse in one batch [92]. Higher productivity and better control over morphology can be achieved with electrospinning in a continuous way, however up till now not many methods have been developed (**Section 2.3.1**).

Even though there are already means to prepare cross-linked fibers, it is still necessary to develop new methods to make more and more polymers available in fibrous forms for biomedical applications. There are three methods described in this thesis, which are based on PSI but could be used for other polymers if the necessary properties are available. These are based on thiol-disulfide chemistry (**Section 6.2.1**),

heterogeneous cross-linking by immersion of fiber membrane into the cross-linkers solution (**Section 6.2.3**) and coaxial electrospinning (**Section 6.2.4**).

### 6.2.1 PSI-CYS reactive electrospinning

During the reactive electrospinning of PSI-CYSE there are two simultaneous reactions affecting electrospinning and fiber morphology. One is the modification of PSI by CYSE (**Figure 13**) and the second is the formation of disulfide bonds as cross-links between the PSI chains (**Figure 17**). These two reactions could not be separated however there was an optimal reaction time for the modification, after which smooth fibers were formed. Different reaction times were tested to determine the minimum reaction time for the preparation of smooth fibers (**Figure 37**). As the reaction went on the amount of thiol sidechains and inevitably cross-links continuously risen, hence first spheres were electrosprayed then with reaction time of 50 minutes there were enough cross-links and polymer-polymer interaction for smooth fibers to be formed. And thus for the preparation of PSI-CYSE the reaction time was always 50 minutes. In the electrospinning of PSI-CYSE, due to the cross-linking reaction (formation disulfide cross-links) shown on **Figure 17**, the viscosity of the solution in the syringe continuously rose just as in any gelation process. Although the rate of the cross-linking reaction inside the syringe was much lower than in open air, it still affected the viscosity of the spinning solution as well as fiber morphology. With 50 minutes reaction time for the synthesis of PSI-CYSE electrospinning was possible for at least 1 hour, hence it is safe to say that the electrospinning window for this system (time before gelation blocs the nozzle) is 1 hour.

Depending on the batch of PSI-CYSE, its reactive electrospinning had two outcomes: either fibers with beads (**Figure 38a**) or smooth fibers (**Figure 38 b, c and d**) were obtained. The explanation for bead formation is the following: in the flying period of the jet there is a constant elongation leading to thinner and thinner fibers, while the surface tension of the solution is trying to split the jet up into spheres (a similar example is running tap water which splits its stream up into water particles after a certain distance from the tap). This means that at high surface tension electrospraying or fibers with beads are produced. However other solution parameters, such as high viscosity works against bead formation, which in the case of PSI-CYSE continuously

changes. And thus a variety in fiber morphology can be originated from the continuously changing solution parameters in PSI-CYSE.

Average fiber diameter according to AFM was 90 ± 30 nm (**Figure 38e**), while according to SEM it was 850 ± 40 nm (**Figure 38f**). The main difference between the samples used for AFM and SEM, is that AFM samples were collected at the beginning of the spinning process, when the viscosity of the solution is low, (**Section 4.9.2**) whereas in the case of SEM the final membrane was measured (**Section 0**). In the case of SEM, fibers prepared from solution of high viscosity were measured, however small fibers can be still found in SEM samples (**Figure 38c**). Since viscosity directly affects fiber diameter and it rises throughout the spinning window, fiber diameter inevitably changes during the electrospinning process. Tang *et al.* experimented with electrospinning the mixture of poly(vinyl alcohol) (PVA), glutaraldehyde and hydrochloric acid. In their case PVA was cross-linked by glutaraldehyde in acid catalysis both inside the syringe and after the jet left the nozzle. Since cross-linking took place in the syringe they also came to the conclusion that only a batch-to-batch electrospinning can be achieved with a well-defined time interval for the electrospinning of each mixture [92].

Sterilization is essential for implants in medical fields and thus it was important to search for a suitable method for the sterilization of PSI-CYS fiber membranes. The most convenient method is dry heat sterilization where samples are kept at high temperatures for a certain amount of time. However, this method is only applicable in the case of heat resistant materials. Thermoanalytical curves (thermal gravimetric, TGA and differential thermal analysis, DTA) for electrospun PSI (reference) and PSI-CYS indicate structural differences between the fibers (**Figure 39**). It can be seen that in both materials there is a slight reduction in mass accompanied by an endothermic reaction till about 120 $^{o}$C, which can be described by the evaporation of remnants of DMF or absorbed water. This can be also observed on **Figure 39c**, where TG is measured in an open container with conditions during dry heat sterilization, whereas according to the FTIR measurement (**Figure 40**) there was no change in the chemical structure of PSI-CYS after heat treatment. Consequently, dry heat sterilization at 160 $^{o}$C for 120 minutes is a suitable method for sterilization of PSI-CYS membranes.

### 6.2.2 Electrospinning of magnetite doped PSI (PSI OAMagn) and PSI-CYS fibers (PSI CYS OAMagn) - 3D electrospinning

Although results related to PSI and PSI-CYS fibers doped with magnetite were presented separately in the results section, they are discussed together to promote better understanding.

The addition of nano particles into fibrous systems prepared by electrospinning is a widely used technique to obtain membranes with higher functionality since in these cases properties of both fibers and nanoparticles can be incorporated into one system [126–129]. Although the easiest way to trap particles into fibers is to directly mix them into the solution used for electrospinning, it is a rarely used method, since particles tend to aggregate in the presence of high polymer concentrations used in electrospinning.

It is well-known that solution properties can change drastically in these mixtures, as it was in the case with PSI solution and magnetite, since solution viscosity rose to 7 times at 5 w/w% magnetite concentration in PSI-OAMagn3 (**Table 7**) compared to that of the pure 25 w/w% PSI/DMF solution's (**Table 1**). Magnetite influenced electrospinning and the resulting fibrous system as well. In most of the cases clots were found along the fibers, which are supposedly aggregated magnetite particles (**Figure 36**). It is not yet clear whether magnetite aggregated during electrospinning (due to the electric field) or as it was mixed into the PSI solution or it was already aggregated before addition. However, the latter is more probable, since the magnetite used for the experiments was a smudge (after preparing the magnetite the solvent was removed with acetone then a slow drying process was applied). There is no information whether the magnetite in this "dry" state is aggregated or not (nor is it possible to determine), however from a previous experimental work it is known, that it cannot be dispersed in pure DMF [130]. Therefore, it is highly possible, that it stayed in the same state inside the polymer solution as it was before (possibly aggregates), causing the electrospinning to result in fibers with magnetite clots. In the mixture of PSI-CYSE and magnetite there were no clots visible under AFM (**Figure 41**), however this system is more complicated from a chemist's point of view. PSI-CYSE (depending on the grafting ratio) has thiol groups which can be easily adsorbed by magnetite. This method is often used in the surface modification of magnetite [131]. Therefore, the oleic acid (which stabilizes magnetite) can be desorbed from the surface while the thiol groups

and with them the polymer itself can be adsorbed. The size of PSI molecules used for the modification was about 30 kDa (**Section 5.1.1**) which is huge compared to the size of commonly used polymers for stabilization therefore it is highly possible, that one polymer molecule attached to more than one particle [111, 132]. There was definitely interaction between the thiol groups and the particles, since at high thiol concentration (PSI-CYS-OAMagn1, 2) (**Table 7**) the solutions gelated roughly immediately after mixing the components together, prohibiting electrospinning, whereas at lower thiol concentration (PSI-CYS-OAMagn3,4, 5) it was possible to electrospin it. Due to the physical/chemical interactions between the particles and the polymer in solution as well as in the clots, fiber diameter rose in general: for example in the case of PSI-OAMagn3 it was 1.43 ± 0.5 μm (**Figure 36b**) whereas in the case of PSIsp10 where the same polymer concentration was used it was 550 ± 70 nm (**Figure 31b**). Also for PSI-CYS-OAMagn3 the average diameter was 500 ± 100 nm (**Figure 41c**) while for PSI-CYS of the same chemical composition it was 90 ± 30 nm.

Magnetite affected not just the microscopic but the macroscopic structure of the membranes as well. In both systems (with or without thiol groups) there were cases when a loose, 3 dimensional fibrous structure emerged from the collector (**Figure 34, Figure 35, Figure 42**), while in other cases it was only a flat sheet. In the case of PSI-OAMagn3 it even reached several centimeters in height (**Figure 35**). There are only a few articles in the literature related to 3D electrospinning, but the general opinion is that charge accumulation in the fibers is causing fiber-fiber repulsion leading to a loose structure [133, 134]. Systems subjected in this thesis are more complex and cannot be described that easily since there are several properties and interactions that need to be taken into consideration for working out a theory. Just to mention a few, which supposedly affect the resulting structure directly: particle-electric field interactions (given the super paramagnetic property of magnetite); polymer-particle interactions; alteration in solution properties such as viscosity, conductivity etc. due to the addition of particles.

Magnetite is superparamagnetic, which property can be exploited in several fields in medicine ranging from imaging to cell culturing [111, 135]. In all cases, even with low magnetite concentrations, the PSI based magnetite doped membranes could be attracted and deformed by a non-uniform external magnetic field (**Figure 42**) The

mechanical stress induced by magnetic interaction may play a decisive role in efficient cell growing which is supported by many studies explaining that a small and controlled mechanical stresses enhance cell proliferation [136–140]. This combined with the high porosity and real 3D structure of these systems can result in new matrices with high functionality for *in vitro* cell growing.

### 6.2.3 Post electrospinning (PSI-DAB, PSI-CYS-DAB, PSI-THD)

The idea for the implementation of post electrospinning cross-linking was to immerse the fibrous membrane into the solution of cross-linker to prepare cross-links between the polymer chains inside the fibers. To see whether this concept is valid, PSIsp10 membranes were immersed into the solution of 0.5 M DAB/EtOH solution for different time periods and then washed with DMF to check dissolution. After only 10 minutes of cross-linking the samples did not dissolve in DMF as a proof that the cross-linking reaction took place, however the 1 x 1 cm square membranes were deformed compared to the original dry membrane (**Figure 43a, b**). With reaction times longer than 10 minutes, samples maintained their shape without any noticeable difference, and thus one can conclude that the necessary reaction time for cross-linking is at least 10 minutes for this system. Also more than 1 hour immersion time (cross-linking time) yielded similar samples with well retained shape and morphology (**Figure 43c**). Compared to the PSIsp10 used in this series (average fiber diameter was 911 ± 41 nm) the average fiber diameter of PSI-DAB was a slightly smaller 800 ± 30 nm in the case of 10 minutes of reaction time (**Figure 44a, b**). The explanation to the diameter change by about 100 nm could be that DAB is a basic chemical with a $pK_a$ value of 10.80, which might not just cross-link PSI but also hydrolyze it, leading to the reduction in fiber diameter. The success of cross-linking was confirmed by FT-IR analysis (**Figure 61a**).

It was also tested whether it is possible to further cross-link PSI-CYS fibers (CYS is a redox sensitive cross-linker containing a disulfide bond) with DAB, (as a non-redox sensitive or permanent cross-linker). The aforementioned fibrous membranes were immersed into the usual DAB/EtOH cross-linking solution for 3 hours. As it was shown before in the case of PSI-DAB fibers, there was no difference between samples with cross-linking times longer than 1 hour. Therefore, it was decided to immerse the

PSI-CYS membranes into DAB solution for 3 hours to ensure proper cross-linking with DAB. Without DAB cross-linking these membranes would have dissolved due to the cleavage of disulfide cross-links in reducing environment. It is worth mentioning, that macroscopically there was no visible change in the texture of the samples after cross-linking with DAB whereas the fiber diameter did not change significantly (760 ±44 nm) compared to the precursor's average diameter of 850 ± 40 nm (**Figure 45a and b**). This slight decrease in diameter is very similar to the decrease in PSI fiber diameter after cross-linking with DAB and thus the possible cause is the same for this phenomenon. In these double cross-linked samples, the redox sensitive disulfide bonds represent a weak cross-link while DAB a sort of permanent one. Redox sensitivity and its use in materials science will be explained later in **Section 6.3.2.3.** The success of cross-linking in PSI-CYS-DAB was confirmed by FT-IR analysis (**Figure 61b**).

In another case post electrospinning cross-linking was tested with the PSI-THD system where PSI membranes were treated in either 0.5 M THD/EtOH or pure THD for different amount of times. Since the resulting PSI-THD membranes were transformed into PASP based membranes immediately after cross-linking, the relating results are discussed later in **Section 6.3.2.2.**

### 6.2.4 Coaxial reactive electrospinning of PSI and THD

In coaxial spinning, a coaxial nozzle is used, through which a core and a shell solution can be pumped separately and the two solutions get in contact with each other only at the tip of the nozzle (**Figure 19a**) [141]. The idea behind gelfiber preparation via coaxial electrospinning is to feed the cross-linker in the core and the polymer in the shell of the needle. Since cross-linking of polymer only happens when the two solutions get in contact and/or mix together, it would only start as the jet leaves the nozzle. However, with the small diameter of the needle and high viscosity of the solutions in coaxial electrospinning, those two would never mix (laminar flow), which would prohibit the mixing of components, thus gelation. But one must consider that during electrospinning as solvents evaporate (if the cross-linking can happen in a heterogeneous reaction) it might be possible to cross-link the polymer shell as the cross-linker diffuses out from the core. Hence, if the processing parameters of such

electrospinning are set right, a continuous gelfiber formation could be achieved without blocking the nozzle by the gelated polymer matrix [92].

As a reference for comparison, fibers containing only PSI were prepared by pumping only the shell solution in the coaxial needle with an empty core during electrospinning. As shown in the SEM pictures (**Figure 46b**), the PSI fibers were smooth without any major defects. The average fiber diameter was 595 ± 44 nm (**Figure 47g**) in a good agreement with the average fiber diameter obtained from standard, single needle electrospinning (500 ± 60 nm) (**Figure 31a, b**).

In this type of electrospinning, it is critical to choose a sufficient cross-linker as a reactant since the solidification of the cross-linker could cause deformation of fibers or even prohibit proper spinning while the solvents evaporate during electrospinning. Although DAB has been shown to be a good candidate for cross-linking PSI [53], it is in solid crystalline state at room temperature, and thus it would cause problems during electrospinning upon the evaporation of solvents. In contrast THD is a liquid at room temperature, hence it cannot cause problems of solidification upon evaporation of solvent. THD has two primary amine functional groups which can react with PSI chains (**Figure 15b**), eventually forming a cross-linked network (**Figure 46a)**. In coaxial electrospinning the gelation time (the time necessary for the mixed solution to lose its liquid properties) is very important as there is a well-defined time interval for the gelation [51]. The beginning of this narrow time frame is when the two solutions first get in contact at the tip of the nozzle, while the end is when the mixture reaches the target. If gelation is too slow, electrospinning will not result in cross-linked fibers. If it is too fast, the gelated solution might block the nozzle and prevent continuous electrospinning. Gelation time can be adjusted by the amount of cross-linker, but usually there is a critical concentration of cross-linker for gelation. As a rule of thumb one can say that the more cross-linker is mixed in, the faster the gelation gets, although properties of gels (such as elasticity) also changes with the amount of cross-linker [57].

In this case, instead of varying the concentration of THD in core-solution, the amount of cross-linker (0.5 M THD in DMF solution) was changed by applying different feeding rates (**Table 4**). Since the feeding rate of shell polymer solution was fixed, by varying the core feeding rate, the ratio of feeding rate of the core to the shell's was varied as well. Although smooth fibers were obtained with low feeding rate of the

core solution (0.12 ml/h, PSI-THD1, **Figure 47a**), these fibers dissolved in DMF due to the insufficient number of cross-links. At higher feeding rate (0.74 ml/h, PSI-THD3, **Figure 47b**) of the core solution the core and shell solutions broke up at the tip of the nozzle and the spinning of the shell and the spraying of the core took place alternately, resulting in a membrane containing spheres and fibers. At 0.5 ml/h of core feeding rate (PSI-THD2, **Figure 47c, d**) a stable fiber formation resulted in fairly smooth fibers where the membrane did not dissolve in DMF, proving the presence of a sufficient number of cross-links inside the matrix. Hence, the best feeding rate for core was 0.5 mL/h.

Compared to pure PSI fibers (**Figure 46b**), THD slightly changed the morphology of the fibers. A large number of droplets incorporated into fibers could be found in all fibrous matrices containing THD. It can be originated from the jet instability caused by the large viscosity difference between PSI solution (~1.8 Pas) in shell and THD solution in core (~1 mPas) as well as the ongoing chemical reaction during fiber formation. It is also important to note that in PSI-THD2 the presence of cross-linker reduced the average fiber diameter significantly (305 ± 41 nm) compared to the PSI fibers (595 ± 44 nm) (**Figure 47g**). The reduced fiber diameter can be originated from the differences between the core and shell solution, meaning that the same electrical field could elongate more fibers when both solutions were fed into the nozzle.

In order to raise jet stability and eliminate the difference in viscosity between the core and the shell solutions, polyethylene oxide (PEO) was mixed to the cross-linker solution, thus the viscosity of the mixture got closer to the viscosity of shell solution. Previous works indicate that PEO is an ideal candidate to improve the electrospinning process or serve as template to assist the formation of electrospun fibers from unspinnable polymers [142]. After optimization, it was found that 2 w/w% PEO in the core solution could significantly increase jet stability (the viscosity of this THD-PEO mixture was ~60 mPas) and resulted in smooth fibers without beads (PSI-THD-PEO, **Figure 47e, f)**. In addition, PEO also made the spinning process easier to control with less occasions of blockage of nozzle due to gelation. It is important to note, that although cross-linking, hence the opening of imide rings was observable in FT-IR, the characteristic absorption bands of PEO were not observable on the spectra (**Figure 48**). This indicates that PEO is not present at the surface of fibers but trapped inside the core.

This observation was similar to Goncalvez's reports that the core component of PVA inside PLA shell could not be observed by ATR-FTIR [143].

The resultant PSI-THD-PEO fibers showed an average fiber diameter of 320 ± 42 nm, which is only a slight change compared to PSI-THD2 (305 ± 41 nm) (**Figure 47g**). The obtained PSI-THD-PEO fiber membrane did not dissolve in DMF, due to enough cross-links inside the fibers (**Figure 64b**), confirming the successful concept of coaxial reactive electrospinning.

## 6.3 Poly(aspartic acid) based gelfibers and their properties

PSI can be hydrolyzed in alkaline environment (pH>7) creating water soluble poly(aspartic acid) (PASP) (**Figure 20**) [6, 13, 51, 53, 55, 57]. Owing to the peptide-based structure, PASP and its derivatives are good candidates for biological applications, but their solubility in water or in physiological conditions prohibits their use as medical implants. The use of PSI for implantation is also hindered, since dissolution of a PSI based fibrous membrane due to hydrolysis happens in less than one day (**Figure 49**) [53]. This limiting factor can be overcome by incorporating chemical cross-links between the linear PASP chains, as it prevents the dissolution of the material in physiological conditions. Hence upon hydrolysis the resulting PASP based network does not dissolve, but only swells in aqueous environment creating a web of hydrogelfibers. Since PASP is not as reactive as its anhydride PSI, the strategy was to introduce cross-links into the PSI based fibrous systems then turn them into the PASP.

### 6.3.1 PASP based gelfibers with disulfide cross-links (PASP-CYS)

Dissolution of PSI-CYS membranes due to hydrolysis was prevented by the disulfide bonds between the PSI chains inside the fibers. Membranes reached their equilibrium form in pH 8 buffer solution in 15 hours and grew by 2-5 % compared to the original dry form (**Figure 50**). Macroscopically these samples were transparent (**Figure 51a**) and looked very similar to PASP based bulk hydrogels in water (**Figure 51b**). The reason behind this is that the fibrous membrane is composed of swollen PASP gelfibers, which should have similar transparency to that of the bulk gel's in general and there is a high amount of water stored both inside and between the fibers. Light refracts, thus changes direction upon entering into another medium with different index of refraction (Fermat's principle). Naturally the gelfibers and the water between

the fibers have a different refractive index, but due to the low polymer concentration in the fibers those must be very close to each other, which enables transparency.

To ensure that the fibrous structure was retained after hydrolysis, microscopic analysis was carried out on PASP-CYS membranes. AFM enables us to investigate samples in solvents in near atomic resolutions. However, the floating fibers often stuck to the cantilever or moved away from the surface preventing proper imaging. Therefore, for AFM analysis samples were always washed with ultrapure water and carefully dried onto cover glasses before analysis. AFM suggested that the fibrous structure was retained after hydrolysis, however due to the adhesion of fibers during the drying process it was not possible to determine whether fibers were separated, deformed or fused together (**Figure 52**). To investigate the real structure of the fibrous membrane, SEM analysis was carried out on previously washed and freeze-dried samples. As it can be seen on **Figure 53** the fibrous structure was partly retained, with fibers fused together and deformed during hydrolysis. The reason behind this can be that there are enough cross-links formed during reactive electrospinning for the samples not to dissolve, however not enough for the fibers to retain their clean fibrous form (notice the bulks at the fiber junctions in **Figure 53**). This is a very common problem of hydrogelfiber membranes since in most of the cases fibers are deformed and fused after immersion into PBS or simple distilled water [54, 92, 93, 109, 144, 145]. However, it is possible to retain the complete fibrous structure of the hydrogelfibers upon immersion into water as it was shown by Knierim et al. In their work, they coated the PVA fibers with poly(p-xylylene) by chemical vapor deposition method. According to their article the fibrous structure was completely maintained [146].

All in all PASP-CYS membranes can be still considered as fibrous membranes, thus the objective of preparing PASP based hydrogelfibers by the thiol-disulfide chemistry based reactive electrospinning was successful.

### 6.3.2 PASP based gelfibers by post electrospinning cross-linking

In post electrospinning cross-linking, the polymer network is created posterior to electrospinning inside the fibers. In this section results related to PASP based gelfibers synthesized by post electrospinning cross-linking are discussed.

#### 6.3.2.1 PASP based gelfiber membranes with DAB cross-links and their pH responsivity

PASP-DAB samples were prepared by the hydrolysis of PSI-DAB membranes. Samples were prepared by two ways: in “route a” after cross-linking of PSI-DAB samples they were immediately washed in ultrapure water then placed in pH 8 buffer solution for hydrolysis, whereas in “route b” after cross-linking of PSI-DAB samples, they were washed with DMF thoroughly then put into pH 8 buffer solution(**Figure 21**). In “route a” washing with ultrapure water did not dissolve the non-cross-linked polymer, and thus cross-linking might have continued during washing and hydrolysis; but in “route b” the non-cross-linked polymer and the remnants of DAB were immediately washed away, preventing further cross-linking during hydrolysis. This difference between the two routes was observable at 10 minutes of cross-linking time, where after hydrolysis the sample from “route a” was a very soft, slightly opaque sheet (**Figure 54a**), while “route b” resulted in a smaller, distorted sample (**Figure 54b**). This difference diminished at cross-linking times longer than 1 hour where samples from both routes looked the same swollen opaque quadrangles with slightly bigger size (approximately 5 %) (**Figure 54c and d**). One can conclude that with 0.5 M DAB/EtOH solution a minimum of 10 minute of cross-linking time is necessary to retain the PSI membrane’s macroscopic morphology after hydrolysis. The chemical structure and the success of hydrolysis was confirmed by FT-IR analysis (**Figure 61a**).

Although cross-linking alone did not change fiber morphology in PSI fibers (**Section 6.2.3, Figure 44a and b**), hydrolysis did. As evidenced by SEM on washed and freeze-dried PASP-DAB samples (with 1 hour cross-linking time) fusion of fibers happened in two ways: in a very few cases fibers fused into flat sheets where fibers were parallel and touched each other (**Figure 56a**) or created an interconnected fibrous structure with connection point where fibers touched each other in any other degree (**Figure 56b**), supposedly both happening during hydrolysis. Zhang et al. reported a similar method for the post electrospinning cross-linking of PSI fibers with 1,2-diaminoethane in methanol solution, where, due to hydrolysis, the fibrous structure was severely damaged [83]. In contrast to their work, cross-linking with DAB proved to be a better option for retaining the fibrous structure of PASP-DAB. Juriga et al. recently reported the auto fluorescent property of PASP based bulk hydrogels [53]. This was also

tested on PASP-DAB fibrous membranes, where they showed the same autofluorescent property (**Figure 67a**).

PASP shows pH sensitive character due to carboxylic groups on the polymer repeating units. The pH responsivity of PASP-DAB was tested using disks of 3 different initial sizes (**Figure 62a, d, g**). After cross-linking and hydrolysis in pH 8 buffer solution those turned into PASP hydrogel disks and swelled significantly while in the next step in pH 3 buffer solution they shrunk. The area of the disks were calculated and it turned out that the swelling and de-swelling was repeatable throughout the 4 cycles of buffer changes (**Figure 63a**). While the described pH responsivity of PASP-DAB membranes is in line with the behavior of PASP based bulk hydrogels [48] there was one aspect where a difference was found. Swelling ratios of the disks are collected on **Figure 63b** and **Table 8** which suggest that the bigger the average initial size of a disk is, the smaller the average of the relative change in the size of the gel disk. In other words, the bigger the disk is, the smaller the change between the swollen and the de-swollen states. However the swelling degree of a hydrogels of the same composition is independent of the initial size [13, 147]. It is also important to note that the bigger the gel disk is, the more time it needs to reach its equilibrium size during swelling and de-swelling [13, 148]. And thus there can be two possible explanations to why the fibrous membranes behaved differently compared to bulk gel disks: either the fibrous membranes did not have enough time to reach their equilibrium size during the measurements or the structural difference between bulk gels and fibrous gels caused it. However the smaller a hydrogel is, the faster it reaches its equilibrium size, therefore in the case of hydrogelfibers of the size of PASP-DAB used in the experiment, 24 hours is more than enough to reach equilibrium [13]. Therefore, the possible explanation is that the gel disk composed of fibers swells slightly differently compared to bulk hydrogels.

#### 6.3.2.2 PASP based gelfibers with THD cross-links (PASP-THD)

Although THD (**Figure 19**) and DAB (**Figure 16**) are quite similar molecules, their applicability in post electrospinning cross-linking was different. Cross-linking in a heterogeneous reaction with 0.5 M THD/EtOH only yielded fiber membranes which dissolved upon hydrolysis in pH 9 buffer solution due to the insufficient number of cross-links. However, treatment of PSI fiber membranes with pure THD resulted in

membranes which did not dissolve after hydrolysis. Upon inspection with SEM, it was found that although 1 hour reaction time was enough to maintain the integrity of samples, the fibrous structure was almost completely diminished. Only flattened and fused "fibers" could be found (**Figure 59a**). At two hours a better fibrous structure was found, however there were still fusion and damage of the fibers (**Figure 59b**), while 3 hour reaction time yielded a fine fibrous structure (**Figure 59c**). And thus THD is another possible cross-linker for post electrospinning cross-linking of PSI fibers [54].

#### 6.3.2.3 Double cross-linked PASP based gelfiber membranes in oxidized (PASP-CYS-DAB) and reduced state (PASP-CYSE-DAB)

Double cross-linked PSI-CYS-DAB fibrous membranes did not dissolve upon hydrolysis leading to the conclusion, that there were enough cross-links in the membrane. During hydrolysis membranes changed their texture into slightly opaque ones (**Figure 57a**), while according to SEM their fibrous properties were retained (**Figure 57b, c**). It was previously shown, that upon hydrolysis PSI-CYS fibers fuse together (**Figure 53**), while in this case, PSI-CYS-DAB fibers retained their morphology. The solely DAB cross-linked fibers also yielded PASP based fibers with better morphology (**Figure 56**), and thus no wonder the addition of DAB cross-links into this system helped. The change in the chemical structure upon hydrolysis was confirmed by FT-IR analysis (**Figure 61b**)

Disulfide bridges are widely used redox sensitive cross-links in drug delivery, since those can be cleaved via reduction by glutathione *in vivo* or by D,L-dithiothreitol (DTT) *in vitro* (**Figure 22**) [149]. *In vitro* DTT can be used to mimic the reducing environment in the body caused by the increased glutathione level. This way gel carriers can be prepared with programmable dissolution [55]. However, this property in the case of long term implants (more than 2 weeks) is not welcome, since materials solely based on disulfide bridges, just as the one reported by Juriga et al., might dissolve too early, leading to complications [53]. If there is another non-redox sensitive cross-link in the system, the implant would not dissolve, only thiol side-chains would be created only inside the matrix, which could be used as a tool for mucoadhesion *in vivo* [150] or cell adhesion enhancement *in vitro* [53] and drug conjugation via thiol groups [151]. In PASP-CYS-DAB fibrous membranes DAB represents the permanent cross-link which

cannot be cleaved by DTT, and thus by immersion of PASP-CYS-DAB membranes into DTT solution, PASP-CYSE-DAB was obtained (**Figure 22**). According to SEM, although the fibrous structure was mostly retained (**Figure 58a, c**), there were sites where fibers adhered together, creating bundles (**Figure 58b, d**). FT-IR analysis of PASP-CYSE-DAB could not prove the success of the reduction, since neither disulfide nor thiol groups are observable by this technique (**Figure 61b**). In conclusion, chemically stable, fibrous, hydrogel membranes could be prepared with thiol groups embedded by the incorporation of reactive electrospinning, post electrospinning cross-linking and further treatments. As Juriga et al. showed bulk hydrogels of similar chemical structure could be applied in *in vitro* cell culturing excellently [53], which might be further enhanced by switching from bulk matrices to fibrous membranes.

### 6.3.3 PASP-THD based gelfibers via coaxial electrospinning and their pH responsivity

Both PSI-THD2 and PSI-THD-PEO could be hydrolyzed into PASP-THD2 and PASP-THD-PEO respectively without any change to their integrity. In the case of PASP-THD2, fused or connected fibers with porous structure were observed with a thin layer of polymer sheet between them (**Figure 60**). The presence of polymer sheet suggests an incomplete cross-linking during electrospinning, which is present at different degrees in all the prepared fibrous samples. One of the reasons for this phenomenon can be that the cross-linker does not have enough time during electrospinning to fully cross-link the whole fiber mass. Therefore, after dipping the fibers into solutions for hydrolysis, while dissolving, the cross-linking can continuously happen inside the fibers resulting in the sheets between the fibers. Also, as there is laminar flow in the syringe there is no mixing of the two solutions. This way cross-linking can only happen at the surface of the two solutions, unless the cross-linker diffuses into the shell solution during electrospinning.

In the first step of the preparation of PASP-THD-PEO, PSI based samples were washed with DMF. After merging the dry electrospun PSI-THD-PEO membranes ($3.03 \pm 0.13$ cm$^2$) (**Figure 64a**) in DMF, membranes shrunk until the unreacted chemicals were washed out and the fibrous sheets got into equilibrium state with their surroundings ($1.28 \pm 0.05$ cm$^2$) (**Figure 64b**). However, in pH 9 buffer solution, as the

hydrophobic PSI based gels turn into hydrophilic PASP based gels, they swell significantly (~39% area change) and become transparent (**Figure 64c**). These PASP-THD-PEO samples looked like bulk gel sheets macroscopically, while SEM on freeze-dried sample showed that although there were connected and fused fibers, the fibrous structure remained after hydrolysis (**Figure 64e, f**). As opposed to PASP-THD2 there were no flat sheets between the fibers which can be explained either by the fast washing with DMF (thus the remaining cross-linker does not have time to cross-link during hydrolysis), or the presence of PEO stabilizes the samples during hydrolysis or both. It is also important to note that the low pore size between fibers in electrospun samples can be a limiting factor in their usage in *in vitro* cell culture, because cells usually settle at the surface of such samples rather than penetrating into them [152]. There were several successful attempts to raise pore size in electrospun membranes based on self-assembly [153], templates [154], alternating current electrospinning [155], etc. In those methods high porosity is obtained via electrospinning directly, while in the case of PASP-THD-PEO due to chemical treatment as fibers fused together. All in all, both fiber diameter and pore size (between fibers) grew significantly in PASP-THD-PEO membranes which can enable cell mobility inside the membrane. Therefore, the highly porous structure of gelfibers is favorable for cell migration inside the matrix, as the pore size in these samples is comparable with the size of cells (~10-30 μm) [156].

PASP based gels show volume change upon change in environmental pH due to the different protolithic state of carboxyl groups on the polymer backbone. Accordingly, samples were in a swollen state (in the maximum size of 7.37 ± 0.11 $cm^2$) in alkali medium (pH 9, **Figure 64c**), while in acidic environment they shrank (5.04 ± 0.07 $cm^2$, pH 4, **Figure 64d**), which is in good agreement with the behavior of PASP based bulk gels [13]. It is interesting to note that the size change of randomly deposited fibers inside the sample can cause a 39% size change macroscopically in the whole area of the sample, which was reproducible throughout the 4 cycles (**Figure 64g**). It was expected to see change in the transparency of samples in different states, however as seen with naked eye, there was no difference between the swollen or the shrunken state.

DOI:10.14753/SE.2018.2178

## 6.4 Comparison of electrospinning based methods for preparation of gelfiber membranes

Three different methods are represented in the thesis for the electrospinning based preparation of hydrogelfibers: reactive electrospinning based on thiol-disulfide cross-linking (**Section 6.2.1**), post electrospinning cross-linking (**Section 6.2.3**) and coaxial nozzle based reactive electrospinning (**Section 6.2.4**). For better understanding important properties of these methods are collected on **Figure 68**.

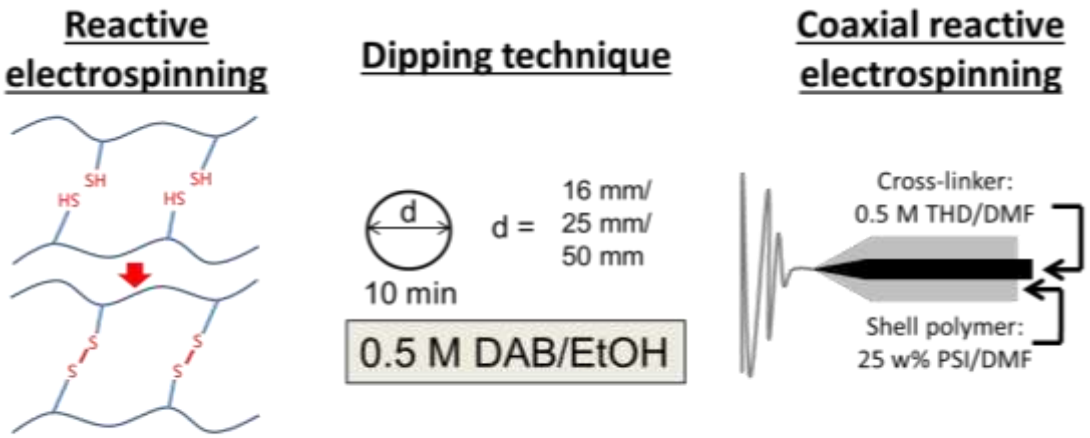


| | Reactive electrospinning (S-S) | Dipping technique | Coaxial reactive electrospinning |
|---|---|---|---|
| Cross-links | YES | YES | YES |
| Preparation type | Batch-to-batch | Batch-to-batch | Continuous |
| Hydrogel fibers | YES | YES | YES |
| pH responsivity | NA | YES | YES |

*Figure 68 Comparison of the three methods discussed in the thesis for the preparation of gelfibers based on electrospinning*

One of the main objectives of the research was to develop methods for the synthesis of fibrous membranes containing polymer networks. All three methods proved to be fit for this purpose since the prepared membranes did not dissolve in their solvents after preparation, they only swelled.

Viewing the productivity of gelfiber preparation, while electrospinning of PSI is continuous, cross-linking of PSI with DAB or THD happens after electrospinning, and thus the preparation of PSI-DAB / PSI-THD can be also considered a batch-to-batch

synthesis. Just as the preparation of PSI-CYS, since electrospinning of PSI-CYSE is also batch-to-batch. In contrast,the coaxial nozzle based reactive electrospinning could be maintained in a continuous way which raises productivity significantly.

Although hydrogel membranes could be prepared by the hydrolysis of PSI based cross-linked membranes, depending on their origin the resulting samples were different in their microscopic structure. Both reactive electrospinning based on thiol-disulfide reaction and coaxial based reactive electrospinning yielded fused fibers in different degrees, while post electrospinning cross-linking with DAB resulted in a well-retained fibrous morphology. Also, combining the standard reactive and post electrospinning method resulted in better fibrous morphology proving the superiority of post electrospinning cross-linking in the matter of microstructure.

pH responsivity of the PASP based membranes was only tested thoroughly on PASP-DAB and PASP-THD-PEO systems. In both cases samples showed pH dependent macroscopic volume change similar to that of PASP based bulk hydrogels' reported in the literature [13].

## 6.5 In vivo biocompatibility and biodegradability of PSI-CYS and PSI-DAB samples

The purpose of the animal experiments was to investigate the medical applicability of PSI-CYS and PSI-DAB based membranes as well as to see their biocompatibility and biodegradability. From a surgeon's point of view suturability (the possibility to suture an implant to fix it at a location) and easy handling (the ability of the implant to withstand the surgical procedure without paying too much attention to the material's wellbeing) are the two most important properties required from an implant. The most important results of the *in vivo* studies are collected in **Table 9**. Handling was easy for both materials and they were implanted without any complication as well. However, problems could arise from the long term storage of these implants. Not especially with PSI-CYS, which could be stored in a sealed container for a long time after sterilization, but with PSI-DAB, which cross-linking and washing/sterilization should be carried out directly before surgery to prevent damage of the fibrous network and the separation of membrane layers. Anyway fixation with suture was also successful without any considerable damage to the implant. Albino rats are commonly

used animals for this purpose, since this animal model has a huge literature with well-defined protocols and are big enough for testing small implants [157–160].

*Table 9 Comparison of the in vivo performance of PSI-CYS and PSI-DAB*

| | | ***PSI-CYS*** | ***PSI-DAB*** |
|---|---|---|---|
| ***IMPLANTATION*** | *Handling and surgery* | *Good suturability and easy handling* | *Good suturability and easy handling* |
| ***3 DAY*** | *Macroscopic result* | *Hydrolysis and swelling by approximately 40 % in size* | |
| | *Biocompatibility* | *Mild accute inflamation and foreign body type reaction* | |
| | *Biodegradation* | *No observable degradation* | |
| | *Tissue invasion* | *No tissue invasion according to histopathology* | *No tissue invasion according to histopathology Attachment of cells to the surface of the samples* |
| ***7 DAY*** | *Macroscopic result* | *Samples either not found or completely covered and incorporated by new tissue* | *Samples lost their integrity and strength Easy trucation by tweezers* |
| | *Biocompatibility* | *Low inflamation and foreign body type reaction* | |
| | *Biodegradation* | *Although degradation was observable macroscopicaly, histopathology showed the remnants of fibrous samples at implantation area* | *Degradation was not observable, however the loss of mechanical strength and integrity indicates it* |
| | *Tissue invasion* | *No* | *Cells invaded the samples for several millimeters Incorporation of samples into the granulation tissue* |

Both types of samples were easily handled by the surgical team. There were no complications during implantation where samples were fixed with one suture each to the back side of the neck muscle (nuchal ligament), under the skin (*sub cutan*) (**Figure 26**). During the implantation the suturability of the membranes was excellent and neither the sutures was torn out, nor the membranes were damaged. Without sutures fixing the samples into one location, in the case of biodegradation it would have been impossible to tell where the samples were previously positioned. However, based on previous experiments (not yet reported) and journal articles from other groups it can be said that often the suture material causes complications instead of the actual implant [161, 162]. During the 3 days (Group A) and 7 days (Group B) observation there were neither visible irritations, nor misbehavior of the animals or any other complications visible to the naked eye. The animals behaved just as they did before surgery: normal food intake, mobility and behavior with the caretakers.

3 days after implantation (Group A) animals were terminated and investigated at the implantation area. In every case, both PSI-CYS (**Figure 65a**) and PSI-DAB (**Figure 66a, b**) samples could be found in their respective animals with natural wound healing and without any observable complication. However both types of samples grew in their size by approximately 40% in diameter and turned from the implanted white paper-like membranes (**Figure 26a**) to soft swollen gels. In the case of PSI-DAB the same size change can be observed *in vitro* as PSI-DAB undertakes hydrolysis in pH 8 buffer solution and grows in the same degree, from 16 mm original diameter to 21 mm (**Figure 62a, b**). This strongly suggests that hydrolysis of PSI based systems indeed occur *in vivo,* which is the first step in the biodegradation of PSI based materials. During hydrolysis gels swell and create a pressure, which can be used for example to create excessive skin tissue for plastic surgery [157]. PSI-CYS and PSI-DAB clearly swelled during hydrolysis, but they were not causing any irritation in the animals macroscopically nor creating excessive skin tissue. It is also noticeable on **Figure 65a** and **Figure 66a, b** that after hydrolysis *in vivo,* the hydrogel membranes were discolored and not transparent compared to the corresponding samples hydrolyzed *in vitro*.

When a foreign object is implanted into a body, its natural response is the so called foreign body reaction [163]. Usually it is a mild inflammation with granulocytes

and hystiocytes trying to restore the damaged area to its natural state for example by attacking or simply segregating the foreign object in a capsule (fibrosis) [164]. Although there is always a foreign body reaction and mild inflammation after any operation it is highly desirable to keep it to a minimum level. The Hematoxylin-Eozin staining used for the evaluation of the slides is a two-component staining system. In very short Hematoxylin is basic/positive and stains the nuclei of a cell with blue by binding to DNA, while Eozin is acidic/negative and binds to positively charged substances and amino acid side-chains (cytoplasm in muscle cells, mitochondria, red blood cells etc.) and marks them pink or red [165]. Histopathology showed that there was acute inflammation in the tissue surrounding both types of samples proving a natural response of the animals to the implants. However, in neither case was this inflammation considerable as a strong reaction. PSI-CYS samples were easily found on the slides in a rim of new tissue surrounding it, and thus showing natural healing (**Figure 65c**), but it seems that fibrin (new tissue) did not invade the membrane. To PSI-DAB the reaction of the body was stronger, while fibrin, granulocytes and hystiocytes invaded the side of the membrane, making it difficult to distinguish the original tissue, the new tissue and the implant. On **Figure 66d** the black arrows indicate the supposed boundary between the sample and the tissue whereas both the new tissue and the fibrous matrix were stained red. Also there are small blue circles in the membrane side of the slide indicating the invasion of granulocytes into it.

Although results similar to 3 days were expected after 7 days in Group B as well, significant differences were found between PSI-CYS and PSI-DAB samples. In the case of PSI-CYS membranes (or in this state PASP-CYS samples) those were either not found or a soft new tissue replaced them (**Figure 65c**). This very soft granulation tissue grew around the stitch but it was easily deformed and removed. Upon cutting it half, there was no evidence for the presence of any remnants of PASP-CYS observable with the naked eye leading to the conclusion that these samples degraded and dissolved in 7 days. As opposed to this PASP-DAB samples were found in a swollen but softer and more fragile state than after 3 days (**Figure 66c**). These samples were easily torn and dissected into separate layers or truncated by tweezers suggesting high reduction in physical strength and consistency. Due to the deformation of the samples and incorporation of surrounding tissue, it was hard to distinguish the samples from the

granulation tissue macroscopically. Furthermore there were no signs of irritation, infection or foreign body reaction neither on nor around the PSI-CYS and PSI-DAB samples (**Figure 65b**, **Figure 66c**), which is a very good results given, that most complications arise from irritation caused by implants.

Although macroscopically PSI-CYS was impossible to find in the implantation area after 7 days, histopathology showed that there was still a fibrous substance (supposedly the PSI-CYS matrix) with a new fibrinous tissue surrounding it (**Figure 65b**). In this state it seemed that the mild inflammation was completely gone and parallel with this vascularization took place, and thus the formation of new blood vessels had already begun. For PSI-DAB samples histopathology showed an excessive drop in the acute inflammation observed on the 3$^{rd}$ day post-implantation. Also the incorporation of the new tissue into the sample evolved into a stage where the boundary between the sample and new tissue was almost impossible to mark exactly (**Figure 65e**).

To see the exact composition of the PSI-DAB matrix after 7 days, a small sample was gathered with a tweezer and investigated by multiphoton microscope without any treatment (**Figure 67a**). Since PSI and PASP based polymers show autofluorescent properties, it was not necessary to dye the sample for investigation [53]. Both the fibrous sample and the cells surrounding it were visible under the microscope glowing in green with similar intensities, and thus it was not possible to distinguish the two properly by digital subtraction. It is still observable that the fibrous structure of the DAB cross-linked sample was retained. Compared to the PASP-DAB samples prepared *in vitro* a similar fibrous structure can be found under the multiphoton microscope just without the cells (**Figure 56c**).

In the natural healing process in the case of implants or any foreign object a new granulation tissue covers and/or invades the sample. This phenomenon was also observable on the SEM pictures of PASP-DAB samples retrieved 7 days post implantation (**Figure 67b, c**), where the cells were flattened out possibly due to the sample preparation process. It is impossible to tell the cell type at this stage, however the most common cells observable at healing wounds and foreign body reaction are fibroblasts [163]. It is also observable on **Figure 67d** that under the cellular shell the fibrous structure was intact without any observable degradation or change in its

morphology. It is also comparable with the fibrous structure of PASP-DAB membranes prepared *in vitro* (**Figure 56a, b**). Furthermore many spheres were found with 6-8 μm in diameter suggesting the presence of either granulocytes or red blood cells inside the matrix close to the surface which is understandable given that histopathology showed vascularization of this type of sample (**Figure 65e**).

### 6.5.1 Role of chemical structure in biological response to PSI-CYS and PSI-DAB based membranes

The main difference between the two samples is in their chemical composition as PSI-CYS contains disulfide bridges as cross-links, which are easily cleaved in the appropriate reducing environment, while in PSI-DAB the cross-linker is more stable compared to the disulfide bridges in PSI-CYS [6]. Although the disappearance of PSI-CYS in less than 7 days would suggest biodegradation, PSI-DAB contradicts it as it did not disappear, which strongly suggests that the reason behind this is the cleavage of disulfide bridges and dissolution of the matrix. However, it is still necessary to conduct a long term experiment involving PSI-DAB to see whether it biodegrades or not. To conclude the *in vivo* experiments one can say that: PSI based systems hydrolyze and swell *in vivo* turning into the corresponding PASP based systems; PSI-CYS degrades under 7 days implanted under the skin although the mechanism has yet to be clarified; PSI-DAB maintains its physical form after 7 days implanted under the skin showing reduction in physical strength and consistency and thus showing signs of degradation.

*In vitro* study on the enzymatic biodegradability of PASP-DAB, PASP-CYS bulk hydrogels was carried out by Juriga *et al*. They showed that PASP-CYS bulk hydrogels degrade in *collagenase type 1* and also in minimal essential media used for cell cultivation while PASP-DAB hydrogels retain their size and form in both of those environments. Their experimental results completely support our findings on the biodegradability and compatibility of PASP-DAB and PASP-CYS *in vivo*.

DOI:10.14753/SE.2018.2178

# 7 Conclusion

In this section the new scientific accomplishments are collected in the following points:

T1. Important parameters in the preparation of polysuccinimide fibers by electrospinning were assessed.

T2. Cross-linked polysuccinimide fibers were prepared by immersing polysuccinimide fibers into the solution of cross-linker's solution post-electrospinning.

T3. Development of a reactive electrospinning strategy based on thiol-disulfide chemistry using a modified polysuccinimide with thiol side-groups.

T4. Preparation of fibrous membranes with real 3D structures were based on the thiol-disulfide reactive electrospinning and the addition of magnetic particles.

T5. Continuous cross-linked fiber preparation was developed based on coaxial reactive electrospinning.

T6. pH sensitive poly(aspartic acid) based gelfiber membranes were successfully prepared.

T7. Polysuccinimide based cross-linked fibrous membranes (-S-S- and DAB) goes through hydrolysis *in vivo* and are biocompatible.

DOI:10.14753/SE.2018.2178

# 8 Summary

Polymeric, fibrous membranes prepared by electrospinning are emerging materials in biomedicine. However, there is still need for new polymers involved in research. Poly(amino acids) with their peptide like chemical structure show biocompatibility and biodegradability and thus they are perfect candidates for bio-based material research. However, poly(amino acids) are water soluble, that severely hinders their application in electrospun medical implants since they immediately dissolve in contact with the aqueous based biological fluids. Therefore the main objective of my research was to develop methods -based on electrospinning- that enable the use of water soluble polymers, specifically poly(aspartic acid) and its derivatives as fibrous membranes for implantation. In this work first fiber formation of polysuccinimide was optimized and then three methods were developed for the preparation of cross-linked polysuccinimide and - by their hydrolysis - cross-linked poly(aspartic acid) based fibrous membranes: a post electrospinning method, where the previously prepared fibers were dipped into the cross-linkers solution (DAB, THD); a reactive electrospinning based, where the thiol group (CYSE) modified polysuccinimide created cross-links during electrospinning; a continuous method based on coaxial electrospinning, where the cross-linker (THD) was fed into the core and the polymer into the shell of the needle. Also, by the addition of magnetite particles into the electrospinning solution, membranes with real 3D structure were created (in cm size).

The poly(aspartic acid) based cross-linked membranes showed similar pH sensitivity to bulk hydrogels of similar chemical structures: the fibrous membranes overall size got smaller in acidic pHs whereas in alkali pH they grew (through several cycles). The biocompatibility and biodegradability of two cross-linked polysuccinimide based systems were tested *in vivo* in albino rats. These experiments showed mild foreign body reaction and tissue invasion into the membranes after one week as well as proved the hypothesis that polysuccinimide undergoes hydrolysis in biological environment.

The developed methods can be generalized for other polymeric systems broadening the available water soluble polymers for fibrous implants. Also the developed poly(aspartic acid) based fibrous membranes could be good candidates for drug delivery, implantation, cell culturing and other biomedical applications.

DOI:10.14753/SE.2018.2178

# 9 Összefoglalás

Elektrosztatikus szálképzéssel készített polimer szálak egyre előkelőbb helyet foglalnak el az orvos-biológiai kutatásokban, ezzel egyre nagyobb igényt teremtve új polimerekre amelyek alkalmasak a szálképzésre. A poli(aminosavak), a fehérjékhez hasonló kémiai felépítésükkel, kiváló biokompatibilis és biodegradábilis alapanyagok lehetnek az orvosi célú fejlesztésekhez. Azonban többnyire vízoldhatóak, amely tulajdonságuk meglehetősen korlátozza használhatóságukat, mint szálas implantátumok, mivel biológiai folyadékokkal érintkezve azonnal feloldódnak. Ezért a kutatásom fő célja olyan új elektrosztatikus szálképzésen alapuló stratégiák fejlesztése, amelyek lehetővé teszik poli(aminosavak), pontosabban a poli(aszparaginsav) alapú szálas, implantálható membránok készítését. Ebben a munkában megvalósítottam és optimalizáltam a poliszukcinimid szálképzését, mely a poli(aszparaginsav) anhidridje. Kidolgoztam három, e polimerre épülő módszert térhálós poliszukcinimid, valamint hidrolízisével poli(aszparaginsav) alapú szálas szövetek előállítására, melyek a következők: keresztkötések létrehozása szálképzést követően a szálak keresztkötő oldatába való áztatásával (DAB, THD); reaktív elektrosztatikus szálképzés, ahol a tiol (CYSE) oldalcsoportokat tartalmazó polimeren szálképzés közben diszulfid hidak keletkeznek; folytonos reaktív elektrosztatikus szálképzés koaxiális tűvel, ahol a keresztkötőt (THD) magfolyadékként, míg a polimert köpeny folyadékként tápláltam. Továbbá, a szálképzéshez használt oldatokhoz mágneses részecskéket adagolva, valós 3D kiterjedéssel rendelkező szöveteket hoztam létre (néhány cm vastagságig). A poli(aszparaginsav) alapú szálas szövedékek pH indukált duzzadási tulajdonsággal rendelkeztek: a szövedékek mérete savas környezetben csökkent, míg lúgosban nőtt (több cikluson keresztül). Két, kémiai összetételében eltérő szövedék *in vivo* biokompatibilitását és biodegradábilitását vizsgálva kiderült, hogy a poliszukcinimid alapú szövedékek a szervezetben hidrolizálnak, valamint egy hetes megfigyelés alatt enyhe idegentest reakciót indukálnak.

A kutatómunkában kifejlesztett stratégiák alkalmasak lehetnek más polimer rendszerek esetén is, így elérhetővé tehetik a vízben oldódó polimereket is mint szálas implantátumok. Továbbá a kifejlesztett poli(aszparaginsav) alapú szövedékek kiváló alapanyagok lehetnek, mint implantátumok és gyógyszerhordozó rendszerek az orvostudományban.

# 10 References

1. Sosnik A, Das Neves J, Sarmento B (2014) Mucoadhesive polymers in the design of nano-drug delivery systems for administration by non-parenteral routes: A review. Prog Polym Sci 39:2030–2075.

2. Tawakkal ISMA, Cran MJ, Miltz J, Bigger SW (2014) A review of poly(lactic acid)-based materials for antimicrobial packaging. J Food Sci. doi: 10.1111/1750-3841.12534

3. Fonseca AC, Gil MH, Simões PN (2014) Biodegradable poly(ester amide)s - A remarkable opportunity for the biomedical area: Review on the synthesis, characterization and applications. Prog Polym Sci 39:1291–1311.

4. Tabata Y (2009) Biomaterial technology for tissue engineering applications. J R Soc Interface 6:S311–S324.

5. Kai D, Liow SS, Loh XJ (2015) Biodegradable polymers for electrospinning: Towards biomedical applications. Mater Sci Eng C 45:659–670.

6. Zrinyi M, Gyenes T, Juriga D, Kim J-H (2013) Volume change of double cross-linked poly(aspartic acid) hydrogels induced by cleavage of one of the crosslinks. Acta Biomater 9:5122–31.

7. Boross L, Sajgó M (1993) A biokémiai alapjai, 2. kiadás. Mezőgazda Kiadó, Budapest

8. Thombre SM, Sarwade BD (2005) Synthesis and biodegradability of polyaspartic acid: A critical review. J Macromol Sci - Pure Appl Chem 42 A:1299–1315.

9. Hasson D, Shemer H, Sher A (2011) State of the Art of Friendly "Green" Scale Control Inhibitors: A Review Article. Ind Eng Chem Res 50:7601–7607.

10. Zohuriaan-Mehr MJ, Pourjavadi A, Salimi H, Kurdtabar M (2009) Protein- and homo poly(amino acid)-based hydrogels with super-swelling properties. Polym Adv Technol 20:655–671.

11. Tomida M, Nakato T, Matsunami S, Kakuchi T (1997) Convenient synthesis of high molecular weight poly(succinimide) by acid-catalysed polycondensation of l-aspartic acid. Polymer (Guildf) 38:4733–4736.

12. Nakato T, Yoshitake M, Matsubara K, Tomida M, Kakuchi T (1998) Relationships between Structure and Properties of Poly(aspartic acid)s. Macromolecules 31:2107–2113.

13. Varga Z, Molnár K, Torma V, Zrínyi M (2010) Kinetics of volume change of poly(succinimide) gels during hydrolysis and swelling. Phys Chem Chem Phys 12:12670–12675.

14. Horvat G, Gyarmati B, Berko S, Szabo-Revesz P, Szilagyi BA, Szilagyi A, Soos J, Sandri G, Bonferoni MC, Rossi S, Ferrari F, Caramella C, Csanyi E, Budai-Szucs M (2015) Thiolated poly(aspartic acid) as potential in situ gelling, ocular mucoadhesive drug delivery system. Eur J Pharm Sci 67:1–11.

15. Wang B, Jeon YS, Park HS, Kim YJ, Kim JH (2015) Mussel-mimetic self-healing polyaspartamide derivative gel via boron-catechol interactions. Express Polym Lett

9:799–808.

16. Lim S, Nguyen MP, Choi Y, Kim J, Kim D (2017) Bioadhesive Nanoaggregates Based on Polyaspartamide- *g* -C18/DOPA for Wound Healing. Biomacromolecules acs.biomac.7b00584.

17. Di Meo C, Cilurzo F, Licciardi M, Scialabba C, Sabia R, Paolino D, Capitani D, Fresta M, Giammona G, Villani C, Matricardi P (2015) Polyaspartamide-Doxorubicin Conjugate as Potential Prodrug for Anticancer Therapy. Pharm Res 32:1557–1569.

18. Sharma A, Kundu S, Reddy M A, Bajaj A, Srivastava A (2013) Design and Engineering of Disulfide Crosslinked Nanocomplexes of Polyamide Polyelectrolytes: Stability under Biorelevant Conditions and Potent Cellular Internalization of Entrapped Model Peptide. Macromol Biosci 13:927–937.

19. Sharma A, Srivastava A (2013) Pronounced influence of pH, metal-ion and solvent isotope on the thermoresponse of synthetic amphiphilic polypeptides. Polym Chem 5119–5128.

20. Németh C, Szabó D, Gyarmati B, Gerasimov A, Varfolomeev M, Abdullin T, László K, Szilágyi A (2017) Effect of side groups on the properties of cationic polyaspartamides. Eur Polym J 93:805–814.

21. Németh C, Gyarmati B, Abdullin T, László K, Szilágyi A (2017) Poly(aspartic acid) with adjustable pH-dependent solubility. Acta Biomater 49:486–494.

22. Craparo EF, Porsio B, Sardo C, Giammona G, Cavallaro G (2016) Pegylated Polyaspartamide-Polylactide-Based Nanoparticles Penetrating Cystic Fibrosis Artificial Mucus. Biomacromolecules 17:767–777.

23. Heo SB, Jeon YS, Kim YJ, Kim SH, Kim JH (2013) Bioinspired self-adhesive polymer for surface modification to improve antifouling property. J Coatings Technol Res 10:811–819.

24. Kim M, Shin SW, Lim CW, Kim J, Um SH, Kim D (2017) Polyaspartamide-based graft copolymers encapsulating iron oxide nanoparticles for imaging and fluorescence labelling of immune cells. Biomater Sci. doi: 10.1039/C6BM00763E

25. HARADA K (1959) Polycondensation of Thermal Precursors of Aspartic Acid1. J Org Chem 24:1662–1666.

26. Cui J, Björnmalm M, Liang K, Xu C, Best JP, Zhang X, Caruso F (2014) Super-soft hydrogel particles with tunable elasticity in a microfluidic blood capillary model. Adv Mater 26:7295–7299.

27. Haider H, Yang CH, Zheng WJ, Yang JH, Wang MX, Yang S, Zrínyi M, Osada Y, Suo Z, Zhang Q, Zhou J, Chen YM (2015) Exceptionally tough and notch-insensitive magnetic hydrogels. Soft Matter 11:8253–8261.

28. Caló E, Khutoryanskiy V V. (2015) Biomedical applications of hydrogels: A review of patents and commercial products. Eur Polym J 65:252–267.

29. Peppas NA, Van Blarcom DS (2016) Hydrogel-based biosensors and sensing devices for drug delivery. J Control Release 240:142–150.

30. Wichterle O, Lím D (1960) Hydrophilic Gels for Biological Use. Nature 185:117–

118.

31. Fusayoshi M (1994) Trends in the Development of Superabsorbent Polymers for Diapers. Superabsorbent Polym 573:88–98.

32. Application of hydrogels. https://www.google.hu/url?sa=i&rct=j&q=&esrc=s&source=images&cd=&cad=rja&uact=8&ved=0ahUKEwi_7cOItNTXAhXEJFAKHXPID6AQjRwIBw&url=http%3A%2F%2Fsticky.kaist.ac.kr%2Fmenu2%2Fmenu3.php&psig=AOvVaw0s2xmqMDstxzcikchAS3aC&ust=1511516287433384.

33. Hennink WE, van Nostrum CF (2012) Novel crosslinking methods to design hydrogels. Adv Drug Deliv Rev 64:223–236.

34. Ghobril C, Grinstaff MW (2015) The chemistry and engineering of polymeric hydrogel adhesives for wound closure: a tutorial. Chem Soc Rev 44:1820–1835.

35. Annabi N, Tamayol A, Uquillas JA, Akbari M, Bertassoni LE, Cha C, Camci-Unal G, Dokmeci MR, Peppas NA, Khademhosseini A (2014) 25th anniversary article: Rational design and applications of hydrogels in regenerative medicine. Adv Mater 26:85–124.

36. Flory PJ (1953) Principles of polymer chemistry. Cornell Universoty Press, Ithaca

37. Flory PJ, Rehner J (1943) Statistical Mechanics of Cross-Linked Polymer Networks II. Swelling. J Chem Phys 11:521–526.

38. Qiu Y, Park K (2012) Environment-sensitive hydrogels for drug delivery. Adv Drug Deliv Rev 64:49–60.

39. Koetting MC, Peters JT, Steichen SD, Peppas NA (2015) Stimulus-responsive hydrogels: Theory, modern advances, and applications. Mater Sci Eng R Reports 93:1–49.

40. Wu XS, Hoffman AS, Yager P (1992) Synthesis and characterization of thermally reversible macroporous poly(N-isopropylacrylamide) hydrogels. J Polym Sci Part A Polym Chem 30:2121–2129.

41. Tomatsu I, Peng K, Kros A (2011) Photoresponsive hydrogels for biomedical applications. Adv Drug Deliv Rev 63:1257–1266.

42. Shiga T (1997) Deformation and viscoelastic behavior of polymer gels in electric fields. Adv Polym Sci 134:131–163.

43. Liu TY, Hu SH, Liu TY, Liu DM, Chen SY (2006) Magnetic-sensitive behavior of intelligent ferrogels for controlled release of drug. Langmuir 22:5974–5978.

44. Ulijn R V, Bibi N, Jayawarna V, Thornton PD, Todd SJ, Mart RJ, Smith AM, Gough JE (2007) Bioresponsive hydrogels. Mater Today 10:40–48.

45. Khare AR, Peppas NA, Massimo G, Colombo P (1992) Measurement of the swelling force in ionic polymeric networks I. Effect of pH and ionic content. J Control Release 22:239–244.

46. Xu Q, Huang W, Jiang L, Lei Z, Li X, Deng H (2013) KGM and PMAA based pH-sensitive interpenetrating polymer network hydrogel for controlled drug release. Carbohydr Polym 97:565–570.

47. Marek SR, Conn CA, Peppas NA (2010) Cationic nanogels based on diethylaminoethyl methacrylate. Polymer (Guildf) 51:1237–1243.

48. Gyenes T, Torma V, Gyarmati B, Zrínyi M (2008) Synthesis and swelling properties of novel pH-sensitive poly(aspartic acid) gels. Acta Biomater 4:733–44.

49. Gyarmati B, Meszar EZ, Kiss L, Deli MA, Laszlo K, Szilagyi A (2015) Supermacroporous chemically cross-linked poly(aspartic acid) hydrogels. Acta Biomater 22:32–38.

50. Gyarmati B, Vajna B, Némethy Á, László K, Szilágyi A (2013) Redox- and pH-responsive cysteamine-modified poly(aspartic acid) showing a reversible sol-gel transition. Macromol Biosci 13:633–40.

51. Gyarmati B, Krisch E, Szilagyi A (2014) In situ oxidation-induced gelation of poly(aspartic acid) thiomers. React Funct Polym 84:29–36.

52. Gyenes T, Torma V, Zrínyi M (2008) Swelling properties of aspartic acid-based hydrogels. Colloids Surf A Physicochem Eng Asp 319:154–158.

53. Juriga D, Nagy KS, Jedlovszky-Hajdu A, Perczel-Kovach K, Chen YM, Varga G, Zrinyi M (2016) Biodegradation and osteosarcoma cell cultivation on poly(aspartic acid) based hydrogels. ACS Appl Mater Interfaces 8:23463–23476.

54. Molnar K, Jedlovszky-Hajdu A, Zrinyi M, Jiang S, Agarwal S (2017) Poly(amino acid)-Based Gel Fibers with pH Responsivity by Coaxial Reactive Electrospinning. Macromol Rapid Commun 201700147:1700147.

55. Krisch E, Messager L, Gyarmati B, Ravaine V, Szilágyi A (2016) Redox- and pH-Responsive Nanogels Based on Thiolated Poly(aspartic acid). Macromol Mater Eng 301:260–266.

56. Tamayol A, Akbari M, Annabi N, Paul A, Khademhosseini A, Juncker D (2013) Fiber-based tissue engineering: Progress, challenges, and opportunities. Biotechnol Adv 31:669–687.

57. Krisch E, Gyarmati B, Szilágyi A (2016) Preparation of pH-responsive poly(Aspartic acid) nanogels in inverse emulsion. Period Polytech Chem Eng 61:19–26.

58. Bresee BRR, Ko W (2003) Fiber Formation During Melt Blowing. INJ Summer

59. Sarkar K, Gomez C, Zambrano S, Ramirez M, de Hoyos E, Vasquez H, Lozano K (2010) Electrospinning to Forcespinning™. Mater Today 13:12–14.

60. Ramakrishna S, Fujihara K, Teo W, Yong T, Ramaseshan R (2006) El e c t r o s p u n n a n o f i b e r s : 9:40–50.

61. Feltz KP, Kalaf EAG, Chen C, Martin RS, Sell SA (2017) A review of electrospinning manipulation techniques to direct fiber deposition and maximize pore size. 46–61.

62. Molnar K, Juriga D, Nagy PM, Sinko K, Jedlovszky-Hajdu A, Zrinyi M (2014) Electrospun poly(aspartic acid) gel scaffolds for artificial extracellular matrix. Polym Int 63:1608–1615.

63. Thoroddsen S (2009) No Title. In:

http://www.eng.nus.edu.sg/EResnews/0902/rd/rd16.html.
http://www.eng.nus.edu.sg/EResnews/0902/rd/rd16.html.

64. Baji A, Mai Y-W, Wong S, Abtahi M, Chen P (2010) Electrospinning of polymer nanofibers: Effects on oriented morphology, structures and tensile properties. Compos Sci Technol 70:703–718.

65. Bohr A, Boetker JP, Rades T, Rantanen J, Yang M (2014) Application of spray-drying and electrospraying/electrospinning for poorly water-soluble drugs: a particle engineering approach. Curr Pharm Des 20:325–48.

66. Jayaraman P, Gandhimathi C, Venugopal JR, Becker DL, Ramakrishna S, Srinivasan DK (2015) Controlled release of drugs in electrosprayed nanoparticles for bone tissue engineering. Adv Drug Deliv Rev 94:77–95.

67. Girardi C, Jullian V, Haddad M, Vansteelandt M, Cabanillas BJ, Kapanda CN, Herent MF, Quetin-Leclercq J, Fabre N (2016) Analysis and fragmentation mechanisms of hirsutinolide-type sesquiterpene lactones by ultra-high-performance liquid chromatography/electrospray ionization linear ion trap Orbitrap mass spectrometry. Rapid Commun Mass Spectrom 30:569–580.

68. Ramakrishna S, Fujivara K, Teo W-E, Lim T-C, Ma Z (2005) An Introduction to Electrospinning and Nanofibers. World Scientific Publishing Co. Pte. Ltd., Singapore

69. Gupta P, Elkins C, Long TE, Wilkes GL (2005) Electrospinning of linear homopolymers of poly(methyl methacrylate): exploring relationships between fiber formation, viscosity, molecular weight and concentration in a good solvent. Polymer (Guildf) 46:4799–4810.

70. Huang GP, Shanmugasundaram S, Masih P, Pandya D, Amara S, Collins G, Arinzeh TL, Arinzeh L (2015) An investigation of common crosslinking agents on the stability of electrospun collagen scaffolds. J Biomed Mater Res Part A 103:762–771.

71. Agarwal S, Greiner A (2011) On the way to clean and safe electrospinning-green electrospinning: Emulsion and suspension electrospinning. Polym Adv Technol 22:372–378.

72. ElectrospinTech Commercially available electrospun products. http://electrospintech.com/products.html#.Wak4r9FLe70.

73. Chen C, Tang Y, Vlahovic B, Yan F (2017) Electrospun Polymer Nanofibers Decorated with Noble Metal Nanoparticles for Chemical Sensing. Nanoscale Res Lett 12:451.

74. Siafaka PI, Okur NÜ, Mone M, Giannakopoulou S, Er S, Pavlidou E, Karavas E, Bikiaris DN (2016) Two different approaches for oral administration of voriconazole loaded formulations: Electrospun fibers versus β-cyclodextrin complexes. Int J Mol Sci 17:1–15.

75. Gross JJ, Chou S-F, Carson D, Woodrow KA (2015) Current strategies for sustaining drug release from electrospun nanofibers. J Control Release 220:584–591.

76. Balogh A, Farkas B, Faragó K, Farkas A, Wagner I, Van Assche I, Verreck G, Nagy

ZK, Marosi G (2015) Melt-blown and electrospun drug-loaded polymer fiber mats for dissolution enhancement: A comparative study. J Pharm Sci 104:1767–1776.

77. Yu M, Dong RH, Yan X, Yu GF, You MH, Ning X, Long YZ (2017) Recent Advances in Needleless Electrospinning of Ultrathin Fibers: From Academia to Industrial Production. Macromol Mater Eng 302:1–19.

78. Yan E, Cao M, Wang Y, Yuan Meng, Zheng H, Hao X, Yu Z, Ba X, Gu X, Zhang D (2016) Degradable polyvinyl alcohol/poly(butylene carbonate) core–shell nanofibers for chemotherapy and tissue engineering. Mater Lett 167:13–17.

79. Qu H, Wei S, Guo Z (2013) Coaxial electrospun nanostructures and their applications. J Mater Chem A 1:11513.

80. Hwang TH, Lee YM, Kong B-S, Seo J-S, Choi JW (2012) Electrospun Core − Shell Fibers for Robust Silicon Nanoparticle-Based Lithium Ion Battery Anodes. Nano Lett 12:802–7.

81. Lu Y, Huang J, Yu G, Cardenas R, Wei S, Wujcik EK, Guo Z (2016) Coaxial electrospun fibers: applications in drug delivery and tissue engineering. Wiley Interdiscip Rev Nanomedicine Nanobiotechnology 8:654–677.

82. Fang J, Wang X, Lin T (2011) Functional Applications of Electrospun Nanofibers. Nanofibers - Prod Prop Funct Appl 287–326.

83. Zhang C, Wu S, Qin X (2014) Facile fabrication of novel pH-sensitive poly(aspartic acid) hydrogel by crosslinking nanofibers. Mater Lett 132:393–396.

84. Gao Q, Takizawa J, Mutsumi K (2012) Hydrophilic non-wovens made of cross-linked fully-hydrolyzed poly(vinyl.pdf. Polymer (Guildf) 54:120–126.

85. Ding B, Kim H-Y, Lee S-C, Shao C-L, Lee D-R, Park S-J, Kwag G-B, Choi K-J (2002) Preparation and characterization of a nanoscale poly(vinyl alcohol) fiber aggregate produced by an electrospinning method. J Polym Sci Part B Polym Phys 40:1261–1268.

86. Kim Y-J, Ebara M, Aoyagi T (2012) Temperature-responsive electrospun nanofibers for “on–off” switchable release of dextran. Sci Technol Adv Mater 13:64203.

87. Dargaville BL, Vaquette C, Rasoul F, Cooper-White JJ, Campbell JH, Whittaker AK (2013) Electrospinning and crosslinking of low-molecular-weight poly(trimethylene carbonate-co-l-lactide) as an elastomeric scaffold for vascular engineering. Acta Biomater 9:6885–6897.

88. Hasanain F, Guenther K, Mullett WM, Craven E (2014) Gamma sterilization of pharmaceuticals--a review of the irradiation of excipients, active pharmaceutical ingredients, and final drug product formulations. PDA J Pharm Sci Technol 68:113–37.

89. Zhang YZ, Venugopal J, Huang ZM, Lim CT, Ramakrishna S (2006) Crosslinking of the electrospun gelatin nanofibers. Polymer (Guildf) 47:2911–2917.

90. Peng YY, Glattauer V, Ramshaw JAM (2017) Stabilisation of Collagen Sponges by Glutaraldehyde Vapour Crosslinking. Int J Biomater. doi: 10.1155/2017/8947823

91. Lu W, Ma M, Xu H, Zhang B, Cao X, Guo Y (2015) Gelatin nanofibers prepared by

spiral-electrospinning and cross-linked by vapor and liquid-phase glutaraldehyde. Mater Lett 140:1–4.

92. Tang C, Saquing CD, Harding JR, Khan S a. (2010) In Situ Cross-Linking of Electrospun Poly(vinyl alcohol) Nanofibers. Macromolecules 43:630–637.

93. Xu F, Sheardown H, Hoare T (2015) Reactive Electrospinning of Degradable Poly(oligoethylene glycol methacrylate)-Based Nanofibrous Hydrogel Networks. Chem Commun 52:1451–1454.

94. Sawhney RK, Hussey L, Hayman RG, Tillotson TM, Us CA, Scott EE (2002) Double-barreled syringe with detachable locking mixing tip. 2:5–7.

95. Jun Zeng, Haoqing Hou, Joachim H.Wendorff AG (2005) Photo-Induced Solid-State Crosslinking of Electrospun Poly(vinyl alcohol) Fibers. Macromol Rapid Commun Rapid Commun 26:1557–1562.

96. Theron JP, Knoetze JH, Sanderson RD, Hunter R, Mequanint K, Franz T, Zilla P, Bezuidenhout D (2010) Modification, crosslinking and reactive electrospinning of a thermoplastic medical polyurethane for vascular graft applications. Acta Biomater 6:2434–47.

97. Langer R, Vacanti JP (1993) Tissue engineering. Science (80- ) 260:920–926.

98. Halim A, Khoo T, Shah JY (2010) Biologic and synthetic skin substitutes: An overview. Indian J Plast Surg 43:23.

99. Schmidt D, Dijkman PE, Driessen-Mol A, Stenger R, Mariani C, Puolakka A, Rissanen M, Deichmann T, Odermatt B, Weber B, Emmert MY, Zund G, Baaijens FPT, Hoerstrup SP (2010) Minimally-invasive implantation of living tissue engineered heart valves: A comprehensive approach from autologous vascular cells to stem cells. J Am Coll Cardiol 56:510–520.

100. Syedain Z, Reimer J, Lahti M, Berry J, Johnson S, Tranquillo RT (2016) Tissue engineering of acellular vascular grafts capable of somatic growth in young lambs. Nat Commun 7:12951.

101. Matriderm. https://ozmedix.com.au/wp-content/uploads/2015/06/Matriderm-Wet.jpg.

102. Pramanik S, Pingguan-Murphy B, Abu Osman NA (2012) Progress of key strategies in development of electrospun scaffolds: bone tissue. Sci Technol Adv Mater 13:43002.

103. Wolf MT, Dearth CL, Sonnenberg SB, Loboa EG, Badylak SF (2015) Naturally derived and synthetic scaffolds for skeletal muscle reconstruction. Adv Drug Deliv Rev 84:208–21.

104. Kleinman HK, Murray JC, McGoodwin EB, Martin GR (1978) Connective tissue structure: cell binding to collagen. J Invest Dermatol 71:9–11.

105. Qazi TH, Mooney DJ, Pumberger M, Gei??ler S, Duda GN (2015) Biomaterials based strategies for skeletal muscle tissue engineering: Existing technologies and future trends. Biomaterials 53:502–521.

106. Pina S, Oliveira JM, Reis RL (2015) Natural-based nanocomposites for bone tissue engineering and regenerative medicine: A review. Adv Mater 27:1143–1169.

107. Logithkumar R, Keshavnarayan A, Dhivya S, Chawla A, Saravanan S, Selvamurugan N (2016) A review of chitosan and its derivatives in bone tissue engineering. Carbohydr Polym 151:172–188.

108. Collins MN, Birkinshaw C (2013) Hyaluronic acid based scaffolds for tissue engineering - A review. Carbohydr Polym 92:1262–1279.

109. Wade RJ, Bassin EJ, Rodell CB, Burdick J a. (2015) Protease-degradable electrospun fibrous hydrogels. Nat Commun 6:6639.

110. Tombácz E, Illés E, Majzik A, Hajdú A, Rideg N, Szekeres M (2007) Ageing in the inorganic nanoworld: Example of magnetite nanoparticles in aqueous medium. Croat Chem Acta 80:503–515.

111. Jedlovszky-Hajdu A, Tombacz E, Banyai I, Babos M, Palko A (2012) Carboxylated magnetic nanoparticles as MRI contrast agents: Relaxation measurements at different field strengths. J Magn Magn Mater 324:3173–3180.

112. Vékás L, Bica D, Marinică O (2006) Magnetic nanofluids stabilized with various chain length surfactants. Rom Reports Phys 58:257.

113. Kamide K, Kataoka A (1969) Theoretical relationships between parameters in the KUHN-MARK-HOUWINK-SAKURADA equation. Die Makromol Chemie 128:217–228.

114. Vlasák J, Rypáček F, Drobník J, Saudek V (1979) Properties and reactivity of polysuccinimide. J Polym Sci Polym Symp 66:59–64.

115. Rutala WA, Weber DJ (2008) Draft guideline for disinfection and sterilization in healthcare facilities. US-Centre Dis Control Prot 1–158.

116. Singh N, Singh RK, Bhunia a K, Stroshine RL (2002) Efficacy of chlorine dioxide, ozone, and Thyme essential oil or a sequential washing in killing Escherichia coli O157:H7 on lettuce and baby carrots. Leb und-Technologie 35:720–729.

117. Noszticzius Z, Wittmann M, Kály-Kullai K, Beregvári Z, Kiss I, Rosivall L, Szegedi J (2013) Chlorine dioxide is a size-selective antimicrobial agent. PLoS One 8:1–10.

118. Matthews BD, Mostafa G, Carbonell AM, Joels CS, Kercher KW, Austin C, Norton HJ, Heniford BT (2005) Evaluation of adhesion formation and host tissue response to intra-abdominal polytetrafluoroethylene mesh and composite prosthetic mesh1. J Surg Res 123:227–234.

119. Shenoy SL, Bates WD, Frisch HL, Wnek GE (2005) Role of chain entanglements on fiber formation during electrospinning of polymer solutions: good solvent, non-specific polymer–polymer interaction limit. Polymer (Guildf) 46:3372–3384.

120. Beachley V, Wen X (2009) Effect of electrospinning parameters on the nanofiber diameter and length. Mater Sci Eng C Mater Biol Appl 29:663–668.

121. Huang Z-MM, Zhang Y-ZZ, Kotaki M, Ramakrishna S (2003) A review on polymer nanofibers by electrospinning and their applications in nanocomposites. Compos Sci Technol 63:2223–2253.

122. Tiwari SK, Venkatraman SS (2012) Importance of viscosity parameters in

electrospinning: Of monolithic and core-shell fibers. Mater Sci Eng C 32:1037–1042.

123. Wang X, Pellerin C, Bazuin CG (2016) Enhancing the Electrospinnability of Low Molecular Weight Polymers Using Small Effective Cross-Linkers. Macromolecules 49:891–899.

124. Ayutsede J, Gandhi M, Sukigara S, Micklus M, Chen HE, Ko F (2005) Regeneration of Bombyx mori silk by electrospinning. Part 3: Characterization of electrospun nonwoven mat. Polymer (Guildf) 46:1625–1634.

125. Buchko CJ, Chen LC, Shen Y, Martina DC (1999) Processing and microstructural characterization of porous biocompatible\rprotein polymer thin films. Polymer (Guildf) 40:7397–7407.

126. Savva I, Krekos G, Taculescu A, Marinica O, Vekas L, Krasia-Christoforou T (2012) Fabrication and characterization of magnetoresponsive electrospun nanocomposite membranes based on methacrylic random copolymers and magnetite nanoparticles. J Nanomater 2012:1–9.

127. Mpekris F, Achilleos M, Vasile E, Vasile E, Krasia-Christoforou T, Stylianopoulos T (2015) Mechanical properties of structurally-defined magnetoactive polymer (co)networks. RSC Adv 5:20011–20019.

128. Liu Y, Zhang X, Xia Y, Yang H (2010) Magnetic Field-Assisted Electrospinning of Aligned Straight and Wavy Polymeric Nanofibers. Adv Mater 22:2454–2457.

129. Nicknejad ET, Ghoreishi SM, Habibi N (2015) Electrospinning of cross-Linked magnetic chitosan nanofibers for protein release. AAPS PharmSciTech 16:1–7.

130. Jedlovszky-Hajdu A, Molnar K, Nagy PM, Sinko K, Zrinyi M (2016) Preparation and properties of a magnetic field responsive three-dimensional electrospun polymer scaffold. Colloids Surfaces A Physicochem Eng Asp 503:79–87.

131. Jedlovszky-Hajdu A, Baldelli Bombelli F, Monopoli MP, Tombacz E, Dawson KA (2012) Surface Coatings Shape the Protein Corona of SPIONs with Relevance to Their Application in Vivo. Langmuir 28:14983–14991.

132. Tombácz E, Tóth IY, Nesztor D, Illés E, Hajdú A, Szekeres M, L.Vékás (2013) Adsorption of organic acids on magnetite nanoparticles, pH-dependent colloidal stability and salt tolerance. Colloids Surfaces A Physicochem Eng Asp 435:91–96.

133. Yousefzadeh M, Latifi M, Amani-tehran M, Teo W, Ramakrishna S A Note on the 3D Structural Design of Electrospun Nanofibers.

134. Bonino C a, Efimenko K, Jeong SI, Krebs MD, Alsberg E, Khan S a (2012) Three-dimensional electrospun alginate nanofiber mats via tailored charge repulsions. Small 8:1928–36.

135. Samal SK, Goranov V, Dash M, Russo A, Shelyakova T, Graziosi P, Lungaro L, Riminucci A, Uhlarz M, Bañobre-López M, Rivas J, Herrmannsdörfer T, Rajadas J, De Smedt S, Braeckmans K, Kaplan DL, Dediu VA (2015) Multilayered Magnetic Gelatin Membrane Scaffolds. ACS Appl Mater Interfaces 7:23098–109.

136. Wilhelm C, Gazeau F (2008) Universal cell labelling with anionic magnetic nanoparticles. Biomaterials 29:3161–74.

137. Lacava LM, Garcia V a. P, Kückelhaus S, Azevedo RB, Sadeghiani N, Buske N, Morais PC, Lacava ZGM (2004) Long-term retention of dextran-coated magnetite nanoparticles in the liver and spleen. J Magn Magn Mater 272–276:2434–2435.

138. Kurazumi H, Kubo M, Ohshima M, Yamamoto Y, Takemoto Y, Suzuki R, Ikenaga S, Mikamo A, Udo K, Hamano K, Li T-S (2011) The effects of mechanical stress on the growth, differentiation, and paracrine factor production of cardiac stem cells. PLoS One 6:e28890.

139. Jain MK, Berg R., Tandon GP (1990) Mechanical stress and cellular metabolism in living soft tissue composites. Biomaterials 11:465–472.

140. Schimmelpfeng J, Dertinger H (1997) Action of a 50 Hz Magnetic Field on Proliferation of Cells in Culture. 183:177–183.

141. Lagerwall JPF, McCann JT, Formo E, Scalia G, Xia Y (2008) Coaxial electrospinning of microfibres with liquid crystal in the core. Chem Commun (Camb) 5420–5422.

142. Jiang S, Hou H, Agarwal S, Greiner A (2016) Polyimide Nanofibers by "Green" Electrospinning via Aqueous Solution for Filtration Applications. ACS Sustain Chem Eng 4:4797–4804.

143. Gonçalves RP, da Silva FFF, Picciani PHS, Dias ML (2015) Morphology and Thermal Properties of Core-Shell PVA/PLA Ultrafine Fibers Produced by Coaxial Electrospinning. Mater Sci Appl 6:189–199.

144. Ji Y, Ghosh K, Li B, Sokolov JC, Clark RAF, Rafailovich MH (2006) Dual-syringe reactive electrospinning of cross-linked hyaluronic acid hydrogel nanofibers for tissue engineering applications. Macromol Biosci 6:811–817.

145. Kim SH, Kim S-H, Nair S, Moore E (2005) Reactive Electrospinning of Cross-Linked Poly(2-hydroxyethyl methacrylate) Nanofibers and Elastic Properties of Individual Hydrogel Nanofibers in Aqueous Solutions. Macromolecules 38:3719–3723.

146. Knierim C, Enzeroth M, Kaiser P, Dams C, Nette D, Seubert A, Klingl A, Greenblatt CL, Jérôme V, Agarwal S, Freitag R, Greiner A (2015) Living Composites of Bacteria and Polymers as Biomimetic Films for Metal Sequestration and Bioremediation. Macromol Biosci 15:1052–1059.

147. Tanaka T, Hocker LO, Benedek GB (1973) Spectrum of light scattered from a viscoelastic gel *. J Chem Phys 59:5151–5159.

148. Li Y, Tanaka T (1990) Kinetics of swelling and shrinking of gels. J Chem Phys 92:1365–1371.

149. Mura S, Nicolas J, Couvreur P (2013) Stimuli-responsive nanocarriers for drug delivery. Nat Mater 12:991–1003.

150. Szilágyi BA, Gyarmati B, Horvát G, Laki Á, Budai-Szucs M, Csányi E, Sandri G, Bonferoni MC, Szilágyi A (2017) The effect of thiol content on the gelation and mucoadhesion of thiolated poly(aspartic acid). Polym Int. doi: 10.1002/pi.5411

151. Yao H, Jiang F, Lu A, Zhang G (2016) Methods to design and synthesize antibody-drug conjugates (ADCs). Int J Mol Sci. doi: 10.3390/ijms17020194

152. Oh SH, Park IK, Kim JM, Lee JH (2007) In vitro and in vivo characteristics of PCL scaffolds with pore size gradient fabricated by a centrifugation method. Biomaterials 28:1664–1671.

153. Mi H-Y, Jing X, Huang H-X, Turng L-S (2017) Instantaneous self-assembly of three-dimensional silica fibers in electrospinning: Insights into fiber deposition behavior. Mater Lett 204:45–48.

154. Chakrapani VY, Kumar TSS, Raj DK, Kumary T V. (2017) Electrospun 3D composite scaffolds for craniofacial critical size defects. J Mater Sci Mater Med 28:119.

155. Pokorny P, Kostakova E, Sanetrnik F, Mikes P, Chvojka J, Kalous T, Bilek M, Pejchar K, Valtera J, Lukas D (2014) Effective AC needleless and collectorless electrospinning for yarn production. Phys Chem Chem Phys 16:26816–26822.

156. Jeong SI, Burns NA, Bonino CA, Kwon IK, Khan SA, Alsberg E (2014) Improved cell infiltration of highly porous nanofibrous scaffolds formed by combined fiber-fiber charge repulsions and ultra-sonication. J Mater Chem B Mater Biol Med 2:8116–8122.

157. Varga J, Janovak L, Varga E, Eros G, Dekany I, Kemeny L (2009) Acrylamide, acrylic acid and n-isopropylacrylamide hydrogels as Osmotic tissue expanders. Skin Pharmacol Physiol 22:305–312.

158. Jaiswal AK, Dhumal R V., Bellare JR, Vanage GR (2013) In vivo biocompatibility evaluation of electrospun composite scaffolds by subcutaneous implantation in rat. Drug Deliv Transl Res 3:504–517.

159. Son S-R, Linh N-TB, Yang H-M, Lee B-T (2013) *In vitro* and *in vivo* evaluation of electrospun PCL/PMMA fibrous scaffolds for bone regeneration. Sci Technol Adv Mater 14:15009.

160. Stankus JJ, Freytes DO, F. BS, William R (2008) Hybrid nanofibrous scaffolds from electrospinning of a synthetic biodegradable elastomer and urinary bladder matrix. J Biomater Sci Polym Ed 19:635–652.

161. Luijendijk RW, Hop WCJ, van den Tol MP, de Lange DCD, Braaksma MMJ, IJzermans JNM, Boelhouwer RU, de Vries BC, Salu MKM, Wereldsma JCJ, Bruijninckx CMA, Jeekel J (2000) A Comparison of Suture Repair with Mesh Repair for Incisional Hernia. N Engl J Med 343:392–398.

162. I MDLPB, Brandão L, Ii C, Tavares L, Ii C (2017) Comparative study of Polypropylene versus Parietex. Acta Cir Bras 32:98–107.

163. Daniell H, Anderson JM, Rodriguez A, Chang DT (2008) FOREIGN BODY REACTION TO BIOMATERIALS. Semin Immunol 20:86–100.

164. Jones KS (2008) Effects of biomaterial-induced inflammation on fibrosis and rejection. Semin Immunol 20:130–136.

165. Ross MH, Kaye GI, Pawlina W (2002) Histology: A Text and Atlas with Cell and Molecular Biology. Lippincott Williams & Wilkins

# 11 Publications of the candidate

## 11.1 Publications related to the thesis

Molnar K, Jedlovszky-Hajdu A, Zrinyi M, Jiang S, Agarwal S (2017) Poly(amino acid)-Based Gel Fibers with pH Responsivity by Coaxial Reactive Electrospinning. Macromol Rapid Commun 201700147:1700147. $IF_{2016}$: 4.638

Jedlovszky-Hajdu A, Molnar K, Nagy PM, Sinko K, Zrinyi M (2016) Preparation and properties of a magnetic field responsive three-dimensional electrospun polymer scaffold. Colloids Surfaces A Physicochem Eng Asp 503:79–87. $IF_{2016}$: 2.765

Molnar K, Juriga D, Nagy PM, Sinko K, Jedlovszky-Hajdu A, Zrinyi M (2014) Electrospun poly(aspartic acid) gel scaffolds for artificial extracellular matrix. Polym Int 63:1608–1615. $IF_{2014}$: 2.409

## 11.2 Publications not related to the thesis

Varga Z, Molnár K, Torma V, Zrínyi M (2010) Kinetics of volume change of poly(succinimide) gels during hydrolysis and swelling. Phys Chem Chem Phys 12:12670–12675. $IF_{2010}$: 4.116

DOI:10.14753/SE.2018.2178

# 12 Acknowledgements

I am very grateful to my supervisor, Angéla Jedlovszky-Hajdú for helping tirelessly and guiding me through my research even during her maternity leave. I am also very grateful to Miklós Zrínyi for inviting me into his group and letting me be a part of it for so many years and of course to both of them for teaching and showing me the wonders of physico-chemistry and colloid sciences. Many thanks to all the recent and past members of the Laboratory of Nanochemistry for the friendly environment and fruitful scientific conversations. Especially to Dávid Juriga and my students Zsófia Németh, Constantinos Voniatis, Rita Varga and Ákos Emri.

Several experiments and measurements were carried out in other laboratories with the help of professionals. Without their help, a good chunk of the thesis would have never been prepared. Therefore I am grateful to György Wéber and his team for the *in vivo* experiments, Lilla Reiniger for histopathology, Katalin Sinkó for SEM, IR, Péter Németh for SEM, Tamás Bozó for teaching me how to use the AFM and all the rest who helped me.

I am also grateful to Seema Agarwal and Andreas Greiner for hosting me in their laboratories in Bayreuth. The coaxial reactive electrospinning strategy was developed during my visit in their laboratories.

And last, but not least I am forever grateful to my family and friends for encouraging me to do this and never give up and also for shaping me to the man I am today. To my parents for raising me and giving guidance, support and advice; to my brother for the discussions and his help in making machines and equipment for my research even late nights; to Kristóf Zólyomi for everything;

to the two forever shining stars of my life, Enikő and Boglárka.

Financial support: Kerpel-Fróniusz Ödön Tehetséggondozó Program, Hungarian Science Foundation OTKA 101704; OTKA 105523; OTKA 115259; NKFIH FK 124147, COST MP1206; ÚNKP-17-3-III-SE-18 New National Excellence Program of the Ministry of Human Capacities

DOI:10.14753/SE.2018.2178

# Supplementary information

## Sample preparation for histopathology

### Water elimination, embedding in paraffin and sample cutting

Water elimination and embedding in paraffin was carried out by a Leica ASP300 enclosed tissue processor with the following protocol:

- samples were put into plastic containers;
- 1 h isopropyl alcohol (IPA);
- 1.5 h IPA;
- 2 h IPA;
- 1.5 h abs. ethanol;
- 2 h abs. ethanol;
- 1 h xilol;
- 1 h xilol;
- 0.5 h xilol;
- 1 h paraffin 60 $^{o}$C;
- 1 h paraffin 60 $^{o}$C;
- 1 h paraffin 60 $^{o}$C.

Then slides of 4 micrometer thickness were cut with a Leica microtom.

### Hematoxylin-Eozin staining

- Paraffin removal: 3 x 3 min xilol
- Resolubilisation:
  - 3 min abs. ethanol
  - 3 min 96 V/V% ethanol
  - 3 min 70 V/V% ethanol
  - 3 min washing in distilled water
  - 10 min Mayer type Hematoxilin staining (for 1L solution in distilled water: 1 g hematoxylin, 50 g $KAl(SO_4)_2$ x 12 $H_2O$, 0.2 g $NaIO_3$, 50 g Trichloroacetaldehyde hydrate, 1 g citric acid)
- 5 min washing in tap water
- 5 min Eozin staining (in the mixture of 60 ml 1 g/V% and 500 ml tap water)